INTERNATIONAL STUDIES IN SCIENCE AND MATHEMATICS

EDITORS

PROF. DR. GÜZİDE ŞENEL

PROF. DR. EDİP BAYRAM

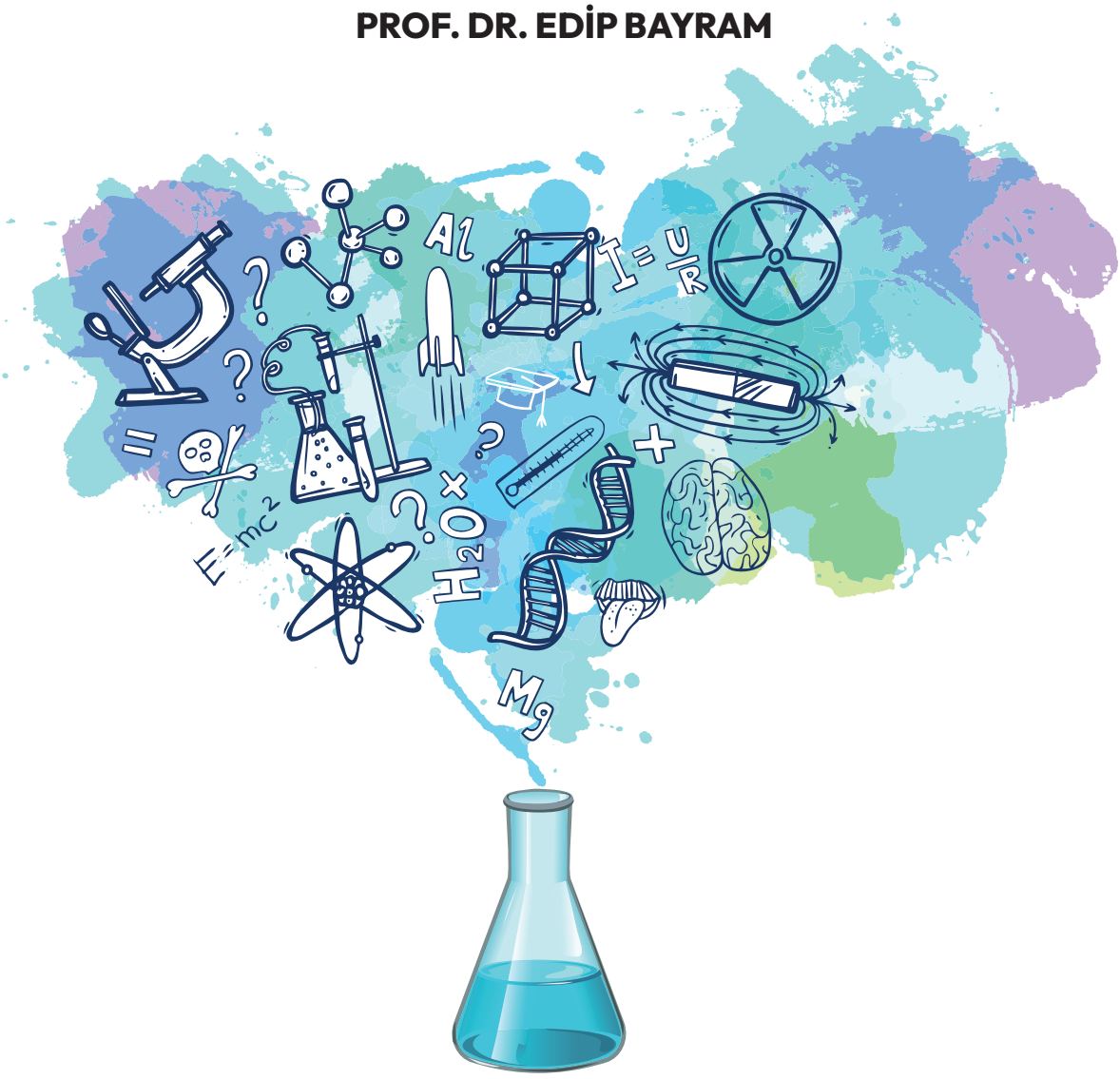

SERÜVEN YAYINEVİ

Genel Yayın Yönetmeni / Editor in Chief • C. Cansın Selin Temana

Kapak & İç Tasarım / Cover & Interior Design • Serüven Yayınevi

Birinci Basım / First Edition • © MART 2026

ISBN • 978-625-8682-81-6

Serüven Yayınevi / Serüven Publishing
Türkiye Adres / Turkey Address: Kızılay Mah. Fevzi Çakmak 1. Sokak
Ümit Apt No: 22/A Çankaya/ANKARA
Telefon / Phone: 05437675765
web: www.seruvenyayinevi.com
e-mail: seruvenyayinevi@gmail.com

Baskı & Cilt / Printing & Volume
Sertifika / Certificate No: 47083

INTERNATIONAL STUDIES IN SCIENCE AND MATHEMATICS

EDITORS

PROF. DR. GÜZİDE ŞENEL
PROF. DR. EDİP BAYRAM

SERÜVEN
YAYINEVİ

CONTENTS

Chapter 1

EVALUATION OF METAPHORS DEVELOPED BY SCIENCE TEACHER CANDIDATES REGARDING THE CONCEPT OF WATER POLLUTION

Nurcan ÖZKAN[1]

1 Nurcan Özkan, Prof. Dr., Trakya University, Education Faculty, Mathematics and Science Education Department, ORCID ID: 0000-0001-5045-6186

INTRODUCTION

Water is essential for all living things on Earth. Rivers, lakes, groundwater, and oceans are vital for both the continuity of ecosystems and the sustainability of human life (URL 1). Since more than two-thirds of the human body is water, people cannot survive even a few days without water. Certain diseases cause a decrease in body water, posing a great danger to human health. For example, the most significant cause of death from diarrhea is dehydration. Water is a fundamental component of blood and tissue fluids in our bodies. Water is essential for all physiological processes occurring in our bodies. It is essential to ensure that water, which is of vital importance, is used without pollution and free from harmful chemicals and disease-causing microorganisms. Similarly, it is important for public health that used and wasted water is disposed of in a way that does not harm people (Ibadullayeva et al., 2019).

Pollution in water resources is of great importance because it is an essential component for all forms of living organisms (Zamani et al., 2012). Indeed, water, which is essential for every stage of life and one of the most important factors for humanity's future survival, and the pollution occurring in it, are constantly gaining importance and becoming more relevant. Because water is one of the fundamental elements that constitute a living environment. Furthermore, thanks to its unique physical, chemical, and biological properties, it itself constitutes a habitat for the living organisms it contains. Therefore, the presence of water in the living environment, its being a living environment itself, and its quality are extremely important (Akın and Akın, 2007). Today, the demand for water is increasing in parallel with population growth, industrial development, and the increase in agricultural activities. Despite this increased demand, water resources are scarce and polluted.

Water pollution is the contamination of water resources such as rivers, lakes, oceans, and groundwater with harmful substances such as radioactive materials, plastics, and chemical waste resulting from human activities (URL 2). In other words, water pollution is defined as the disruption of the natural composition of water sources or the appearance of substances in the water that were not previously present, due to the increase in the concentration values of substances in the natural composition of water sources as a result of certain human activities (Uzun et al., 2014). Water pollution also means the contamination of water sources with harmful chemical, physical, and biological substances. These pollutants enter the water for a variety of reasons, including industrial waste, pesticides, household waste, and even erosion caused by natural disasters. As a result, drinking water, agricultural irrigation, and natural habitats are severely affected. Therefore, understanding and preventing water pollution is a critical requirement for a sustainable future (URL 1).

Water pollution, a prominent environmental problem today that can lead to serious health problems, poses a significant threat to societies. Because water is the natural resource most affected by and most vulnerable to environmental pollution. Water pollution not only affects water resources, but also profoundly impacts ecosystems, underwater life, and human health (URL 2). Water resources, essential for the life of living beings, economic development, and the environment, are limited and vulnerable to negative external influences. Indeed, in today's world, a large portion of water resources have had their natural composition altered, or polluted, as a result of various human activities. If this situation continues, access to fresh water will become difficult in the future, and aquatic life in the disrupted aquatic environment will face a number of negative consequences.

Water that is safe for human consumption should contain sufficient oxygen and essential minerals, and should be clear (Akın, 2009). Considering that one liter of wastewater pollutes eight liters of clean water (Aksungur and Firidin, 2008) and renders it unusable, the likelihood of disruption to the natural cycle of water resources in the near future cannot be denied. In underdeveloped and developing countries, 95% of wastewater and 70% of industrial waste are discharged into water sources without any treatment, resulting in 1.4 billion people worldwide living without access to clean water (Gümrükçüoğlu et al., 2008). Considering that billions of people today lack access to water and adequate hygiene conditions (Çolakoğlu, 2009), the importance of this issue becomes clear.

Although the fact that three-quarters of the Earth's surface is covered with water gives the impression of an abundance of water in the world, only about 0.74% of it is potable. The world population, which was 1 billion in the last quarter of the 18th century at the beginning of the Industrial Revolution, reached 2.5 billion in 1950 and approximately 6.5 billion at the end of 2005. The rapid increase in the world's population, the excessive development of industry and technology, and the insufficient establishment or widespread adoption of environmental awareness are among the reasons why the amount of potable water in the world is gradually decreasing. In addition, the irresponsible pollution of potable water sources creates irreversible problems (Atalık 2006; Dağlı, 2005; Haviland, 2002).

Water pollution profoundly affects ecosystems, human health, and the economy. The most important consequences of water pollution are listed below:

Impact on Ecosystems

a) Biodiversity decline: Polluted water reduces the habitats of living species, leading to species extinction and a decrease in biodiversity.

b) Ecosystem imbalances: Water pollution disrupts food chains and natural water cycles in ecosystems. Conditions such as eutrophication, in particular, lead to sudden algal blooms in ecosystems.

Impact on Human Health

a) Increase in diseases: Contaminated water leads to the spread of waterborne diseases such as cholera, typhoid, and hepatitis.

b) Risk of poisoning: Chemical and heavy metal pollution can lead to chronic diseases and poisoning in the long term.

Economic Effects

a) Agriculture and fisheries: Polluted water causes yield losses in agricultural lands and also seriously affects the fishing industry.

b) Infrastructure and sanitation costs: High costs are required to clean water sources and improve wastewater treatment plants.

Measures taken to address water pollution must be sustainable in order to be effective. This is possible by implementing environmental sustainability, that is, by ensuring the continuity of natural resources (Yılmaz and Bayrakçeken, 2017). For example, the pollutants released into the water should be less than the resources spent to treat them (Küçük and Güneş, 2013). Protecting the quality of natural resources such as air and soil, as well as water, human health, biodiversity, and animal and plant life are also forms of environmental sustainability (Kaypak, 2011).

While laws, regulations, and many other rules are effective in raising awareness among individuals about water pollution, there is also an educational aspect to this issue. At this point, it is also necessary to instill educational practices and theoretical skills. Currently, many practices are being carried out within the scope of skills training in the field of educational sciences. Environmental literacy, environmental issues, and environmental education are particularly noteworthy types of these practices (Karatekin and Yılmaz, 2019; NAAEE, 2011; Roth, 2002).

When examining research on water and environmental issues within the field of educational sciences, it is observed that the data collection tools used vary. These studies generally involve the application of scales or surveys (surveys); observation or interviews (focus groups or semi-structured); asking questions related to written materials (open-ended/sentence completion); and research on perception analysis. Although metaphor studies have been preferred by some researchers (Gürlen and Köseoğlu, 2019; Köseoğlu, 2017; Uysal and Yılmaz, 2019) in identifying the conceptual infrastructure and determining perceptions, sufficient studies on metaphorical perceptions related to the concept of "water pollution" have not been found in the relevant

literature (Yılmaz and Yanarateş, 2020). Therefore, it was deemed appropriate to conduct a metaphorical perception study based on the concept of water pollution. The word metaphor is derived from the Greek word "Metapherein," where meta means to change and pherein means to endure (Levine, 2005). The term metaphor comes from the Latin and Greek root metaphora. The traditional definition of metaphor is a tool that allows one to see one thing in terms of another (Cameron, 1999). Massengil Show and Mahlios (2008) described metaphor as "analogical tendencies acting as a cognitive bias underlying the individual's subconscious." This means that the goal is to enable the person to express and describe their life experiences in sequence. Yob (2003) states that metaphor is used to understand and discover something specific, concrete, new, or highly fictional.

Metaphors are extraordinary tools that provide rich descriptions and meanings reflecting individuals' cultures and contexts; therefore, they are used for various purposes in education by illuminating cultural, institutional, and personal structures (Wallace, 2001). Metaphors, as a way of examining prospective teachers' thoughts, enable the identification of conceptual tendencies and their ability to use them logically in their work and lives. Perhaps this is the most powerful tendency of metaphors. In pursuit of these goals, metaphors are preferred in research as analogical tools, serving as a semantic tool for the underlying benefits and specific experiences and frameworks of human consciousness (Neisser, 2003). In addition, metaphors help people understand nature and the environment by conveying meaning from seemingly meaningless experiences and deriving meaning from their interpretations of objective realities. Therefore, metaphors enable people to understand nature and the environment. For example, scientists often use metaphors when developing theoretical frameworks and analytical tools for perceiving the world (Morgan, 1998; Yıldırım and Şimşek, 2021). Therefore, the primary function of metaphor is to stimulate active learning thought processes and to achieve the desired outcome in the fundamental learning process through these effects (Carroll and Mack, 1999).

The aim of this research is to reveal prospective teachers' metaphorical perceptions of the concept of "water pollution" using qualitative research techniques, given the increasing water pollution in today's world.

MATERIAL AND METHODS

a) Research Model

This research employed a qualitative research method. Qualitative research is a method that utilizes techniques such as interviews, document analysis, and observation, presenting events as a whole and in their natural context, thereby facilitating a qualitative process (Yıldırım and Şimşek, 2021). The study utilized phenomenology, a qualitative research approach (Gümüş

and Akhan, 2024). The phenomenological design focuses on phenomena that we notice but do not examine in depth. Phenomena can manifest in our lives in various forms, such as perception, experience, concepts, events, orientations, and situations. We may encounter these phenomena in different ways in our daily lives, but this familiarity does not mean we fully understand them. For studies where we want to investigate phenomena that are not entirely unfamiliar to us but that we do not fully comprehend, phenomenology constitutes a suitable research design (Yıldırım and Şimşek, 2021). In this respect, since the research revealed the perceptions of the participants regarding the concept of "water pollution" and reached common themes, the research was conducted using a "phenomenological" design.

b) Working Group

The study group consists of prospective teachers studying in the 3rd and 4th years at Trakya University (Faculty of Education, Department of Science Education) during the 2025–2026 academic year. Data were collected from prospective teachers on a voluntary basis.

c) Data Collection and Analysis

Metaphors can be considered one of the tools that educators can use in all areas of education to achieve different goals (Arslan and Bayrakçı, 2006; Parks, 2010; Saban, 2008). It is suggested that metaphors be used in research to reveal students' understanding and perceptions in the teaching process (Botha, 2009). It can be described as an effective qualitative data collection tool in the detailed examination of cases or events (Güneş and Fırat, 2016). In research where metaphors function as a data collection tool, the use of expressions such as "like/similar" is expected to create a clear association with the subject and source of the metaphor (Doğan, 2017). The aim is also to identify the rationale behind the comparison using the conjunction "because".

Convenience sampling was used to determine the study group. This type of sampling helps the study to be carried out in a more practical and faster way (Yıldırım and Şimşek, 2021). The sample consists of 41 prospective teachers in total: 19 girls and 3 boys from the 3rd year, and 17 girls and 2 boys from the 4th year.

A semi-structured interview form was used as a data collection tool in this study. In this context, prospective teachers were given blank forms to fill in the statement "Water pollution is like/similar to …….. Because ……." in order to learn about their perceptions of "water pollution" using metaphors. The data they created through metaphors forms the main theme of the study. Teacher candidates participating in the study were asked to complete a sentence by writing the first word that came to their mind regarding the concept of water pollution at the beginning of the sentence, and

its explanation at the end. They were given approximately fifteen minutes to write down their metaphors and justifications.

The data obtained in the research were analyzed using content analysis. Content analysis is considered one of the most important analytical techniques frequently used in social and natural sciences. It is a technique in which objective and systematic inferences are made from certain characteristics of the given message, in accordance with specific rules (Büyüköztürk et al., 2016).

First, each form obtained from prospective teachers was examined. Each of the forms read was numbered. Then, the metaphors and justifications written for each concept were categorized. Metaphors expressing similar meanings have been grouped together. Associations made by prospective teachers through metaphors were analyzed in line with expert opinions.

RESULTS AND DISCUSSION

In this section, first, the metaphors developed by prospective teachers were identified and presented in a table, and then the frequency and percentage values of the metaphors were determined (Table 1).

Table 1. Metaphors Developed by Participants Regarding the Concept of "Water Pollution"

Code	Metaphors	f	%
1	A rusty key	2	5.3
2	A silent enemy	2	5.3
3	The first domino to fall	2	5.3
4	Hidden poison	1	2.4
5	A ruined road	1	2.4
6	A rotten apple	1	2.4
7	An invisible killer	1	2.4
8	A silently progressing collapse	1	2.4
9	A virus spreading through the body	1	2.4
10	Pile of garbage	1	2.4
11	Fire	1	2.4
12	Yeast	1	2.4
13	A dead battery	1	2.4
14	A broken clock	1	2.4
15	Taking a breath away	1	2.4
16	A rainbow with its colors darkened	1	2.4
17	Disease	1	2.4
18	A dagger plunged into the heart of nature	1	2.4
19	A dirty mirror	1	2.4
20	A leaky piggy bank	1	2.4
21	Clogging the veins of nature	1	2.4
22	A foundation beginning to crack	1	2.4
23	Blockage of the lifeblood	1	2.4
24	A tree slowly being poisoned	1	2.4
25	A chain reaction	1	2.4
26	Invisible handcuff	1	2.4
27	An old guitar with frayed strings that won't stay in tune	1	2.4
28	A wimming on the edge of a cliff	1	2.4
29	A spoiled medicine	1	2.4
30	A dirty curtain	1	2.4
31	A light going out	1	2.4
32	A insidious disease	1	2.4
33	A slowly spreading poison	1	2.4
34	Spider web	1	2.4
35	Snowball	1	2.4
36	Echo (reverb)	1	2.4
37	A self-sustaining chaos	1	2.4
38	Inanimate	1	2.4
Total	38	41	100

Table 1 shows that prospective teachers created 38 metaphors related to the concept of "water pollution". The most frequently used metaphors by

prospective teachers were a rusty key, a silent enemy, and the first domino topple, all at 5.3%. Each metaphor is represented by two individuals. The remaining 35 metaphors were developed by one individual each (2.4%).

In this study, conducted to determine prospective teachers' perceptions of the concept of "water pollution," the metaphors created were categorized. When grouping the answers, care was taken to ensure that they consisted of metaphors covering similar topics and subtopics. The metaphors produced by the participants were grouped under 5 different categories. These categories, their frequencies, and percentages are given in Table 2.

Table 2. Distribution of Metaphors Generated by Participants Regarding the Concept of "Water Pollution" According to Categories

Categories	Metaphors	f	%
Regarding the results	A ruined road, pile of garbage, a broken clock, a rainbow with its colors darkened, a dirty mirror, a dirty curtain, a chain reaction, a light going out, an old guitar with frayed strings that won't stay in tune	9	23.7
Regarding the necessity of taking precautions	A rusty key, an invisible killer, a dead battery, a leaky piggy bank, a foundation beginning to crack, a tree slowly being poisoned	6	15.8
Regarding the disruption of the natural balance and destructive natural elements	The first domino to fall, a rotten apple, a silently progressing collapse, fire, taking a breath away, a dagger plunged into the heart of nature, clogging the veins of nature, blockage of the lifeblood	8	21.1
Regarding factors threatening healthy living	A hidden poison, a silent enemy, a virus spreading through the body, disease, invisible handcuff, swimming on the edge of a cliff, a spoiled medicine, a insidious disease, a slowly spreading poison, a self-sustaining chaos	10	26.2
Regarding the living environment or event	Yeast, spider web, snowball, echo, inanimate	5	13.2
Total		38	100

As shown in Table 2, metaphors are grouped under 5 categories. Categories: Regarding the results, regarding the necessity of taking precautions, regarding the disruption of the natural balance and destructive natural elements, regarding factors threatening healthy living, and regarding the living environment or event.

Category 1: Regarding the results

This category contains a total of nine different metaphors (23.7%). Each metaphor is represented by an individual. Metaphors: A ruined road, pile of garbage, a broken clock, a rainbow with its colors darkened, a dirty mirror,

a dirty curtain, a chain reaction, a light going out, an old guitar with frayed strings that won't stay in tune. Here are some of the reasons behind the development of certain metaphors in this category:

"Water pollution is like a pile of garbage. Because as it accumulates, it disrupts the balance of nature and makes habitats uninhabitable."

"Water pollution is like a broken clock. Because once the balance of water is disrupted, the rhythm and timing of all of nature are disrupted."

"Water pollution is like a rainbow with its colors darkened. Because even though it contains all the shades of life, the pollution hides them."

"Water pollution is like a dirty mirror, because it prevents nature from reflecting its true face."

"Water pollution is like an old guitar with frayed strings that won't stay in tune. Because when humans disrupt the balance of nature, the world can no longer play any song in the tone it should."

"Water pollution is like a light going out. Because as clean water diminishes, life begins to darken."

Category 2: Regarding the necessity of taking precautions

There are a total of six different metaphors (15.8%) in this category. Of these metaphors, only the rusty key is represented by two individuals; the others are represented by a single individual. Metaphors: A rusty key, an invisible killer, a dead battery, a leaky piggy bank, a foundation beginning to crack, a tree slowly being poisoned. Here are some of the reasons behind the development of certain metaphors in this category:

"Water pollution is like a rusty key. Because it renders the water that opens the door to life unusable, making it difficult for living beings to access their basic needs."

"Water pollution is like an invisible killer. Because toxic substances that mix with water slowly and imperceptibly threaten living organisms."

"Water pollution is like a dead battery. Because when water is polluted, its energy and life cease; it can no longer power nature or us."

"Water pollution is like a tree that is slowly being poisoned. Because while it may appear majestic and strong from the outside, from within it destroys the water, the essential source of life, and all the living things it contains."

"Water pollution is like a leaky piggy bank. Because it causes the most valuable resource we've been saving for our future to silently disappear."

Category 3: Regarding the disruption of the natural balance and destructive natural elements

There are a total of eight different metaphors in this category (21.1%). Of the metaphors, only the first domino toppled is represented by two individuals; the others are represented by a single individual. Metaphors: The first domino to fall, a rotten apple, a silently progressing collapse, fire, taking a breath away, a dagger plunged into the heart of nature, clogging the veins of nature, blockage of the lifeblood. Here are some of the reasons behind the development of certain metaphors in this category:

"Water pollution is like a rotten apple; it spoils the healthy apples next to it."

"Water pollution is like the first domino to toppled. Because it initiates irreversible destruction that affects not only the water but also the soil, plants, animals, and ultimately human health."

"Water pollution is like a dagger plunged into the heart of nature. Because it wounds the entire ecosystem."

"Water pollution is like clogging the veins of nature. Because if the water is polluted, the flow of life stops."

"Water pollution is like taking a breath away. Because if the water is polluted, nature cannot breathe and life comes to a standstill."

"Water pollution is like a silently progressing collapse. Because its effects are not sudden, but cumulative."

"Water pollution is like fire; if left unchecked, it causes great harm to the environment and living beings."

Category 4: Regarding factors threatening healthy living

There are ten different metaphors in this category (26.2). Only the silent enemy metaphor is represented by two individuals, the others by a single individual. Metaphors: A hidden poison, a silent enemy, a virus spreading through the body, disease, invisible handcuff, swimming on the edge of a cliff, a spoiled medicine, a insidious disease, a slowly spreading poison, a self-sustaining chaos. Here are some of the reasons behind the development of certain metaphors in this category:

"Water pollution is like a virus spreading through the body. Because its effects are felt slowly but deeply."

"Water pollution is like invisible handcuff. Because it takes away the freedom of water and slowly enslaves all the living things that depend on it."

"Water pollution is like an insidious disease. Because it spreads unnoticed and over time negatively affects the lives of all living things."

"Water pollution is like swimming on the edge of a cliff. Because no matter how careful we are, the moment we lose control, it's the end for us."

"Water pollution is like a self-reinforcing chaos. Because the decomposition of organisms that die due to pollution consumes the dissolved oxygen in the water; this triggers anaerobic respiration, leading to the release of toxic gases and the formation of a "dead zone" where life becomes even more impossible."

Category 5: Regarding the living environment or event

There are a total of five different metaphors in this category (13.2%). All metaphors are represented by a single individual. The metaphors are: Yeast, spider web, snowball, echo, inanimate. Here are some of the reasons behind the development of certain metaphors in this category:

"Water pollution is like a snowball; it grows bigger as it rolls, making it harder to control."

"Water pollution is like an echo. Because its consequences always come back to us."

"Water pollution is like yeast. Just as a small amount is enough to leaven bread, even the smallest drop of contaminated water can pollute the entire body of water."

CONCLUSION

Water pollution poses a serious threat to both the natural environment and human health. Increased water pollution, caused by factors such as industrial activities, agricultural practices, and improper waste management, necessitates urgent action. Protecting water resources is vital for a sustainable future (URL 3). Furthermore, educational programs should be organized in schools, universities, and community centers to raise awareness about water pollution. Campaigns conducted through television, the internet, and social media will be effective in preventing water pollution and raising environmental awareness (URL 1).

Ensuring the sustainability of water and water resources is crucial for life, as water resources are used in a wide variety of areas (drinking, irrigation, industry). Therefore, the utilization of this resource must be sustainable in the future, just as it has been in the past and is today. However, today the rate at which water and resources can regenerate has been exceeded, and resources are rapidly becoming polluted and losing their sustainability. With the ever-increasing population, the demand for water and resources has also increased. In line with this increased demand and pollution, the quality and quantity of water and resources have decreased (Göksu and Ziya, 2015). In addition to anthropogenic influences, natural processes (changes in precipitation inputs, erosion, weathering of crustal material) also degrade surface water quality,

and industrial, agricultural, recreational, or other purposes negatively impact drinking water. The progression of this situation is also leading to undesirable levels of water pollution.

International cooperation is also important in combating water pollution. Many countries have signed various agreements and protocols to combat water pollution. In addition, technologies and innovative solutions are being developed to conserve water resources, thereby aiming for more efficient water use (URL 3).

In this study, 41 prospective teachers developed 38 different metaphors. When the metaphors produced by the prospective teachers were examined, a rusty key, a silent enemy, and the first domino falling, along with two individuals, were the most frequently used metaphors. The other 35 metaphors were used by only one individual. This shows that prospective teachers define water pollution as part of their daily life experiences and/or as an integral part of their professional knowledge, synthesized from those experiences. These metaphors were then categorized according to their similarities and grouped into 5 categories. Table 2 shows that the strongest category in terms of frequency and intensity is "Regarding factors threatening healthy living".

When examining studies on water pollution, it is observed that they address topics such as water pollution in ecosystems, environmental pollution and poverty, global water management, environmental education and water education, water quality, water problems and strategies, water security, water pollution and society, conscious water consumption, water pollution and viruses, science education and environmental problems, environmental literacy, water literacy, and water footprint. However, only two articles were found that dealt with the subject of water pollution and had a direct metaphorical perception relationship (Köseoğlu, 2017). The metaphor study was redone with the aim of contributing to this field through additional solutions such as providing diversity, expanding the sample size, using alternative methods, and maintaining the relevance of the study.

In her study, Köseoğlu (2017) aimed to determine university students' perceptions of the concepts of "water" and "water pollution" through metaphors. The study group consisted of 258 undergraduate students studying at Hacettepe and Gazi Universities during the 2015-2016 academic year. Participants were given a semi-structured questionnaire that included the statement, "Water/water pollution is similar to this because...". The study's findings showed that students perceived water as a necessity and an indispensable part of life, while they perceived water pollution as the end of life. Metaphors developed regarding the concept of water pollution have been divided into three conceptual categories: "consequences", "disruption of the

natural balance", and "the need for action". Many of the metaphors developed differ from those presented in this study.

In their study, Yılmaz and Yanarateş (2020) aimed to determine metaphorical perceptions of water pollution through data triangulation. The research was conducted with the participation of prospective teachers from 11 different departments studying at a state university. The study employed four different qualitative and quantitative research methods: Metaphor studies (phenomenology), semi-structured individual and focus group interviews, meta-thematic analysis, and survey (scale application). The study shows that prospective teachers produced 135 different metaphors. Among these, addiction (5), ignorance (5), garbage (5), rotten fruit (5), rotten lungs (12), the end of the world (29), thought pollution (6), past mistakes (8), sick body (6), human life (18), heartbreak (4), cancer (35), dark pit (6), apocalypse (8), dirty objects (19), coronavirus (12), bad habits (13), oil poured down the sink (10), germs (6), breathlessness (6), death (28), dead battery clock (9), war (18), cigarette (18), the beginning of the end (11), carotid artery (10), incurable disease (9), unproductive field (20), virus (22), old age (6), harmful bacteria (7) and poison ivy (6) are the most frequently used metaphors. When the metaphors produced by the departments were examined, the most different metaphors were produced in the social studies (51), pedagogical formation group (50), classroom and science (45), Turkish (36), mathematics (34), art and crafts (31), preschool (26), psychological counseling and guidance (19), music (13) and computer and instructional technologies (12) teaching departments, respectively. Metaphors produced regarding water pollution are grouped under 9 different categories. When compared with this study, it is seen that very few of the metaphors are similar.

This research reveals how university students, who will play important roles in society in the future, perceive the concept of water pollution. It is believed that the metaphors that emerge in this context will be important research tools in future studies on the perception of water pollution issues.

REFERENCES

Akın, G. (2009). *Ekoloji-Çevrebilim ve Çevre Sorunları*. Ankara: Tiydem Yayıncılık.

Akın, M., and Akın, G. (2007). Suyun önemi, Türkiye'de su potansiyeli, su havzaları ve su kirliliği. *Ankara Üniversitesi Dil ve Tarih-Coğrafya Fakültesi Dergisi*, *47*(2), 105-118.

Aksungur, N., and Firidin, Ş. (2008). Su kaynaklarının kullanımı ve sürdürülebilirlik. *Sumae Yunus Araştırma Bülteni*, *8*(2), 9-11.

Arslan, M. M., and Bayrakçı, M. (2006). Metaforik düşünme ve öğrenme yaklaşımının eğitim- öğretim açısından incelenmesi. *Millî eğitim, 171*, 100-108.

Atalık, A. (2006). Küresel ısınmanın su kaynakları ve tarım üzerine etkileri. *Bilim ve Ütopya*, *139*, 18-21.

Botha, E. (2009). Why metaphor matters in education. *South African of Education, 29*, 431-444.

Büyüköztürk, Ş., Kılıç Çakmak, E., Akgün, Ö. E., Karadeniz, Ş., and Demirel, F. (2016). *Bilimsel Araştırma Yöntemleri.* (20. Baskı). Ankara: Pegem Akademi Yayıncılık.

Cameron, L., and Low, G. (1999). Metaphor. *Language Teaching*, *33*, 77-96.

Carroll, J. M., and Mack, R. L. (1999). Metaphor, computing systems, and active learning. *International Journal of Human-Computer Studies*, *51*(2), 385-403.

Çolakoğlu, E. (2009). Ortak bir değer olarak su ve su etiği. *ZKÜ Sosyal Bilimler Dergisi, 5*(9), 109–116.

Dağlı, H. (2005). İçme suyu kalitesi ve insan sağlığına etkileri. Bizim İller. *İller Bankası Aylık Yayın Organı, 3*, 16-21.

Doğan, Y. (2017). Ortaokul öğrencilerinin çevre kavramına ilişkin sezgisel algıları: Bir metafor analizi. *Ahi Evran Üniversitesi Kırşehir Eğitim Fakültesi Dergisi, 18*(1), 721-740.

Göksu, M., and Ziya, L. (2015). *Su Kirliliği*. Ankara: Akademisyen Kitapevi.

Gümrükçüoğlu, M., Baştürk, O., and Yüksek, M. (2008). *Sürdürülebilir Su Yönetiminde Nehir Kirliliği Üzerine Bir Çalışma*. TMMOB 2. Su Politikaları Kongresi. Ankara. 20-22 Mart 2008. 521-529.

Gümüş, H. E., and Akhan, N. E. (2024). Sosyal bilgiler ve fen bilgisi öğretmen adaylarının sürdürülebilirlik, kalkınma ve sürdürülebilir kalkınma kavramlarına yönelik metaforik algılarının karşılaştırılması. *International Primary Educational Research Journal, 8*(3), 359-373. doi: 10.38089/iperj.2024.190

Güneş, A., and Fırat, M. (2016). Açık ve uzaktan öğrenmede metafor analizi araştırmaları. *Açıköğretim Uygulamaları ve Araştırmaları Dergisi, 2*(3), 115-129.

Gürlen, E., and Köseoğlu, P. (2019). Üniversite öğrencilerinin "toprak ve toprak kirliliği" kavramlarına ilişkin algılarının metafor ile analizi. *Bolu Abant İzzet Baysal Üniversitesi Eğitim Fakültesi Dergisi, 19*(1), 243-256.

Haviland, W. A. (2002). *Kültürel Antropoloji* (Çev: Hüsamettin İnaç, Seda Çiftçi). No: 143. Sosyoloji Serisi: 3. İstanbul: Kaktüs Yayınları.

Ibadullayeva, J., Jumaniyazova, K., Azimzadeh, S., Canıgür, S., and Esen, F. (2019). Çevre kirliliğinin insan sağlığı üzerindeki etkileri. *Türk Tıp Öğrencileri Araştırma Dergisi*, *1*(3), 52-58.

Karatekin, K., and Yılmaz, A. (2019). *Çevre Okuryazarlığı.* Ankara: Pegem Akademi Yayıncılık.

Kaypak, Ş. (2011). Küreselleşme sürecinde sürdürülebilir bir kalkınma için sürdürülebilir bir çevre. *KMÜ Sosyal ve Ekonomik Araştırmalar Dergisi, 13*(20), 19-33.

Köseoğlu, P. (2017). An analysis of university students' perceptions of the concepts of "water" and "water pollution" through metaphors. *EURASIA Journal of Mathematics Science and Technology Education, 3*(8), 4343-4350. doi: 10.12973/eurasia.2017.00930a.

Küçük, M., and Güneş, G. (2013). Sivil toplum kuruluşları ve çevresel sürdürülebilirlik. *Sosyal ve Beşeri Bilimler Dergisi, 5*(2), 298-311.

Levine, P. M. (2005). Metaphors and images of classrooms. *Kappa Delta Pi Record, 41*(4), 172-175. https://doi.org/10.1080/00228958.2005.10532066

Massengill Shaw, D., and Mahlios, M. (2008). Pre-service teachers' metaphors of teaching and literacy. *Reading Psychology*, *29*(1), 31-60.

Morgan, G. (1998). *Yönetim ve Örgüt Teorilerinde Metafor*. İstanbul: BZD Yayıncılık.

North American Association for Environmental Education (NAAEE). (2011). *Developing a Framework for Assessing Environmental Literacy*. North American Association for Environmental Education, Washington, D.C., USA.

Neisser, J. U. (2003). The swaying form: Imagination, metaphor, embodiment. *Phenomenology and the Cognitive Sciences, 2*, 27-53.

Park, C. L. (2010). Making sense of the meaning literature: An integrative review of meaning making and its effects on adjustment to stressful life events. *Psychological Bulletin, 136,* 257-301. http://dx.doi.org/10.1037/a0018301

Roth, C. E. (2002) *A Questioning Framework for Shaping Environmental Literacy* (US, Earthlore associates & The Center for Environmental Education of Antioch New England Institute).

Saban, A. (2008). Okula ilişkin metaforlar. *Kuram ve Uygulamada Eğitim Yönetimi Dergisi, 14*(55), 459-496.

URL 1. Su Kirliliği Nedir? Su Kirliliği Nedenleri ve Sonuçları (Güncelleme tarihi: 8 Kasım 2025)

URL 2. Çevreni Koru. Su Kirliliği Nedir? Nedenleri ve Nasıl Önlenir?

URL 3. Su.gen.tr. Su Kirliliğinin Zararları ve Çevresel Etkileri.

Uysal, H., and Yılmaz, A. (2019). Prospective teachers' views on beauty criteria. *International Journal of Educational Methodology, 5*(3), 337-346.

Uzun, A., Keleş, R., and Bal, İ. (2014). Sapanca Gölü içme suyu havzasında otoyol ve demiryolundan kaynaklanan kirliliğin yağmur suyu sulak alan metoduyla giderilmesi. *APJES, II*(I), 09-15.

Wallace, S. (2001). Guardian angels and teachers from hell: Using metaphor as a measure of schools' experiences and expectations of general national vocational qualifications. *International Journal of Qualitative Studies in Education*, *14*(6), 727-739.

Yıldırım, A., and Şimşek, H. (2021). *Sosyal Bilimlerde Nitel Araştırma Yöntemleri* (12. Baskı), Ankara: Seçkin Yayıncılık.

Yılmaz, A., and Bayrakçeken, S. (2017). Öğretmen adaylarının elektrokimya konusundaki kavram yanılgılarının belirlenmesi. *Bayburt Eğitim Fakültesi Dergisi, 12*(24), 881-906.

Yılmaz, A., and Yanarateş, E. (2020). Öğretmen adaylarının "su kirliliği" kavramına yönelik metaforik algılarının veri çeşitlemesi yoluyla belirlenmesi. *Kastamonu Education Journal*, 28(3), 1500-1528, doi: 10.24106/kefdergi.722554

Yob, I. M. (2003). Thinking constructively with metaphors. *Studies in Philosophy and Education, 22*, 127–138.

Zamani, A. A., Yaftian, M. R., and Parizanganeh, A. (2012). Multivariate statistical assessment of heavy metal pollution sources of groundwater around a lead and zinc plant. *Iranian Journal of Environmental Health Sciences & Engineering*, *9*(29), 1-10.

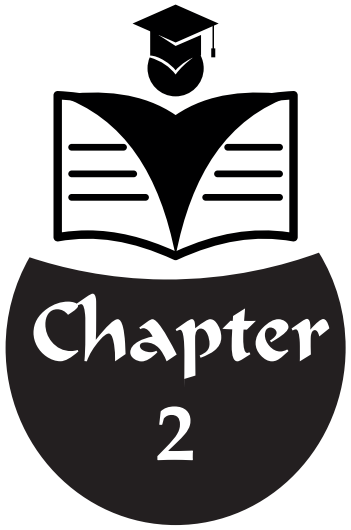

SOME ALGEBRAIC AND SMOOTHNESS PROPERTIES OF q-NUMERICAL RADIUS AND q-CRAWFORD NUMBER FUNCTIONS

Rukiye Öztürk Mert[1]

1 Asst. Prof. Dr., Hitit University, Faculty of Engineering and Natural Sciences, Department of Mathematics, Çorum, Türkiye, rukiyeozturkmert@hitit.edu.tr, ORCID: 0000-0001-8083-5304

1. Introduction

The establishment of the norm as $\|\cdot\|$ is done by the inner product $(\cdot,\cdot)$ in a complex Hilbert space $\mathfrak{H}$. The collection of all bounded linear operators that act on $\mathfrak{H}$ is denoted by the Banach algebra $B(\mathfrak{H})$. This is how the operator norm is explained:

$$\|\mathfrak{B}\| = \sup_{\|x\|=1} \{\|\mathfrak{B}x\|: \ x \in \mathfrak{H}\}, \mathfrak{B} \in B(\mathfrak{H}).$$

The numerical range $W(\mathfrak{B})$ is the image of $\mathfrak{H}$ under the quadratic form $x \to (\mathfrak{B}x, x)$ connected $\mathfrak{B} \in B(\mathfrak{H})$. Explicitly,

$$W(\mathfrak{B}) = \{(\mathfrak{B}x, x): \ x \in \mathfrak{H}, \ \ \|x\| = 1\}$$

is the numerical range for a $\mathfrak{B}$ on $\mathfrak{H}$.

The well-established fact is that the spectrum for an operator is within the numerical range's closure. Furthermore, according to the Toeplitz-Hausdorf Theorem, the numerical range is always convex. The operator $\mathfrak{B}$ is self-adjoint iff the set $W(\mathfrak{B})$ is contained within the set $\mathbb{R}$. The numerical radius of $\mathfrak{B}$ is $w(\mathfrak{B})$, where $w(\mathfrak{B})$ is the supremum of $\{|\gamma|: \ \gamma \in W(\mathfrak{B})\}$.

It is known that

$$\frac{\|\mathfrak{B}\|}{2} \leq w(\mathfrak{B}) \leq \|\mathfrak{B}\|$$

(see [1]).

For a more in-depth analysis of the features of the numerical range and radius, refer to [1-3].

$\mathfrak{B}$ is a bounded linear operator and $q \in \mathbb{C}$, $0 < |q| \leq 1$. The definitions for the q-numerical range $W_q(\mathfrak{B})$ and the q-numerical radius $w_q(\mathfrak{B})$ of $\mathfrak{B}$, respectively, are given as follows:

$$W_q(\mathfrak{B}) = \{(\mathfrak{B}x, y): \ x, y \in \mathfrak{H}, \ \ \|x\| = \|y\| = 1, \ \ (x, y) = q\},$$

$$w_q(\mathfrak{B}) = \sup_{z \in W_q(\mathfrak{B})} |z| \, .$$

Note that when $q = 1$, the traditional numerical range $W(\mathfrak{B})$ and numerical radius $w(\mathfrak{B})$ are arrived at by these definitions. The idea of the q-numerical range was first put forward by [4] in 1977 for linear transformations on n-dimensional unitary space. [5] later proved the convexity for the q-numerical range. Further details were explored by [6] and [7]. The numerical range for square matrices was characterized by [8]. Additionally, q-numerical ranges of shift operators have been examined in depth in [8-10]. [11] highlighted the significance of the q-numerical range in describing the property for quantum operations, and [12] investigated various bounds for the q-numerical radius.

An extensive analysis regarding the continuity of the p-numerical radius and Davis-Wielandt-related functions can be found throughout the literature [13-17].

In [18-20], the authors investigated how the aforementioned issues converge, along with the investigation of spectral features found in converging operator sequences.

Estimates concerning a comparison of the operator norms of analytic functions and the numerical radius were obtained in [21], with further refinements provided in [22] using power differences of associated operators.

The spectral characteristics and gaps of direct sums of operators were explored in [23-25]. Operators linked to gap relations were outlined in [26] in comparison with operator norms with the spectral and numerical radii of tensors. Relationships between operator norms and spectral radii for various block operator matrices including anti-diagonal, upper triangular, and nxn block matrices have been investigated in [27-29].

Furthermore, [30] examined the key features of weighted numerical radius.

In [31], estimates were provided for the numerical radii of Hardy-type operators.

Finally, [32] derived evaluation formulas for the joint δ-numerical radius and for the function of the Crawford number, presenting significant estimates within the context of sectorial coordinate operators.

This study has been investigated the algebraic and smoothness properties for q-numerical radius and q-Crawford number functions. The research has been established fundamental inequalities for these functions and proves that the uniform convergence of operator-function sequences ensures the convergence of their respective q-numerical radii and q-Crawford numbers. Furthermore, the paper has been demonstrated that these functions inherit key regularity traits from their associated operator-functions, such as Holder continuity and uniform absolute continuity, which implies that they are differentiable almost everywhere. These findings provide new insights into the spectral characteristics of operators.

2. Main Section

Proposition 2.1. For any two operator functions $\mathcal{A}, \mathcal{B}: [0,1] \to B(\mathfrak{H})$ and q is a complex number with $0 < |q| \leq 1$, the subsequent statements are accurate:

i. $w_t^q(\mathcal{A} + \mathcal{B}) \leq w_t^q(\mathcal{A}) + w_t^q(\mathcal{B})$;
ii. $c_t^q(\mathcal{A} + \mathcal{B}) \leq c_t^q(\mathcal{A}) + c_t^q(\mathcal{B})$

where $0 \leq t \leq 1$.

Theorem 2.2. The following is true for any operator-functions $\mathcal{A}, \mathcal{B}: [0,1] \to B(\mathfrak{H})$ and $q \in \mathbb{C}$, $0 < |q| \leq 1$:

i. $\left|w_t^q(\mathcal{A}) - w_t^q(\mathcal{B})\right| \leq w_t^q(\mathcal{A} - \mathcal{B})$, $0 \leq t \leq 1$;
ii. $\left|c_t^q(\mathcal{A}) - c_t^q(\mathcal{B})\right| \leq c_t^q(\mathcal{A} - \mathcal{B})$, $0 \leq t \leq 1$.

Proof.

i. The Proposition 2.1 property (i) is the basis of the conclusion that $w_t^q(\mathcal{A}) \leq w_t^q(\mathcal{A} - \mathcal{B}) + w_t^q(\mathcal{B})$

and

$$w_t^q(\mathcal{B}) \le w_t^q(\mathcal{A}-\mathcal{B}) + w_t^q(\mathcal{A}), 0 \le t \le 1.$$

Then from last inequalities it is obtained that

$$\left|w_t^q(\mathcal{A}) - w_t^q(\mathcal{B})\right| \le w_t^q(\mathcal{A}-\mathcal{B}), 0 \le t \le 1.$$

ii. Similarly, from the property (ii) of Proposition 2.1 we have
$c_t^q(\mathcal{A}) \le c_t^q(\mathcal{A}-\mathcal{B}) + c_t^q(\mathcal{B})$

and

$c_t^q(\mathcal{B}) \le c_t^q(\mathcal{A}-\mathcal{B}) + c_t^q(\mathcal{A}), 0 \le t \le 1.$

Then from above inequalities it follows that

$$\left|c_t^q(\mathcal{A}) - c_t^q(\mathcal{B})\right| \le c_t^q(\mathcal{A}-\mathcal{B}), 0 \le t \le 1.$$

Now give one definition.

Definition 2.3 [33]. A sequence of operators $(\mathcal{T}_n) \subset B(\mathfrak{H})$ is said to uniformly converge to the operator $\mathcal{T} \subset B(\mathfrak{H})$, if for any $\varepsilon > 0$, there exists a positive integer number n_ε such that for all integer $n > n_\varepsilon$ is hold

$$\|\mathcal{T}_n - \mathcal{T}\| < \varepsilon.$$

Now it will be investigated convergence properties of $w_t^q(\cdot)$ and $c_t^q(\cdot)$ via uniformly convergence of operator-functions.

Theorem 2.4. If the operator-function sequences $(\mathcal{A}_n(t))$ in $B(\mathfrak{H})$ uniformly converges to the operator-function $(\mathcal{A}(t)) \in B(\mathfrak{H})$, $0 \le t \le 1$, then

$$w_t^q(\mathcal{A}) = \lim_{n\to\infty} w_t^q(\mathcal{A}_n)$$

and

$$c_t^q(\mathcal{A}) = \lim_{n\to\infty} c_t^q(\mathcal{A}_n), 0 \le t \le 1.$$

Proof. From Theorem 2.2 we have

$$\left|w_t^q(\mathcal{A}_n) - w_t^q(\mathcal{A})\right| \le w_t^q(\mathcal{A}_n - \mathcal{A}) \le \|\mathcal{A}_n(t) - \mathcal{A}(t)\|, n \ge 1$$

and

$$\left|c_t^q(\mathcal{A}_n) - c_t^q(\mathcal{A})\right| \leq w_t^q(\mathcal{A}_n - \mathcal{A}) \leq \|\mathcal{A}_n(t) - \mathcal{A}(t)\|, n \geq 1$$

for every $0 \leq t \leq 1$.

From these evaluations the validity of theorem it is clear.

Theorem 2.5. Assume that there exists positive constant K and $\alpha \in (0,1]$, such that for every $t, s \in [0,1]$ is satisfied the condition

$$\|\mathcal{A}(t) - \mathcal{A}(s)\| \leq K|t-s|^{\alpha}.$$

In this case are true

$$\left|w_t^q(\mathcal{A}) - w_s^q(\mathcal{A})\right| \leq K|t-s|^{\alpha}$$

and

$$\left|c_t^q(\mathcal{A}) - c_s^q(\mathcal{A})\right| \leq K|t-s|^{\alpha}.$$

Proof. Indeed, for any $t, s \in [0,1]$ we have

$$\begin{aligned} w_t^q(\mathcal{A}) &= \sup_{x,y\in S_1(\mathfrak{H})} |(\mathcal{A}(t)x, y)| \\ &\leq \sup_{x,y\in S_1(\mathfrak{H})} |(\mathcal{A}(s)x, y)| + \|\mathcal{A}(t) - \mathcal{A}(s)\| \\ &\leq w_s^q(\mathcal{A}) + \|\mathcal{A}(t) - \mathcal{A}(s)\| \\ &\leq w_s^q(\mathcal{A}) + K|t-s|^{\alpha} \end{aligned}$$

and similarly,

$$w_s^q(\mathcal{A}) \leq w_t^q(\mathcal{A}) + K|t-s|^{\alpha}.$$

So, it is obtained that

$$\left|w_t^q(\mathcal{A}) - w_s^q(\mathcal{A})\right| \leq K|t-s|^{\alpha}.$$

By the similar technique it is clear that

$$c_t^q(\mathcal{A}) \leq c_s^q(\mathcal{A}) + K|t-s|^{\alpha}$$

and

$$c_s^q(\mathcal{A}) \le c_t^q(\mathcal{A}) + K|t-s|^\alpha$$

for every $t, s \in [0,1]$. Therefore, we have

$$\left|c_t^q(\mathcal{A}) - c_s^q(\mathcal{A})\right| \le K|t-s|^\alpha, t, s \in [0,1].$$

Corollary 2.6. For fixed operator-function $\mathcal{A}(\cdot)$ satisfying condition in Theorem 2.5 the functions $w_t^q(\mathcal{A}), c_t^q(\mathcal{A}) : [0,1] \to \mathbb{R}$ belongs to the class of Holder functions H_α with degree α.

Now give one definition.

Definition 2.7 [34]. An operator-function $\mathcal{A}(\cdot)$: $[0,1] \to B(\mathfrak{H})$ is termed uniformly absolutely continuous in $[0,1]$, if given $\varepsilon > 0$ there exists a $\delta > 0$ such that

$$\sum_{k=1}^n \|\mathcal{A}(t_k) - \mathcal{A}(s_k)\| < \varepsilon$$

for every finite family of non-overlapping open intervals

$$\{(s_k, t_k): (s_k, t_k) \subset [0,1],\ k = 1,2,\dots,n\}$$

with $\sum_{k=1}^n (t_k - s_k) < \delta$.

In this case it will be denoted $\mathcal{A} \in AC[0,1]$.

Theorem 2.8. If operator-function $\mathcal{A} \in AC[0,1]$, then real-valued functions $w_t^q(\mathcal{A}), c_t^q(\mathcal{A}) \in AC[0,1]$.

Proof. In this case for any finite family of non-overlapping open intervals $(s_k, t_k) \subset [0,1],\ k = 1,2,\dots,n$. We have

$$\sum_{k=1}^n \left|w_{t_k}^q(\mathcal{A}) - w_{s_k}^q(\mathcal{A})\right|$$

$$= \sum_{k=1}^n \left| \sup_{\substack{x,y \in S_1(\mathfrak{H}) \\ (x,y)=q}} |(\mathcal{A}(t_k)x, y)| - \sup_{\substack{x,y \in S_1(\mathfrak{H}) \\ (x,y)=q}} |(\mathcal{A}(s_k)x, y)| \right|$$

$$\leq \sum_{k=1}^{n} \sup_{\substack{x,y\in S_1(\mathfrak{H}) \\ (x,y)=q}} |((\mathcal{A}(t_k)-\mathcal{A}(s_k))x,y)|$$

$$\leq \sum_{k=1}^{n} \|\mathcal{A}(t_k)-\mathcal{A}(s_k)\|$$

And similarly

$$\sum_{k=1}^{n} \left| c_{t_k}^{q}(\mathcal{A}) - c_{s_k}^{q}(\mathcal{A}) \right|$$

$$= \sum_{k=1}^{n} \left| \inf_{\substack{x,y\in S_1(\mathfrak{H}) \\ (x,y)=q}} |(\mathcal{A}(t_k)x,y)| - \inf_{\substack{x,y\in S_1(\mathfrak{H}) \\ (x,y)=q}} |(\mathcal{A}(s_k)x,y)| \right|$$

$$\leq \sum_{k=1}^{n} \sup_{\substack{x,y\in S_1(\mathfrak{H}) \\ (x,y)=q}} |((\mathcal{A}(t_k)-\mathcal{A}(s_k))x,y)|$$

$$\leq \sum_{k=1}^{n} \|\mathcal{A}(t_k)-\mathcal{A}(s_k)\|$$

From these evaluations and definition of uniformly absolutely continuous it is established the statement of theorem.

Corollary 2.9. Under the conditions of last theorem, the functions $w_t^q(\mathcal{A}), c_t^q(\mathcal{A}) : [0,1] \to \mathbb{R}$ is differentiable almost everywhere belonging to Lebesque space $L^1(0,1)$.

Theorem 2.10. If the operator-function $\mathcal{A}(\cdot)$: $[0,1] \to B(\mathfrak{H})$ is uniformly absolutely continuous, then

$$\sup_{\substack{x,y\in S_1(\mathfrak{H}) \\ (x,y)=q}} \int_0^1 |(\mathcal{A}(t)x,y)|dt \leq \int_0^1 \sup_{\substack{x,y\in S_1(\mathfrak{H}) \\ (x,y)=q}} |(\mathcal{A}(t)x,y)|dt$$

and

$$\int_0^1 \inf_{\substack{x,y\in S_1(\mathfrak{H}) \\ (x,y)=q}} |(\mathcal{A}(t)x,y)|dt \leq \inf_{\substack{x,y\in S_1(\mathfrak{H}) \\ (x,y)=q}} \int_0^1 |(\mathcal{A}(t)x,y)|dt\,.$$

In this case it is sufficient to noted that the functions

$$(\mathcal{A}(t)x,y), x,y \in \mathfrak{H}, (x,y)=q, w_t^q(\mathcal{A}) \text{ and } c_t^q(\mathcal{A}), 0 \leq t \leq 1$$

are continuous in $[0,1]$.

References

1. Gustafson K. E., and Rao, D. K. M. (1997). Numerical Range: The Field of Values of Linear Operators and Matrices. New York: Springer.
2. Halmos, P. R. (1982). A Hilbert Space Problem Book. New York: Springer – Verlag.
3. Bhunia, P., Dragomir, S. S., Moslehian, M. S., & Paul, K. (2022). Lectures on Numerical Radius Inequalities. Infosys Science Foundation Series. New York: Springer.
4. Marcus, M., and Andersen, P. (1977). Constrained Extrema of Bilinear Functionals. Monatsh Math., 84(3), 219-235.
5. Tsing, N.K. (1984). The Constrained Bilinear Form and The c-Numerical Range. Linear Algebra Appl., 56, 195-206.
6. Li, C.-K., Mehta, P.P., and Rodman, L. (1994). A Generalized Numerical Range: the Range of a Constrained Sesquilinear Form. Linear Multilinear Algebra, 37(1-3), 25-49.
7. Li, C.-K., and Nakazato, H. (1998). Some Results on The q-Numerical. Linear Multilinear Algebra, 43(4), 385-409.
8. Chien, M.-T. and Nakazato, H. (2002). Davis-Wieland Shell and q-Numerical Range. Linear Algebra Appl., 340(1-3), 15-31.
9. Chien, M.-T. (2012). The Numerical Radius of a Weighted Shift Operator. RIMS Kokyuroku, 1778, 70-77.
10. Chien, M.-T, and Nakazato, H. (2007). The q-Numerical Radius of Weighted Shift Operators with Periodic Weights. Linear Algebra Appl., 422, 198-218.
11. Duan, R., Feng, Y., and Ying, M. (2009). Perfect Distinguishability of Quantum Operations. Phys Rew Lett., 103(21), 4pp.
12. Moghaddam, S.F., Mirmostafaee, A.K., and Janfada, M. (2024). q-Numerical Radius Inequalities for Hilbert Space. Linear Multilinear Algebra, 72(5), 751-763.
13. Cağlayan Ü., and Ismailov Z.I. (2024). On The Continuity Properties of Davis-Wielandt Radius and Crawford Number Functions. E. Otkun Çevik içinde, Matematik Alanında Analizler (s. 16-24), Afyonkarahisar: Yaz Yayınları.
14. Otkun Çevik E., and Ismailov Z.I. (2024). On The Continuity of Ratio Numerical Radius and Ratio Crawford Number Functions. E. Otkun Çevik

içinde, Matematik Alanında Analizler (s. 25-34), Afyonkarahisar: Yaz Yayınları.

15. Ismailov Z.I., and Ipek Al, P. (2024). On the Continuity Property of Berezin Number Function. International Research in the Field of Mathematics-I (s. 29-34), Konya: Eğitim Yayınevi.

16. Cağlayan Ü., and Ipek Al, P. (2024). On the Continuity with Respect to Denominator of Ratio Numerical Radius and Ratio Crawford Number Functions. International Academic Studies in Sciences and Mathematics, June 2024 (s. 121-132), Ankara: Serüven Yayınevi.

17. Ipek Al, P., and Cağlayan Ü. (2024). The Monotonicity and Uniformly Continuity Properties of p-Numerical Radius Function. Fen Bilimleri ve Matematik Alanında Yeni Yaklaşımlar, Haziran 2024 (s. 132-142), Ankara: Platanus Publlishing.

18. Cağlayan Ü., and Ismailov Z.I. (2024). On The Convergence Properties Of p-Numerical Radii And p-Crawford Numbers Sequences. O. Talaz, A. Demirçalı. içinde, Current Studies in Science and Mathematics (s. 5-18), Ankara: Platanus Publishing.

19. Ipek Al, P., and Ismailov Z.I. (2024). On the Convergence Properties of (p,q)-Numerical Radii and (p,q)-Crawford Numbers Sequences. International Research in the Field of Mathematics-I (s. 67-77), Konya: Eğitim Yayınevi.

20. Bhunia, P., Ipek Al, P., and Ismailov, Z. I. (2024). On the Convergence of Some Spectral Characteristics of the Converging Operator Sequences. Proceedings-Mathematical Sciences, 134(1), 1-15.

21. Ipek Al, P., Öztürk Mert, R., and Ismailov, Z. I. (2024). Operator Norm-Numerical Radius Gaps for Analytic Function of Hilbert Space Operators. Konuralp Journal of Mathematics, 12(1), 80-85.

22. Ismailov Z. I., and Otkun Çevik E. (2022). On the one Spectral Relation for Analytic Function of Operator. Journal of Nonlinear Science and Applications, 15, 301-307.

23. Ismailov, Z., and Öztürk Mert, R. (2022). Gaps Between Some Spectral Characteristics of Direct sum of Hilbert Space Operators. Operators and Matrices, 16(2), 337-347.

24. Otkun Çevik, E., and Ismailov, Z. I. (2022). Some Gap Relations Between Operator Norm with Spectral and Numerical Radii of Direct Sum Hilbert Space Operators. Lobachevskii Journal of Mathematics, 43(2), 366-375.

25. Ismailov, Z. I., and Ipek Al, P. (2022). Some Spectral Characteristic Numbers of Direct Sum of Operators. Turkish Journal of Analysis and Number Theory, 10(1), 21-26.

26. Ismailov, Z. I., and Ipek Al, P. (2021). Gaps Between Operator Norm and Spectral and Numerical Radii of the Tensor Product of Operators. Turkish Journal of Analysis and Number Theory, 9(2), 22-24.

27. Ipek Al, P., and Ismailov, Z. I. (2021). On the Spectral Radius of Antidiagonal Block Operator Matrices. Journal of Mathematical Chemistry, 59(10), 2206-2217.

28. Otkun Çevik, E., and Ismailov, Z. I. (2021). Spectral Radius and Operator Norm of Infinite Upper Triangular Double Band Block Operator Matrices. Journal of Analysis & Number Theory, 9(2), 19-22.

29. Otkun Çevik, E., and Ismailov, Z. I. (2021). Spectral Radius and Operator Norm of nxn Triangular Block Operator Matrices. Journal of Analysis & Number Theory, 9(1), 7-12.

30. Ismailov, Z. I., and Ipek Al, P. (2025). Generalization of the Numerical Radius, Crawford Number and Numerical Index Functions in the Weighted Case. Filomat, 39(11), 1-16.

31. Ismailov, Z. I., and Ipek Al, P. (2025). On the Numerical Radius of Hardy-Typ Operators. Editor:Fatma Lorcu, Matematik Konuları (s. 75-86), Afyonkarahisar: Yaz Yayınları.

32. Ismailov Z. I., and Otkun Çevik E. (2026). Some Inequalities for Bounds of Joint δ-Numerical Radius and Joint δ-Crawford Number Functions. Linear and Multipoint Algebra, 74(2), 192-212.

33. Kato, T. (1966). Perturbation Theory for Linear Operators. New York: Springer –Verlag.

34. Yeh, J. (2006). Real Analysis: Theory of Measure and Integration. World Scientific.

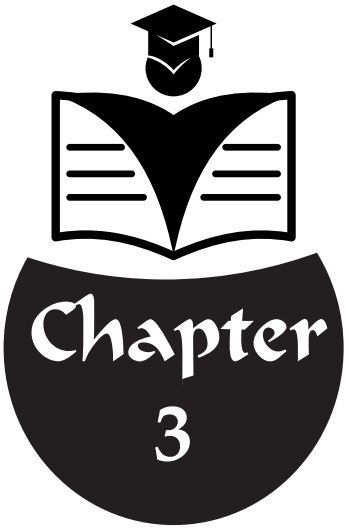

ROBUST ALTERNATIVES TO t-TEST AND THEIR APPLICATIONS TO HEALTH SCIENCES

Gökhan Uyar[1]
Abdullah Yalçınkaya[2]
Özlem Kaymaz[3]

1 Gökhan UYAR, Lecturer (PhD) , Ankara University Faculty of Science Department of Statistics, https://orcid.org/0000-0002-4551-6671
2 Abdullah YALÇINKAYA, Asst. Prof. Dr., Ankara University Faculty of Science Department of Statistics, https://orcid.org/0000-0003-2280-6438
3 Özlem KAYMAZ, Assoc. Prof. Dr., Ankara University Faculty of Science Department of Statistics, https://orcid.org/0000-0003-1235-8117

1. Introduction

The traditional two sample t-test is a well-known statistical procedure for testing whether the means of two independent groups are equal under the assumption of normality. It is stated that when the assumptions are met, the t-test is known to be the most powerful unbiased test for determining the differences between means, see Bridge & Sawilowsky (1999), Tiku & Akkaya (2004). However, non-normal distributions are more common in real-world data; see for example Şenoğlu & Tiku (2001) and the references therein. In practice, also, datasets may also contain one or more observations identified as outliers represent observations with extreme differences from the rest of the data. When the assumption of normality is violated or when the data contain outliers, the efficiency of the least squares (LS) estimators and the power of the test based on them is reduced. Even minor deviations from normality can lead to a considerable loss of power (Tukey, 1958).

Hence, t-tests based on robust (location - scale) estimators have been proposed in the literature as alternatives to the traditional t-test. Robust estimators are used to minimize the adverse effect of outliers in the estimation of the mean and variance, leading to more reliable and unbiased results under violation of the normality assumption.

A substantial body of research has been conducted to evaluate the robustness of the traditional t-test and its robust variants under various types of assumption violations from different perspectives. In these studies, the robustness of the t-test and the proposed robust methods has been examined across different sample sizes, and effect sizes, varying degrees of heteroscedasticity, and different levels of skewness and kurtosis to assess the degree of deviation from normality, see Table 1 for some examples.

Table 1. Literature review for the robustness of t-test according to different cases

	Sample Sizes	Variance Rates	Effect Sizes	Kurtosis γ_K, Skewness γ_S Correlation ρ, or Distribution	Proposed robust estimators in t-test
Rasch et al. (2011)	10 – 100	1:1 – 1:10	0 – 5	γ_K: 0 – 15, γ_S: 0 – 3	
Nguyen et al. (2016)	10 – 400	1:1 – 1:20	0 – 0.8	γ_K: 0 – 25, γ_S: 0 – 6	
Fradette et al. (2003)	10 – 80	1:1	0.25 – 0.75	ρ: -0.5 – 0.5, Exponential, Chi-squared	Trimmed means, Winsorized variances
Yusof et al. (2012)	15 – 25	1:36		g-distributions, h-distributions	Trimmed means, Median, MAD

Upon examination of these studies, robust estimators such as trimmed means and M-estimators emerge as alternatives to sample mean. When comparing t-tests based on robust estimators with the traditional t-test under normality, they exhibit similarly high statistical power. However, in the presence of deviations from normality, the power of the traditional t-test decreases, while the power of t-tests based on robust estimators remains relatively high.

In this study, we examined the traditional two-sample t-test and several robust two-sample t-tests used to assess the equality of means between independent groups. We investigated the Type-1 error rates and statistical power of these tests under the assumption of equal variances across two different outlier scenarios using a simulation study;

Case 1: The first group contains outliers in both the lower (minimum) and upper (maximum) tails.

Case 2: Both two groups contain outliers in both the lower (minimum) and upper (maximum) sections.

Finally, we evaluated the robustness of the tests using real application data representing both scenarios.

This study, designed to highlight the importance of using robust methods when the assumptions of the t-test are violated, is intended to serve as a valuable reference for researchers.

The remainder of the study is organized as follows: Section 2 presents the mathematical expression of the traditional two-sample t-test. Section 3 provides a detailed description of the robust two-sample t-tests considered in this study. Section 4 outlines the design and results of the simulation study. Section 5 presents the real data application, and the final section contains the conclusion.

2. Two-Sample t-Test

In this study, we focus on independent two sample t-test and rather than its one sample counterpart. Two sample t-test is used to test the equality of the means for independent groups.

For two independent groups, the mean of the jth group is μ_j and the variance of the jth group is σ_j^2. The null hypothesis for the two-sample t-test is defined by $H_0: \mu_1 = \mu_2$ vs the alternative hypothesis $H_1: \mu_1 \neq \mu_2$.

Suppose that X_{ij} $(i = 1, \dots, n_j;\ \ j = 1, 2)$ be a random sample from the jth group. The sample mean and variance for jth group are defined as

$$\bar{X}_j = \sum_{i=1}^{n_j} \frac{X_{ij}}{n_j} \tag{1}$$

and

$$S_j^2 = \frac{\sum_{i=1}^{n_j} (X_{ij} - \bar{X}_j)^2}{n_j - 1} \tag{2}$$

respectively.

Under the assumption that homogeneity of variances and normality are met, the traditional t test statistics for independent samples is defined as

$$t = \frac{\overline{X}_1 - \overline{X}_2}{\sqrt{S_p^2\left(\frac{1}{n_1} + \frac{1}{n_2}\right)}} \tag{3}$$

where S_p^2 is the estimate of the pooled (common) variance defined by

$$S_p^2 = \frac{(n_1 - 1)S_1^2 + (n_2 - 1)S_2^2}{n_1 + n_2 - 2}. \tag{4}$$

The test statistic in Eq. (3) has a t distribution with $v = n_1 + n_2 - 2$ degrees of freedom.

3. Robust Two-Sample t-Tests

In this section, robust estimators defined as an alternative to the well-known least squares (LS) estimators and the tests based on them are introduced. Among the robust estimators proposed as alternatives to LS estimators, trimmed mean (as an L-estimator), W24, BS82, Huber (as M-estimators) and MML (Modified Maximum Likelihood Estimation) are considered.

3.1 t-Test based on Trimmed Mean Estimator

The trimmed mean is one of the most commonly used L-estimator in the literature.

L-estimator T is defined as

$$T = \sum_{i=1}^{n} a_i x_{(i)}$$

where $x_{(1)} \leq x_{(2)} \leq \cdots \leq x_{(n)}$ are ordered statistics, and $a_1, a_2, \ldots, a_n$ are real numbers which satisfy $0 \leq a_i \leq 1, i = 1, 2, \ldots, n$ and $\sum a_i = 1$. The numbers $a_1, a_2, \ldots, a_n$ are called as the weights. L-estimators first proposed by Daniel (1920) are defined as the linear combination of the ordered statistics (Hoaglin & Mosteller, 1983).

The sample mean ($\bar{x}$) is a conventional L-estimator where $a_1 = a_2 = \ldots = a_n = \frac{1}{n}$.

The trimmed mean, as its name suggests, is a sample's mean after each tail has had a particular proportion of the extreme order statistics removed. The trimmed mean is used to eliminate the outlier effect and is defined as

$$\hat{\mu}_{tr}(\alpha) = \frac{1}{n(1-2\alpha)}\left\{(1-r)\left[x_{(g+1)} + x_{(n-g)}\right] + \sum_{i=g+2}^{n-g-1} x_{(i)}\right\}. \quad (5)$$

For this L-estimator, a_i $(i = 1, 2, \ldots, n)$ weights are

$$a_i = \begin{cases} 0, & if\ i \le g\ or\ i \ge n+g+1 \\ \frac{(1-r)}{n(2-\alpha)}, & if\ i = g+1\ or\ i = n-g \\ \frac{1}{n(1-2\alpha)}, & if\ g+2 \le i \le n-g-1 \end{cases}.$$

where $g = [\alpha n]$, $r = \alpha n - g$, and α is the trimming percentage of data. The estimator of the σ corresponding to the trimmed mean is defined as

$$\hat{\sigma}_{tr} = \left[\frac{\sum_{i=1}^{n} a_i (x_i - \mu_{tr})^2}{1 - \sum_{i=1}^{n} a_i^2}\right]^{1/2}. \quad (6)$$

The t-test statistics based on the trimmed mean estimator is given below

$$t_{tr} = \frac{\hat{\mu}_{1tr} - \hat{\mu}_{2tr}}{\sqrt{S_{ptr}^2\left(\frac{1}{n_1} + \frac{1}{n_2}\right)}} \quad (7)$$

where

$$S_{ptr}^2 = \frac{(n_1 - 1)\hat{\sigma}_{1tr}^2 + (n_2 - 1)\hat{\sigma}_{2tr}^2}{n_1 + n_2 - 2}. \quad (8)$$

3.2 t-Test based on M-Estimators

M-estimators are robust estimators based on the minimax principle that ensure the minimization of a specific objective function (Huber, 1964; Huber, 1981). Among these, W24 estimators (using the wave function proposed by Andrews et al., 1972; Andrews, 1974) and BS82 (using the bi-square function proposed by Beaton & Tukey, 1974), which are commonly used in the literature and can be obtained without the need for iterative methods, are

introduced. These estimators are called as one-step M-estimators because they can be solved in a single step.

3.2.1 t-Test based on W24 Estimator

W24, estimator of the location parameter is defined as

$$\hat{\mu}_W = T_0 + (hS_0)\tan^{-1}\left(\frac{\sum_{i=1}^{n}\sin(z_i)}{\sum_{i=1}^{n}\cos(z_i)}\right) \tag{9}$$

where $T_0 = median(y_i)$, $S_0 = median|y_i - T_0|$, $h = 2.4$, and $z_i = (y_i - T_0)/hS_0$. Here, only z_i values that satisfy the condition $|z_i| \leq \pi$ are used.

The estimator of the σ corresponding to the W24 estimator is defined as

$$\hat{\sigma}_W = hS_0\left[n\frac{\sum\sin^2(z_i)}{(\sum\cos(z_i))^2}\right]^{1/2}. \tag{10}$$

The t-test statistics based on the W24 estimator is given below

$$t_W = \frac{\hat{\mu}_{1W} - \hat{\mu}_{2W}}{\sqrt{S_{pW}^2\left(\frac{1}{n_1} + \frac{1}{n_2}\right)}} \tag{11}$$

where

$$S_{pW}^2 = \frac{(n_1 - 1)\hat{\sigma}_{1W}^2 + (n_2 - 1)\hat{\sigma}_{2W}^2}{n_1 + n_2 - 2}. \tag{12}$$

3.2.2 t-Test based on BS82 Estimator

BS82 estimator of the location parameter is defined as

$$\hat{\mu}_B = T_0 + (hS_0)\frac{\sum_{i=1}^{n}\psi(z_i)}{\sum_{i=1}^{n}\psi'(z_i)} \tag{13}$$

where $T_0 = median(y_i)$, $S_0 = median|y_i - T_0|$, $h = 8.2$, and $z_i = (y_i - T_0)/hS_0$.

The weight function $\psi(z)$ and its derivative are defined as

$$\psi(z) = \begin{cases} z(1 - z^2)^2, & |z| \leq 1 \\ 0, & otherwise \end{cases} \tag{14}$$

and $\psi'(z) = 1 - 6z^2 + 5z^4$, respectively.

The estimator of the σ corresponding to the BS82 estimator is defined as

$$\hat{\sigma}_B = hS_0\left[n\frac{\sum\psi^2(z_i)}{(\sum\psi'(z_i))^2}\right]^{1/2}. \tag{15}$$

The t-test statistics based on the BS82 estimator is given below

$$t_B = \frac{\hat{\mu}_{1B} - \hat{\mu}_{2B}}{\sqrt{S_{pB}^2\left(\frac{1}{n_1}+\frac{1}{n_2}\right)}} \tag{16}$$

where

$$S_{pB}^2 = \frac{(n_1-1)\hat{\sigma}_{1B}^2 + (n_2-1)\hat{\sigma}_{2B}^2}{n_1+n_2-2}. \tag{17}$$

3.2.3 t-Test based on Huber's M-Estimator

Let $y_1, y_2, \ldots, y_n$ be a random sample from the distribution $\frac{1}{\sigma} f\left(\frac{y-\mu}{\sigma}\right)$. Huber (1964, 1981) supposed that the f distribution is a long-tailed symmetric distribution and developed a new method to estimate μ.

The proposed methodology employs the log-likelihood function, defined as follows:

$$\ln L = -nln\sigma + \sum_{i=1}^{n} lnf(z_i) \tag{18}$$

where $z_i = (y_i - \mu)/\sigma$. If f is known in Eq. (18), the maximum likelihood estimator of the parameter μ is obtained as

$$\frac{\partial lnL}{\partial \mu} = \frac{1}{\sigma}\sum_{i=1}^{n}\xi(z_i) = 0 \tag{19}$$

where $\xi(z) = -\frac{f'(z)}{f(z)}$.

When written as $w_i = w_i(z) = \frac{\xi(z_i)}{z_i}$ where $\sum_{i=1}^{n} w_i(y_i - \mu) = 0$ in Eq. (19),

$$\hat{\mu}_H = \frac{\sum_{i=1}^{n} w_i y_i}{\sum_{i=1}^{n} w_i} \tag{20}$$

is obtained.

Given σ ve $\xi(z)$, the solution to Eq. (19) can be obtained using iterative methods easily. Nevertheless, in practice, both σ and $\xi(z)$ are unknown. Huber (1964) proposed the $\xi(z)$ function as

$$\xi(z) = \begin{cases} z & |z| \leq c \\ csgn(z) & |z| > c \end{cases} \tag{21}$$

In equation (21), c is usually assumed to be 1.345. Eq. (20) with using the $\xi(z)$ function in Eq. (21) is called the Huber's M-estimator.

When σ is unknown, the estimator

$$\tilde{\sigma}_0 = \frac{median|y_i - median(y_i)|}{0.6745}$$

is used.

The estimator of σ corresponding to $\hat{\mu}_H$ is defined as

$$\hat{\sigma}_H = \left\{ \frac{n\tilde{\sigma}_0^2 \left[\sum_{i=1}^{n} \xi^2 \left(\frac{y_i - \hat{\mu}_H}{\tilde{\sigma}_0}\right)\right]}{\left[\sum_{i=1}^{n} \xi' \left(\frac{y_i - \hat{\mu}_H}{\tilde{\sigma}_0}\right)\right]^2} \right\}^{1/2}. \tag{22}$$

The t-test statistics based on the Huber's M-estimator is given below

$$t_H = \frac{\hat{\mu}_{1H} - \hat{\mu}_{2H}}{\sqrt{S_{pH}^2 \left(\frac{1}{n_1} + \frac{1}{n_2}\right)}} \tag{23}$$

where

$$S_{pH}^2 = \frac{(n_1 - 1)\hat{\sigma}_{1H}^2 + (n_2 - 1)\hat{\sigma}_{2H}^2}{n_1 + n_2 - 2}. \tag{24}$$

3.3 t-Test based on MML Estimator

The MML method proposed by Tiku (1967) is a non-iterative approach that provides explicit estimators for model parameters. When iterative methods are employed, several convergence issues may arise — such as convergence to incorrect values, failure to converge, or converging local maxima instead of global maxima due to multiple roots. Therefore, the MML

method effectively overcomes the computational challenges typically associated with ML method.

MML estimator of the location parameter μ is defined as

$$\hat{\mu}_{MML} = \frac{\left\{\sum_{i=r+1}^{n-r} y_{(i)}\right\} + r\beta(y_{(r+1)} - y_{(n-r)})}{m} \tag{25}$$

where $m = n - 2r + 2r\beta$ and $r = [0.5 + 0.1n]$.

MML estimator of the scale parameter is defined as

$$\hat{\sigma}_{MML} = \frac{B + \sqrt{B^2 + 4AC}}{2\sqrt{A(A-1)}} \tag{26}$$

where $A = n - 2r$, $B = r\alpha\{y_{(i+1)} - y_{(n-i)}\}$, and

$$C = \sum_{i=r+1}^{n-r} y_{(i)}^2 + r\beta\{y_{(n-r)}^2 - y_{(r+1)}^2\} - m\hat{\mu}_{MML}^2$$

Here, α and β are table values given in Tiku & Akkaya (2004).

The t-test statistics based on the MML estimator is given below

$$t_{MML} = \frac{\hat{\mu}_{1MML} - \hat{\mu}_{2MML}}{\sqrt{S_{pMML}^2\left(\frac{1}{n_1} + \frac{1}{n_2}\right)}} \tag{27}$$

where

$$S_{pMML}^2 = \frac{(n_1 - 1)\hat{\sigma}_{1MML}^2 + (n_2 - 1)\hat{\sigma}_{2MML}^2}{n_1 + n_2 - 2}. \tag{28}$$

4. Simulation Study

In this section, the Type I error rates and the powers (1 – β) of the traditional t-test and robust methods are examined to evaluate the differences between the means of two independent samples. The purpose of the simulation study is to compare the performances of the test methods under two different scenarios (Case 1 and Case 2) and to identify the conditions under which reliable results are obtained.

Two independent samples are randomly generated from a standard normal distribution with a mean of 0 and variance of 1. Sample sizes (n = 15,

30, 50, and 100) and effect sizes (d) (small: 0.2, medium: 0.5, large: 0.8) are examined for both Case1 and Case2 (see Cohen, 1988). Each simulation scenario is replicated 10,000 times. In all scenarios, a balanced design with equal sample sizes and equal variances was assumed.

In Case 1, 10% of the observations in one group are replaced with outliers, with 5% taken from the lower tail end and 5% from the upper tail after sorting the data from smallest to largest. Case 2, 10% of the observations in both independent groups are replaced with outliers in a similar manner, with 5% from the lower tail end and 5% from the upper tail. In both scenarios, traditional t-test, Trimmed Mean, Huber's M, BS82, W24, and MML methods are applied for each sample size, and their results are compared.

In this section, Type I error rates, defined as the probability of rejecting a true null hypothesis, are calculated for each method. In addition, deviations of the observed Type I error rates from the nominal significance level of 0.05 are evaluated. Similarly, the power of the test, defined as the probability of rejecting a false null hypothesis when it is actually false, is assessed for each method. The test methods achieving the highest power under each scenario are also identified. The type 1 error rates and the test power values are presented in Tables 2 and 3.

Table 2. Type I error values for Case 1 and Case 2

Case 1	Traditional t-test	Trimmed Mean	Huber M	BS82	W24	MML
n=15	0.0259	0.0599	0.0755	0.0538	0.0536	0.0585
n=30	0.0201	0.0756	0.0754	0.0465	0.0526	0.0543
n=50	0.0225	0.0829	0.0719	0.0466	0.0504	0.0515
n=100	0.0257	0.0989	0.0767	0.0513	0.0471	0.0499
Case 2	Traditional t-test	Trimmed Mean	Huber M	BS82	W24	MML
n=15	0.0136	0.0557	0.0734	0.0483	0.0482	0.0611
n=30	0.0135	0.0605	0.0799	0.0422	0.0454	0.0542
n=50	0.0115	0.0789	0.0730	0.0464	0.0445	0.0514
n=100	0.0117	0.0969	0.0761	0.0489	0.0478	0.0509

According to the results presented in Table 2, the following conclusions are drawn:

For Case 1:

- When n=15, 30, and 50, the W24 method performs best.
- When n=100, the MML method is preferred.

For Case 2:

- When n=15, the BS82 method is preferred.
- When n=30, 50, and 100, the MML method performs best.

These methods are shown to maintain the Type 1 error rate closer to the nominal significance level.

Table 3. Power values for Case 1 and Case 2

Case 1	d	Traditional t-test	Trimmed Mean	Huber M	BS82	W24	MML
n=15	0.2	0.0736	0.1510	0.1815	0.1387	0.1359	0.1481
	0.5	0.2332	0.4109	0.4367	0.3668	0.3660	0.3915
	0.8	0.4925	0.7180	0.7409	0.6615	0.6638	0.6890
n=30	0.2	0.1028	0.2377	0.2480	0.1846	0.1750	0.2029
	0.5	0.4121	0.6474	0.6589	0.5795	0.5697	0.6065
	0.8	0.7977	0.9284	0.9332	0.9046	0.9021	0.9150
n=50	0.2	0.1390	0.3308	0.3193	0.2456	0.2453	0.2605
	0.5	0.6155	0.8438	0.8310	0.7732	0.7800	0.7938
	0.8	0.9541	0.9930	0.9928	0.9863	0.9853	0.9884
n=100	0.2	0.2581	0.5389	0.4685	0.4048	0.3938	0.4117
	0.5	0.9123	0.9849	0.9725	0.9677	0.9645	0.9654
	0.8	0.9995	0.9999	0.9999	0.9999	0.9999	0.9999
Case 2	d	Traditional t-test	Trimmed Mean	Huber	BS82	W24	MML
n=15	0.2	0.0485	0.1368	0.1797	0.1156	0.1157	0.1515
	0.5	0.1839	0.3842	0.4470	0.3215	0.3238	0.3927
	0.8	0.4461	0.6974	0.7409	0.5964	0.5976	0.6852
n=30	0.2	0.0690	0.2209	0.2399	0.1521	0.1483	0.2001
	0.5	0.3603	0.6472	0.6650	0.5008	0.4921	0.6039
	0.8	0.7665	0.9324	0.9335	0.8459	0.8493	0.9202

n=50	0.2	0.1027	0.3227	0.3213	0.2152	0.2061	0.2647
	0.5	0.5891	0.8466	0.8317	0.7151	0.7000	0.7991
	0.8	0.9476	0.9933	0.9909	0.9681	0.9703	0.9880
n=100	0.2	0.1988	0.5475	0.4621	0.353	0.3444	0.4054
	0.5	0.8907	0.9848	0.9748	0.9407	0.9347	0.9691
	0.8	0.9994	0.9999	0.9998	0.9996	0.9998	0.9998

According to the results presented in Table 3, the following recommendations can be made:

For both Case 1 and Case 2:

- When n=15 and 30, the Huber method is recommended for all effect sizes.
- When n=50 and 100, the trimmed mean method is recommended for all effect sizes.

As a result, the simulation study demonstrates that the performance of the test methods varies depending on the outlier conditions, sample sizes, and effect sizes. According to the literature, the traditional t-test is asymptotically the most powerful test when the underlying assumptions are satisfied and no outliers are present. However, the simulation results indicate that the power of the traditional t-test decreases in the presence of outliers and violations of the normality assumption. In contrast, the robust methods generally exhibit higher power than the traditional t-test. Furthermore, the findings suggest that both sample size and the presence of outliers are significant factors affecting test performance.

5. Applications to Real Data

In this section, the performance of the test methods considered in the simulation study (traditional t, W24, BS82, Huber M, trimmed mean, and MML) is demonstrated using real data. The results of them are then discussed in light of the findings from the simulation study. The data used in both applications is obtained by randomly selecting a balanced subsample from the original data. This subsample consisted of observations that satisfied the

specified statistical conditions, namely homogeneity of variances and the presence and location of outliers.

In the first application, the Hepatitis C Virus (HCV) dataset obtained from the UCI Machine Learning Repository (Dua & Graff, 2019) was used to represent Case 1 in the simulation study. This data set was collected to investigate liver diseases associated with the Hepatitis C virus (HCV) using biochemical markers. It consists of two independent groups comprising healthy blood donors and Hepatitis C patients. A total of 80 observations of serum albumin (ALB) levels are included in the analysis. The boxplot and QQ-plot of ALB levels are presented below.

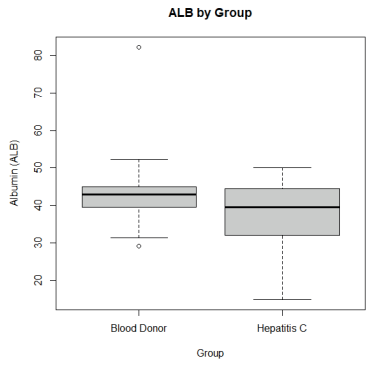

Figure 1. Boxplot of the HCV data

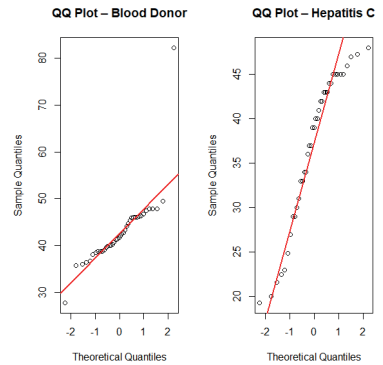

Figure 2. Q-Q plot of the HCV data

It is observed that only one group has two outliers, located in both the lower and upper tails of the distribution, consistent with the scenario defined as Case 1 in the simulation study. In contrast, the other group does not exhibit any outliers. The two independent groups do not satisfy the normality assumption; however, the assumption of variance homogeneity is met (Levene's test, p=0.058).

Table 4. Results of tests for HCV data.

Estimators	MD	DF	95% CI (Lower, Upper)	SE	t-value	p-value
Traditional t	6.0923	76	(2.3988, 9.7858)	1.8545	3.2852	0.0015
W24	4.8823	76	(1.7712, 7.9934)	1.5621	3.0862	0.0014
BS82	4.8877	76	(1.7654, 8.0099)	1.5677	3.0786	0.0014
Huber M	4.6471	76	(1.8424, 7.4519)	1.4082	3.2584	0.0008
Trimmed Mean	5.0655	76	(2.4565, 7.6746)	1.3100	3.8182	0.0001
MML	5.2969	76	(1.9115, 8.6823)	1.6998	3.1162	0.0026

MD: Mean Difference, DF: Degrees of freedom, CI: Confidence Interval, SE: Standard Error

The results presented in Table 4 show that p-values for all the test methods are below the significance level (α=0.05); therefore, the null hypothesis is rejected. However, the tests based on robust methods display lower standard errors (SE) and narrower confidence intervals (CI) compare to the traditional t-test. In particular, the Huber's M-estimator and trimmed mean methods exhibit the smallest SE and narrowest CI values among the methods considered. These real-data findings are consistent with results obtained in the simulation study for Case 1.

In the second application, Framingham Heart Study (FHS) dataset obtained from Kaggle (see Francis - noeyislearning) was used to represent Case 2 in the simulation study. The dataset originates from the well-known longitudinal Framingham Heart Study (Dawber et al., 1951). This application aims to compare total cholesterol (totChol) levels between two independent groups individuals with heart disease and those without heart disease. The dataset includes a total of 80 observation. The boxplot and QQ-plot of totChol levels are presented below.

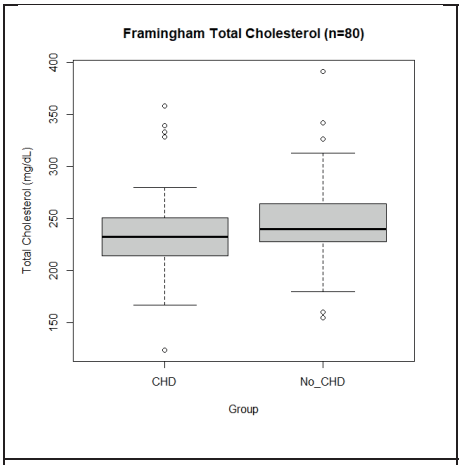

Figure 3. Boxplot of the FHS data

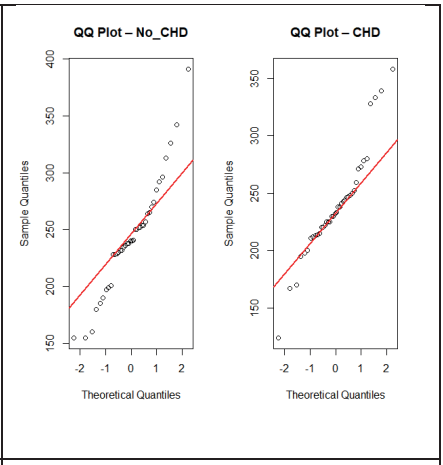

Figure 4. Boxplot of the FHS data

It is observed that both groups contain outliers in the lower and upper tails of the distribution, consistent with the scenario defined as Case 2 in the simulation study. Although the normality assumption is violated for two independent groups, the assumption of variance homogeneity is satisfied (Levene's test, p=0.67).

Table 5. Results of tests for FHS data

Estimators	MD	DF	95% CI (Lower, Upper)	SE	t-value	p-value
Traditional t	5.2250	78	(-15.8065, 26.2565)	10.5641	0.4946	0.6223
W24	6.4660	78	(-11.5303, 24.4624)	9.0395	0.7153	0.2383
BS82	6.7129	78	(-10.9952, 24.4210)	8.8947	0.7547	0.2263
Huber M	6.6064	78	(-8.6744, 21.8872)	7.6755	0.8607	0.1960
Trimmed Mean	4.2778	78	(-10.9529, 19.5084)	7.6503	0.5592	0.2888
MML	5.4588	78	(-11.4734, 22.3910)	8.5050	0.6418	0.5229

MD: Mean Difference, DF: Degrees of freedom, CI: Confidence Interval, SE: Standard Error

The results presented in Table 5 show that p-values for all the test methods are greater than the significance level (α=0.05); therefore, the null hypothesis is not rejected. However, the tests based on robust methods yield lower standard errors (SE) and narrower confidence intervals (CI) compare to the traditional t-test. In particular, the Huber's M-estimator and trimmed mean methods exhibit the smallest SE and narrowest CI values among all methods. These real data findings are consistent with the results obtained in the simulation study for Case 2.

6. Conclusions

Under ideal conditions, where normality and variance assumptions are met, the traditional two-sample t-test is asymptotically the most powerful test for comparing group means. However, when the assumption of normality is violated, or the data contain outliers, the efficiency of LS estimatiors and the power of test based on them are reduced.

In this study, robust estimators are employed to minimize the adverse effects of outliers on the estimation of the mean and variance, leading to more reliable and unbiased results under violations of the normality assumption. Accordingly, the finding suggests that t-test based on robust estimators should be preferred over the traditional t-test when the data include outliers. Moreover, the findings provide practical guidance for applied researchers in selecting appropriate test procedures under different contamination and sample size conditions.

References

Andrews, D. F. (1974). A robust method for multiple linear regression. *Technometrics*, 16, 523-531.

Andrews, D. F., Bickel, P. J., Hampel, F., Huber, P., Rogers, W., & Tukey, J. W. (1972). *Robust Estimation of Location: Survey and Advances*. Princeton University press: Princeton, N. J.

Beaton, A. E. and Tukey, J. W. (1974). The fitting of power series, meaning polynomials, illustrated on band-spectroscopic data. *Technometrics, 16*, 147-186.

Bridge, P. D., & Sawilowsky, S. S. (1999). Increasing physicians' awareness of the impact of statistics on research outcomes: Comparative power of the t-test and Wilcox Rank-Sum test in small samples applied research. *Journal of Clinical Epidemiology, 52*(3), 229-235. https://doi.org/10.1016/S0895-4356(98)00168-1

Cohen, J. (1988). *Statistical power analysis for the behavioral sciences* (2nd ed.). Lawrence Erlbaum Associates.

Daniel, C. (1920). Observations weighted according to order. *American Journal of Mathematics, 42*, 222–236.

Dawber, T. R., Meadors, G. F., & Moore, F. E. (1951). Epidemiological approaches to heart disease: The Framingham Study. *American Journal of Public Health, 41*(3), 279–286. https://doi.org/10.2105/AJPH.41.3.279

Dua, D., & Graff, C. (2019). *UCI machine learning repository*. University of California, Irvine, School of Information and Computer Sciences. http://archive.ics.uci.edu/ml

Fradette, K., Keselman, H. J., Lix, L., Algina, J., & Wilcox, R. R. (2003). Conventional and robust paired and independent-samples t tests: type I error and power rates, *Journal of Modern Applied Statistical Methods, 2*(2), 22. Doi: 10.22237/jmasm/1067646120

Francis (noeyislearning) (n.d.). *Framingham Heart Study dataset* [Data set]. Kaggle. https://www.kaggle.com/datasets/noeyislearning/framingham-heart-study

Hoaglin, D. C., & Mosteller, F. (1983). *Understanding robust and exploratory data analysis*. John Wiley & Sons.

Huber, P. J. (1964). Robust estimation of a location parameter. *Annals of Mathematical Statistics, 35*, 73–101.

Huber, P. J. (1981). *Robust statistics*. John Wiley & Sons.

noeyislearning. (n.d.). *Framingham Heart Study dataset*. Kaggle. https://www.kaggle.com/datasets/noeyislearning/framingham-heart-study

Nguyen, D. T., Kim, E. S., Rodriguez de Gil, P., Kellermann, A., Chen, Y. H., Kromrey, J. D., & Bellara, A. (2016). Parametric tests for two population means under normal and non-normal distributions. *Journal of Modern Applied Statistical Methods, 15*(1), 9.

Rasch, D., Kubinger, K. D., & Moder, K. (2011). The two-sample t test: pretesting its assumptions does not pay off. *Statistical Papers, 52*(1), 219-231. https://doi.org/10.1007/s00362-009-0224-x

Şenoğlu, B., & Tiku, M. L. (2001). Analysis of variance in experimental design with nonnormal error distributions. *Communications in Statistics - Theory and Methods, 30*(7), 1335–1352. https://doi.org/10.1081/STA-100104748

Tiku, M. L. (1967). Estimating the mean and standard deviation from a censored normal sample. *Biometrika, 54*(1–2), 155–165.

Tiku, M. L., & Akkaya, A. D. (2004). *Robust estimation and hypothesis testing*. New Delhi, India: New Age International.

Tukey, J. W. 1958. Bias and Confidence in not quite large samples. *Annals of Mathematical Statistics, 29*, 614.

Yusof, Z. M., Abdullah, S., Yahaya, S. S. S., Othman, A. R., Malaysia, U. S., Othman, A. R., & Jauh, P. P. P. J. (2012). A robust alternative to the t-test. *Modern Applied Science, 6*(5), 27-33. http://dx.doi.org/10.5539/mas.v6n5p27

Zimmerman, D. W. (2004). A note on preliminary tests of equality of variances. *British Journal of Mathematical and Statistical Psychology, 57*(1), 173-181. https://doi.org/10.1348/000711004849222

Chapter 4

COMPARATIVE ANALYSIS OF OPTICAL BAND GAP ENERGIES IN SPIN-COATED ZNO/PMMA-co-PEA NANOCOMPOSITES: A STUDY VIA TAUC AND ASF FORMALISMS

M. Selin SUNAY[1]

1 Dr. Öğr. Üyesi Mimar Sinan Güzel Sanatlar Üniversitesi, Kültür Varlıklarını Koruma ve Onarım Yüksekokulu, Kültür Varlıklarını Koruma ve Onarım Bölümü, İstanbul, TÜRKİYE. selin.sunay@msgsu.edu.tr
ORCID ID: 0000-0002-4054-6302

INTRODUCTION

Polymers are widely used in many manufacturing processes, including construction, healthcare, and packaging, due to their flexibility, lightness, durability, and low strength. Polymers are distinguished by their facile processing characteristics and their capacity for integration into high-quality thin-film architectures. They are compatible with a diverse range of fabrication methodologies, including solution-processing techniques such as immersion coating, rotational coating, solution deposition, and various advanced functional coating technologies. Consequently, polymers have become indispensable components within the optoelectronics industry, where they serve critical functions across a broad spectrum of high-performance applications [1].

Despite their versatility, polymers generally exhibit inferior mechanical, thermal, and electrical properties relative to metals and ceramics. Conventional polymer systems—including homopolymers, copolymers, polymer blends, and chemically modified derivatives—frequently fail to satisfy the rigorous performance requirements of advanced engineering applications [2]. While polymer selection is traditionally governed by mechanical, thermal, electrical, optical, and magnetic characteristics, a more holistic approach necessitates the consideration of additional parameters. These include the hydrophilic-hydrophobic balance, chemical stability, and biocompatibility, as well as specialized optoelectronic properties. Furthermore, chemical functionalities—such as solubility, wettability, and rheological behavior during molding—play a critical role. Beyond their intrinsic properties, polymers are frequently leveraged as matrices to enhance the processability and structural versatility of composite materials.

Lately, extensive research has been conducted on organic/inorganic composite materials with diverse compositions. The incorporation of inorganic nanoparticles into polymer matrices enables the synthesis of advanced functional materials tailored for diverse industrial sectors. Recent breakthroughs in nanotechnology have facilitated the precise design and

fabrication of inorganic nanostructures that leverage critical cooperative physical phenomena, such as superparamagnetism, size-dependent bandgap modulation, ferromagnetism, and optimized electron and phonon transport properties [1]. The emergence of advanced characterization techniques and fundamental insights at the nanometric and molecular scales has become a primary catalyst for the development of innovative hybrid architectures. These advancements are driving transformative progress across a broad spectrum of disciplines, including sensing technologies, nanoelectronics, photonics, and solid-state lighting, as well as bio-medicine, heterogeneous catalysis, and systems for energy storage and conversion [3]. The incorporation of inorganic nanoparticles—including silica, transition metal oxides, metallic phosphates, nanoclays, and metal chalcogenides—extends beyond enhancing mechanical and thermal stability. These constituents introduce novel functionalities governed by their chemical composition, morphology, particle size, and crystallinity. Consequently, the integration of such fillers can significantly tune or augment a material's electronic, magnetic, and redox properties, as well as its optical refractive index and overall density [4]. In summary, the synthesized nanocomposites demonstrate enhanced optical, mechanical, magnetic, and optoelectronic characteristics.

The poly(methyl methacrylate-co-ethyl acrylate) used in this study is a copolymer commonly known as PMMA-co-PEA, designed to balance the rigid and brittle nature of pure PMMA with the flexibility of PEA. In the optical world, this material is considered an "ideal balance" polymer offering high transparency and improved mechanical strength. Like pure PMMA, this copolymer is exceptionally transparent. It typically allows for over 90% light transmission in the visible spectrum. The addition of PEA (Ethyl Acrylate) disrupts the polymer chain regularity slightly but does not introduce significant scattering centers, meaning it remains "water-clear." The refractive index of the copolymer is generally close to 1.49, which is the standard for PMMA. However, it can be fine-tuned by adjusting the monomer ratio. In addition, various product options, including photonic

crystals [5] and protected inorganic structures[6], can be produced through structures derived from the specific use of this content.

In the advancement of polymer-inorganic nanocomposites for targeted at photonic devices, inorganic nanoparticles specifically noble metals like **Au** and **Ag**, as well as semiconductors such as **TiO_2**, **ZnO**, and **PbS** are frequently employed as photofunctional dopants to tailor the material's photonic properties [7]. Among many inorganic materials, zinc oxide (ZnO), which was also used in this study, is one of the most attractive semiconductors. Zinc oxide (ZnO) is a wide-bandgap semiconductor characterized by high optical transparency and distinct luminescent properties within the near-ultraviolet (UV) and visible spectra [8]. Owing to these attributes, ZnO has emerged as a high-potential candidate for a diverse range of electronic and optoelectronic applications. These include antireflective coatings and transparent conducting oxides (TCOs) in solar cells, as well as functional components in chemiresistors, electro-optical modulators, heat mirrors, and elastic wave filters [9]. Owing to its substantial exciton binding energy of approximately 60 meV, ZnO supports stable excitonic transitions at ambient temperatures, potentially yielding superior radiative recombination efficiency and lower lasing thresholds. Recent studies have focused on the structural and electronic optimization of ZnO to broaden its technological utility. Specifically, bandgap engineering has emerged as a critical strategy for tailoring ZnO for advanced ultraviolet (UV) photodetection and light-emitting applications.

Poly(methyl methacrylate-co-ethyl acrylate) (PMMA-co-PEA) doped with Zinc Oxide (ZnO) nanoparticles creates a nanocomposite with a unique blend of optical characteristics. By embedding inorganic ZnO into the acrylic copolymer matrix, you effectively tune how the material interacts with light. The band gap structure of PMMA-co-PEA/ZnO nanocomposites, the subject of this study, is a fascinating example of how "tuning" materials at the nanoscale can alter their electronic properties.

For this purpose, thin polymeric films of a specific thickness were first

obtained by applying PMMA-co-PEA copolymer to glass surfaces using the drop casting method. Subsequently, nanocomposite films obtained by coating polymer film surfaces, dried at room temperature, with a solution consisting of dispersed ZnO(15nm) nanoparticles using the spin coating method in different numbers of layers were subjected to heat treatment at 180°C for 30 minutes. Optical measurements were performed at room temperature using a Varian Cary 100 Bio UVV spectrophotometer.

2. MATERIALS

2.1 Fabrication of PMMA-co-PEA Films via Solution Casting:

The powdered PMMA-co-PEA (polymethyl methacrylate-polyethyl acrylate) copolymer, purchased from Sigma Aldrich, with an average molecular weight of Mw~101,000 $g.mol^{-1}$ and a glass transition temperature (Tg) of 104°C, is a thermoplastic polymer. It is hard and transparent. Before starting the planned experiments and analyses, the copolymer was prepared for analysis by dissolving it in THF (Tetrahydrofourane), which is the most suitable solvent for it. Afterwards, its density was measured with a Micromeritics AccuPyc II 1340 Gas Pycnometer and found to be ρ: 1.2110 g/cm^3.

To ensure a homogeneous distribution, the polymeric solution was stirred at room temperature using a magnetic stirrer for a specific duration. The solution was then deposited onto pre-cleaned 2.5 x 2.5 cm^2 glass substrates—previously treated with alcohol—via the drop-casting method. To maintain a consistent film thickness (d = 3.5- 4μm) an equal volume (number of drops) was applied to each substrate at ambient temperature. Finally, the samples were allowed to dry at ambient temperature for 1 day to yield PMMA-co-PEA copolymeric films. The flowchart representation of this deposition and patterning process is illustrated in Figure 1.

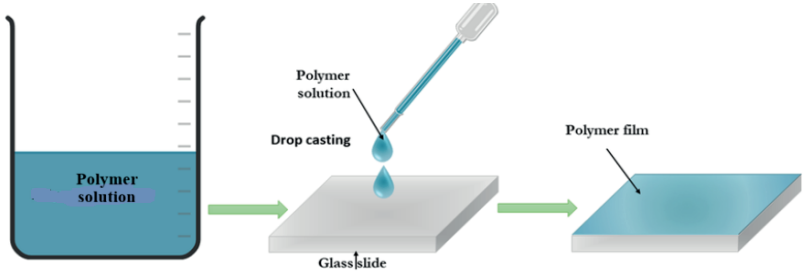

Drop casting of the synthesized copolymer onto a clean glass substrate. [Color figure can be viewed at wileyonlinelibrary.com]

Figure 1: Casting of PMMA-co-PEA thin films.

Copolymeric films of uniform thickness were deposited and allowed to dry at ambient temperature for a duration of 24 hours. The SEM images of poly(methyl methacrylate-co-ethylacrylate)(PMMA-PEA) pure polymer films at room temperature are shown in Figure 2.

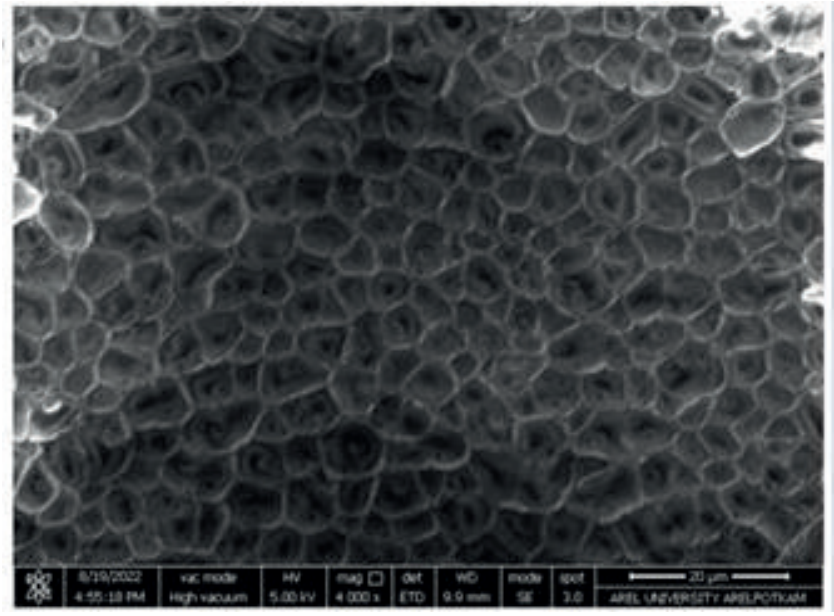

Figure 2: SEM images of nano-sized PMMA-co-PEA thin films used in this study (Images were taken at room temperature before annealing).

2.2. Preparation of PMMA-co-PEA / ZnO Nanocomposite Films

Owing to their high specific surface area, 15 nm ZnO nanoparticles exhibit a significant propensity for agglomeration in metal oxide suspensions. To mitigate this and ensure long-term colloidal stability and homogeneous dispersion, the suspension was supplemented with the non-ionic surfactant Pluronic F127. The solution was continuously stirred using a magnetic bar for 3 hours at ambient temperature, succeeded by a 24-hour equilibration period to achieve a steady-state distribution. Polymer-metal oxide nanocomposite films were synthesized through the layer-by-layer deposition of 15 nm ZnO particles onto pure polymer films using the spin-coating method. Samples were prepared with 1, 5, and 10 layers to evaluate the impact of coating thickness on the composite properties. These steps are shown schematically in

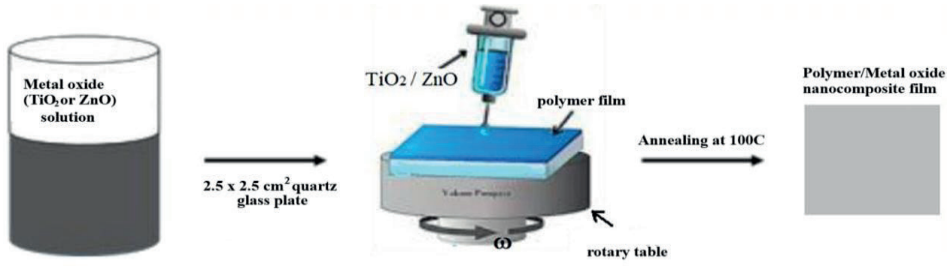

Figure 3: Casting of Polymer/Metal Oxide Nanocomposite films.

3. EXPERIMENTAL

3.1 UVV Measurements

The optical properties of the PMMA-co-PEA/ZnO nanocomposite films were characterized via UV-Vis spectroscopy (Varian Cary 100 Bio) within the 190–600 nm range.

3.2 Field Emission Gun Scanning Electron Microscope (FEGSEM-EDS) Measurement

The surface topography of the polymer thin films was characterized using a FEI QUANTA 450 FEG Field Emission Scanning Electron Microscope (FE-SEM) operated at an accelerating voltage of 10–20 kV.

4. RESULTS AND DISCUSSIONS

4.1. Electronic Absorption Spectroscopic Analysis

The principles of Ultraviolet-Visible Molecular Absorption Spectrometry involve the excitation of valence electrons to higher energy states through the absorption of ultraviolet or visible light. The Beer-Lambert Law provides a mathematical framework for the interdependence of absorbance and transmittance is defined by the following expression [10]:

$$A = -\log_{10}\frac{I}{I_0} = -\log_{10} T \qquad (1)$$

In this context, *A* stands for absorbance, *T* for transmittance, and *I* and I_0 for the intensities of transmitted and incident light. As light undergoes electromagnetic wave propagation within a material, it undergoes absorption, scattering, or transmission. The absorbance is fundamentally governed by the material's molecular structure. In the absence of intrinsic photon absorption such as luminescence or electronic transitions the measured absorbance (A), is attributed solely to structural heterogeneities acting as scattering centers. Consequently, as defined by Eq. (1), an elevation in the density of these scattering centers attenuates the transmitted light intensity, (I), leading to a reciprocal increase in the calculated absorbance.

The UV–Vis spectrums of PMMA-co-PEA/ZnO(15nm) nanocomposite films are displayed in Fig. 4.

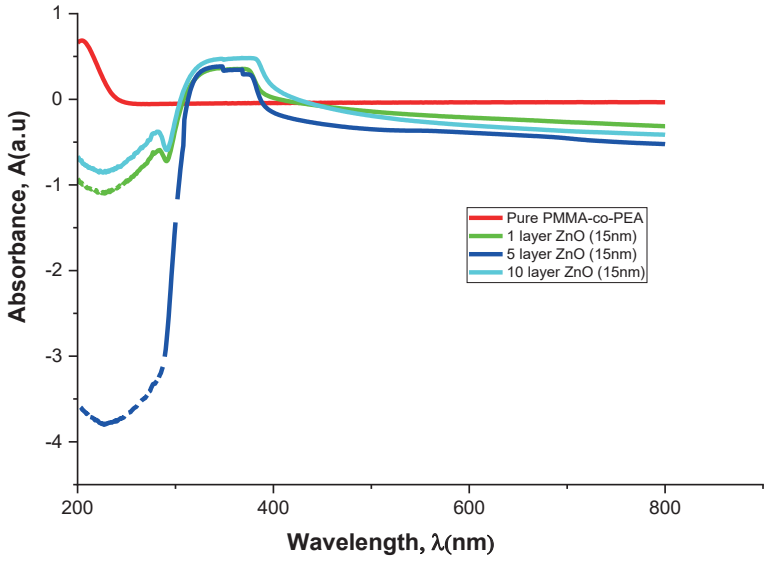

Figure 4: Optical absorption spectrum of PMMA-co-PEA/ZnO(15nm) nanocomposite films for various layers of ZnO.

The results show that the highest absoption peak measure for pure copolymer(PMMA-co-PEA) between 190nm and 200nm (λ< 250nm region I). The pronounced enhancement in Region I is assigned to the electronic π→π * transition, which is induced by the carbonyl groups incorporated into the PMMA-co-PEA structure.

The incorporation of ZnO into the pure PMMA-co-PEA matrix induces a bathochromic shift in the absorption edge toward lower photon energies, effectively narrowing the optical band gap of the functionalized composites. Compared to the UV region, the absorption spectra of the functionalized polymer exhibit enhanced intensities within the visible spectrum. This suggests that the incident photon energy is sufficient to promote electronic transitions from the valence band to the conduction band. Consequently, while absorption remains attenuated beyond 380 nm, there is a marked enhancement across the visible range. This phenomenon stems from ZnO's typical wide band gap property, indicating that the material has begun to absorb UV light strongly. Furthermore, increasing the number of ZnO layers

also increases the maximum absorption values. ZnO nanoparticles, employed as photon-scattering centers in the composite, increase the absorption values in Region-II (λ >250nm).

Except for pure copolymer (PMMA-co-PEA), ZnO-doped nanocomposites exhibit very similar absorption coefficients and a decreasing behavior in the region after 400 nm (visible light). These results demonstrate that increasing the concentration of ZnO dopants effectively preserves the high optical transparency of the nanocomposite in the visible spectrum while simultaneously enhancing its UV-shielding efficiency.

4.2. Absorption (*α*) and Extinction (*k*) Coefficients

The band gap energy (E_g) is a critical indicator of a material's suitability for optoelectronic implementations. Consequently, the optical absorption coefficient (a) serves as a constituent parameter for characterizing this energy and detecting structural transitions within the band system, as it quantifies the material's capacity for wavelength-specific photon absorption[11]. The absorption coefficient provides a robust basis for comparison across materials with different thicknesses and is characterized by the following relationship [12]:

$$\alpha = \frac{(2.303)A}{d} \tag{2}$$

in which A indicates the absorbance and d signifies the thickness of the sample. The wavelength dependence of the optical absorption coefficient for PMMA-co-PEA/ZnO nanocomposites is illustrated in Figure 6. Notably, the evolution of the absorption coefficient in Figure 5 is consistent with the absorbance characteristics presented in Figure 4 .

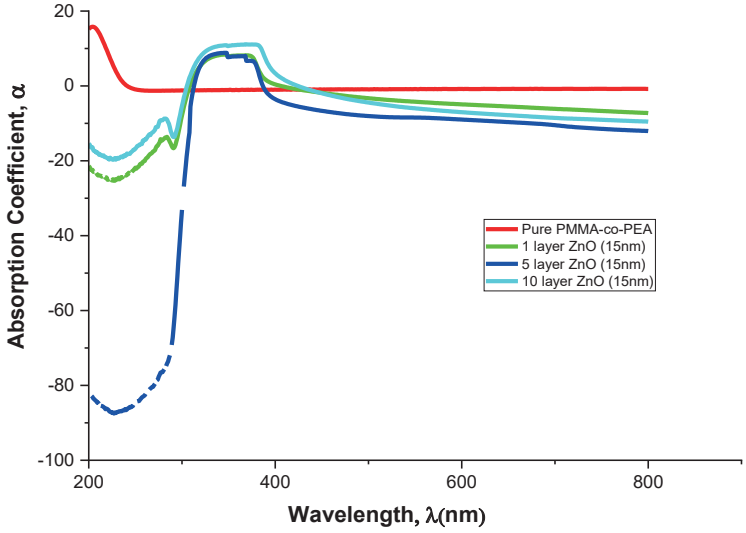

Figure 5: Optical absorption coefficient (α) of PMMA-co-PEA/ZnO(15nm) nanocomposite films for various layers of ZnO.

The optical properties of the samples were evaluated in terms of extinction coefficient (k), which governs the dissipation of electromagnetic energy within the medium. This parameter, corresponding to the imaginary part of the complex refractive index, reflects the probability of electronic transitions and total attenuation per unit thickness. The calculation of (k) was performed using the relationship expressed below[13];

$$k = \frac{\alpha\lambda}{4\pi} \tag{3}$$

Where (a) is the absorption coefficient and (λ) is the photon wavelength, Fig. 6 presents the extinction coefficient (k) as a function of wavelength for the PMMA-co-PEA / ZnO nanocomposite system.

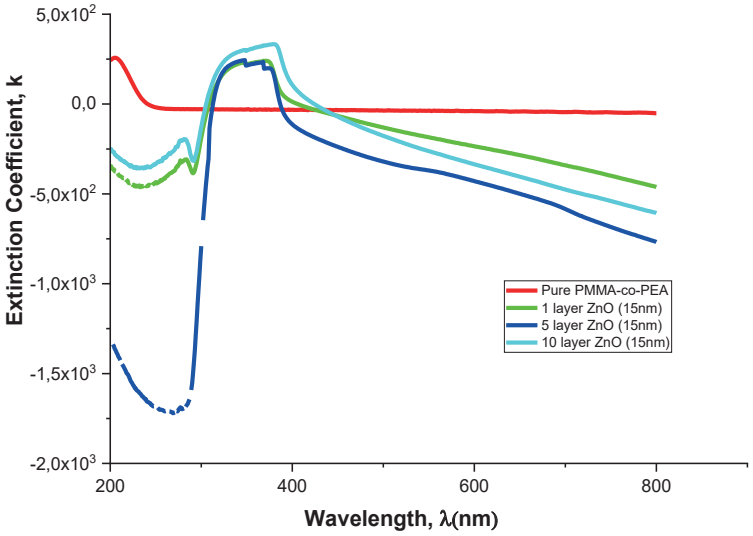

Figure 6: The variation of the damping coefficient of PMMA-co-PEA/ZnO nanocomposite films with wavelength.

As shown in Fig.6, in *Region II* (λ>250nm), the extinction coefficient *k* exhibits a linear decrease with decreasing wavelength and then

and then exhibit an upward trend in *Region I* (λ<250nm). The observed enhancement in the absorption coefficient with thicker ZnO layers can be ascribed to the intensified interaction between the incident photons and the material, resulting in energy attenuation [14].

4.3 Estimation of Optical Band Gap Energy

The band gap energy of a semiconductor represents the minimum energy required to transition an electron from the valence band to the conduction band. Precise determination of this value is essential for predicting the light-induced processes in semiconductors, particularly when evaluating their efficiency in photocatalytic applications. [15].

4.3.1 Tauc Method

The Tauc method proceeds from the assumption that the energy-dependent absorption coefficient, (a) is governed by the following relation[15]:

$$\alpha h\nu = B(h\nu - E_g)^m \quad (4)$$

In this expression, α represents the absorption coefficient, $(h\nu)$ denotes the photon energy, B is a proportionality constant, and E_g signifies the optical band gap between the valence and conduction bands. The exponent The term m classifies the electronic transition type; specifically, Equation (4) describes direct allowed transitions when m = 1/2 and indirect allowed transitions for m = 2. These transitions are graphically represented in Figure 7 and Figure 8, respectively.

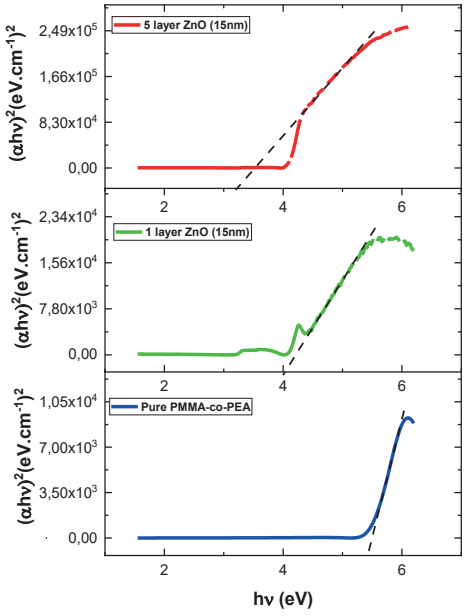

Figure 7: Tauc plots $(\alpha h\nu)^2$ vs. $(h\nu)$ for PMMA-co-PEA/ZnO nanocomposite films to evaluate the direct optical band gap energies (E_d).

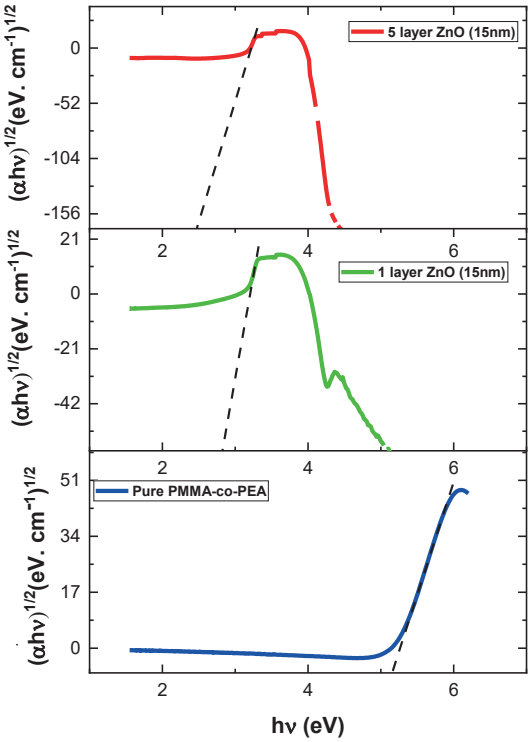

Figure 8: Tauc plots $(\alpha h\nu)^{1/2}$ vs. $(h\nu)$ for PMMA-co-PEA/ZnO nanocomposite films to evaluate the indirect optical band gap energies (E_i).

Both plots exhibit well-defined linear regions at higher photon energies, indicating that the optical band gap for both direct (E_d) and indirect (E_i) allowed transitions can be determined for the PMMA-co-PEA/ZnO nanocomposite thin films. These values were derived by extrapolating the linear portions of the curves in Fig. 7 and Fig. 8 to the ($h\nu$) axis intercept. The resulting E_d and E_i values are summarized in Table 1.

Both graphs have smooth linear regions on the right hand side. This shows that, both direct (E_d) and indirect (E_i) allowed transition band gap energies can be calculated for PMMA-co-PEA/ZnO nanocomposite thin films. E_d and E_i optical band gap energies were calculated from the cut-off point at the ($h\nu$) axis of the linear straight lines in Fig. 7 and Fig. 8. The obtained E_d and E_i values are given in Table 1.

Table 1. Investigation of the Urbach energy (E_u), refractive index (n), and optical bandgap energies of PMMA-co-PEA/ZnO nanocomposite films, determined via Tauc and Absorption Spectrum Fitting (ASF) methods.

ZnO(15nm) layer number	Tauc Method					ASF Method				
	E_d(eV)	E_i(eV)	n_d	n_i	E_u(eV)	E_d(eV)	E_i(eV)	n_d	n_i	E_u(eV)
0	5,42	5,16	1,94	1,97	5,14	5,43	5,16	1,94	1,97	5,14
1	4,03	2,6	2,16	2,51	3,05	4,02	2,65	2,17	2,49	3,04
5	3,21	2,47	2,34	2,56	3,2	3,2	2,42	2,57	2,57	3,2

4.3.2 Absorbance Spectrum Fitting Method (ASF)

Precise quantification of film thickness is fundamental to the Tauc method for determining the optical band gaps of composite samples. Furthermore, to enhance the accuracy of the absorption coefficient (a), appropriate corrections must be applied to account for reflective losses. Souri and Shomalian introduced an optimized analytical expression by combining the Beer-Lambert law and Tauc formalism, specifically designed to minimize the impact of these two factors on optical band gap determination[16]. Using the ASF procedure, Eq.(4) can be rewritten as the following [17], [18], [19], [20],[16]:

$$A(\lambda) = B_1\lambda \left[\frac{1}{\lambda} - \frac{1}{\lambda_g}\right]^m + B_2 \quad (5)$$

Where A(λ) is the measured absorbance value for λ wavelength, λg, is the wavelength corresponding to the optical band gap, $B_1=[B(hc)^{m-1}d/2{,}303]$, *c* is the speed of the light, *h* is Planck's constant, *d* is the thickness of sample and is a constant which takes into account the reflection. This method utilizes absorbance spectra rather than the absorption coefficient to determine optical properties. Similar to the Tauc approach, different values

of m are evaluated to find the optimum fit. The value of λ_g is then extracted from the plot of $(A\lambda^{-1})^{1/m}$ versus λ^{-1}. As illustrated in Figures 9 and 10, λ_g for direct *(m =1/2)* and indirect *(m = 2)* transitions is determined by the intersection of the linear extrapolation with the photon energy axis. Table 1 lists the band gap values (E_g) of the PMMA-co-PEA/ZnO nanocomposite films, as derived from Equation (6).

$$E_g = \frac{1239{,}83}{\lambda_g} \tag{6}$$

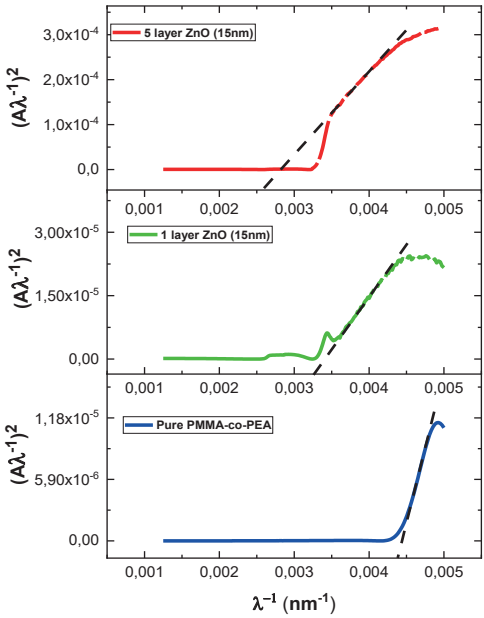

Figure 9: To determine the allowed direct transition energies (E_d) of PMMA-co-PEA/ZnO nanocomposite films, the Absorption Spectrum Fitting (ASF) method was employed by plotting $(A\lambda^{-1})^2$ versus (λ^{-1}).

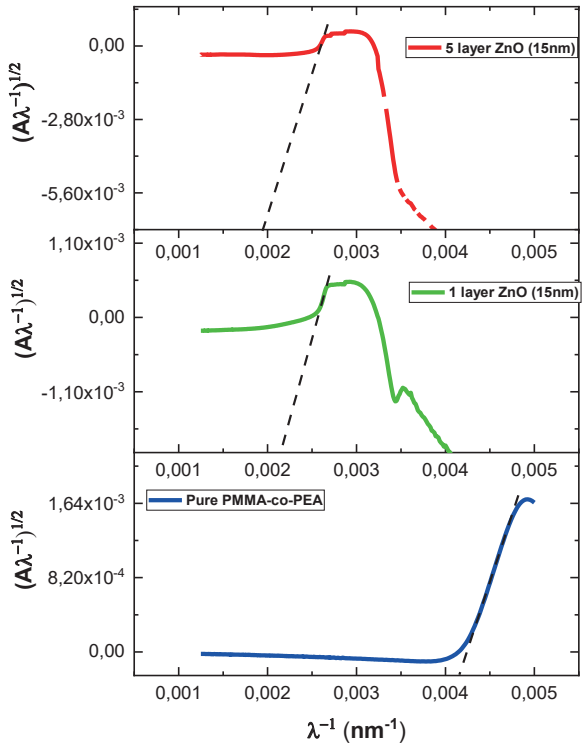

Figure 10: To determine the allowed indirect transition energies (E_i) of PMMA-co-PEA/ZnO nanocomposite films, the Absorption Spectrum Fitting (ASF) method was employed by plotting $(A\lambda^{-1})^{1/2}$ versus (λ^{-1}).

As shown in Table 1, the optical band gap values derived from the Tauc and ASF methods exhibit strong mutual agreement. For both models, the E_d and E_i transition energies of the PMMA-co-PEA/ZnO nanocomposite films decrease as the ZnO content increases. This trend is ascribed to the proliferation of localized energy levels within the band gap, which act as localized states that effectively reduce the optical band gap by introducing intermediate energy levels between the valence and conduction bands. [21]. This result is expected, as the incorporation of conductive additives into the insulating PMMA-co-PEA matrix enhances the overall conductivity of the bio-nanocomposites, transitioning them into a semi-conductive state. As illustrated in Table 1, the PMMA-co-PEA/ZnO nanocomposite films exhibit lower energy requirements for E_i compared to E_d. These findings align with

similar studies in the literature, where E_i values were consistently found to be lower than E_d [22]. Furthermore, the optical band gap energy (E_g) is influenced by several critical parameters, including material crystallinity, structural anisotropy, and temperature, as well as the influence of external factors such as pressure and electromagnetic fields[23].

4.4 Estimation of Urbach Energy

Urbach energy (Eu) is a parameter that prevents the absorption of low-energy photons, especially in tuned or amorphous semiconductors, just below the fundamental absorption limit. Simply put, it is a measure of the amount of order in a material's crystal structure. In an ideal crystal structure, there is a sharp gap (band gap) between energy bands. However, in real materials (especially polymer-inorganic nanocomposites like the one you're working with), "tails" form at the ends of the valence and conduction bands due to structural defects, thermal vibrations, or impurities. These are called Urbach tails. For various amorphous and crystalline materials, the optical absorption coefficient (a) near the fundamental absorption edge exhibits an exponential dependence on photon energy (hν), adhering to the empirical relation established by Urbach [24].

$$\alpha = \alpha_0 \exp\left(\frac{h\nu}{E_u}\right) \tag{7}$$

In accordance with Eq. (7), the Urbach energy (Eu) is derived from the reciprocal slope of the linear portion of the lnα vs. (hν) plot. Figure 11 illustrates the variation of lnα as a function of photon energy (hν) for the PMMA-co-PEA/ZnO nanocomposites, with the resulting Eu values, derived from these slopes, summarized in Table 1.

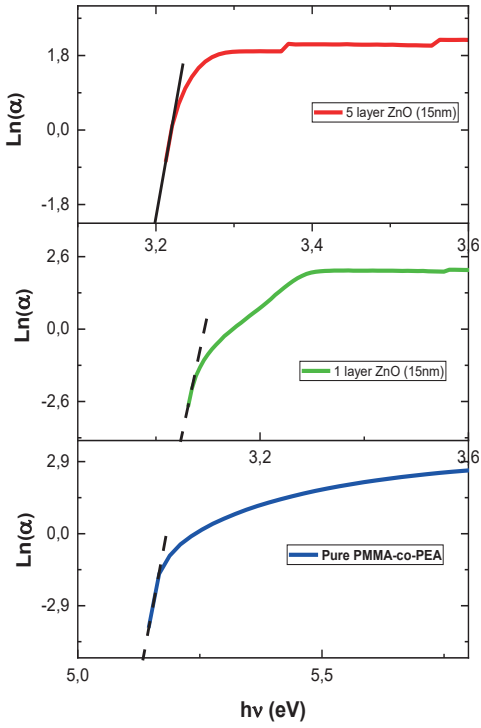

Figure 11: (lnα) versus (hν) plots of the PMMA-co-PEA/ZnO nanocomposite films. The Urbach energy (E_u) for each composite was derived by calculating the slope of the linear portion of the absorption edge.

The Urbach energy (E_u) may also be derived using direct absorption data, eliminating the dependency on film thickness. Following the ASF method, Equation (7) is expressed as:

$$A(\lambda) = C \exp\left(\frac{hc}{E_u}\right) \quad (8)$$

Here, C is (α_0 d/2,303). The variation of ln(A) with respect to λ^{-1} for nanocomposites is given in Figure 12. Urbach energy values were derived from the slope of the ln(A)- λ^{-1} graph using equation (8), and the obtained data are given in Table I.

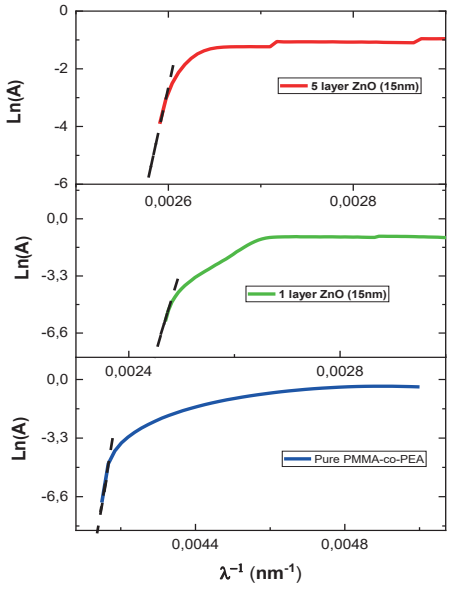

Figure 12: (lnA) versus (λ^{-1}) plots of the PMMA-co-PEA/ZnO nanocomposite films. The Urbach energy (E_u) for each composite was derived by calculating the slope of the linear portion of the absorption edge.

A comparative analysis of Urbach energy (E_u) values calculated via the Tauc and Absorption Spectrum Fitting (ASF) methods reveals nearly congruent results. It is observed that an increase in the number of ZnO layers correlates with a progressive rise in (E_u) values. This elevation in (E_u) indicates heightened structural amorphousness, confirming that the incorporation of additional ZnO layers disrupts the crystalline order within the PMMA-co-PEA matrix.

4.5 Determination of Refractive Indices

For the nanocomposite films, the refractive index (n) was derived as a function of the optical band gap (Eg), which was determined via both Tauc and Absorption Spectrum Fitting (ASF) methods using Equation (9)[25].

$$\frac{n^2-1}{n^2-1} = 1 - \sqrt{\frac{E_g}{20}} \qquad (9)$$

In this context, n represents the linear refractive index at λ_g. The dependence of the refractive index of PMMA-co-PEA/ZnO nanocomposite films on the ZnO layer thickness is presented in Table 1. Notably, the results obtained from both methodologies demonstrate high consistency.

An increase in the ZnO layer numbers enhances the density of scattering centers within the nanocomposite, promoting multiple scattering phenomena. This phenomenon induces a reduction in the effective phase velocity of light as it propagates through the medium, thereby leading to a corresponding increase in the refractive index (n = c/v).

5. Conclusion

Electronic Absorption Spectroscopy (UVV) was employed to evaluate the optical parameters of PMMA-co-PEA nanocomposite films as a function of the number of spin-coated ZnO layers. The optical band gap energy (E_g) was determined through both Tauc and Absorption Spectrum Fitting (ASF) methods. The results obtained from both analytical approaches exhibited high consistency, yielding nearly identical (Eg) values. Furthermore, increasing the ZnO content in the composites increased photon scattering, which led to an increase in refractive indices (n). This increase in refractive indices is considered promising for optoelectronic applications of these nanocomposite films.

Acknowledgments

This study was funded by the Scientific Research Projects (BAP) unit of Mimar Sinan Fine Arts University.

I would also like to thank Prof. Dr. Demet AKTAŞ for the optical analyses carried out in the Spectroscopy Research Laboratory of the Physics Engineering Department at Istanbul Technical University (ITU) and Istanbul Arel University Polymer Technologies and Composite Application and Research Center (POTKAM) for the SEM imaging analyses.

REFERENCES

[1] Shanghua, L., Meng Meng, L., Muhammet S. Toprak, Do Kyung Kim & Mamoun Muhammed.(2010). (2010) Nanocomposites of polymer and inorganic nanoparticles for optical and magnetic applications. Nano Reviews, 1:1, 5214, DOI: 10.3402/nano.v1i0.5214

[2] Jeon, I.Y., and Baek, J.B.(2010). Nanocomposites Derived from Polymers and Inorganic Nanoparticles, Materials, 3(6), 3654-3674; https://doi.org/10.3390/ma3063654

[3] Parola, S., Julián-López, B., Carlos, L.D., Sanchez, C. (2016) .Optical Properties of Hybrid Organic-Inorganic Materials and their Applications. Adv. Funct. Mater., 26, 6506–6544, DOI: 10.1002/adfm.201602730

[4] Sanchez, C., Julián, B., Belleville, P., Popall, M. (2005). Applications of hybrid organic-inorganic nanocomposites. J. Mater. Chem. 2005, *15*, 3559–3592.

[5] Chomski E., Ozin G. A.(2000). Panoscopic Silicon—A Material for "All" Length Scales. Adv. Mater., 12, 1071-1078, DOI: 10.1002/1521-4095(200007)12:143.0.CO;2-J

[6] Moon J. H., Kim S., Yi G. R., Lee Y. H., Yang S. M. (2004). Fabrication of Ordered Macroporous Cylinders by Colloidal Templating in Microcapillaries. Langmuir, 20, 2033-2035, DOI: 10.1021/la0358015

[7] Caseri, W. (2009). Inorganic nanoparticles as optically effective additives for polymers. Chem Eng Comm. 196: 549–72. https://doi.org/10.1080/00986440802483954

[8] Nunes, P., Fernandes, B., Fortunato, E., Vilarinho, P., Martins, R. (1999). Performance presented by ZnO thin films deposited by spray pyrolysis. Thin Solid Films, 337: 176, https://doi.org/10.1016/S0040-6090(98)01394-7

[9] Chopra, L., Major, S., Pandya, D. K., Rastogi, R. S., Vankar, V.D. (1983). Thermal device applications. Thin Solid Films, 1021: 1-4

[10] Zainudin, A.A., Fen, Y.W., Yusof, N.A., Oma N.A.S.(2017). Structural, optical and sensing properties of ionophore doped graphene based bionanocomposite thin film, Optik, 144, pp. 308-315, 10.1016/j.ijleo.2017.07.001

[11] Kurt, A., Demirelli, K. (2010). A study on the optical properties of three-armed polystyrene and poly(styrene-b-isobutyl methacrylate). Polym. Eng. Sci., 50 (2010), pp. 268-277, 10.1002/pen.21530

[12] Al-Ani, S.K.J. (1993). Determination of the optical gap of amorphous materials, Int. J. Electronics, 75, pp. 1153-1163, 10.1080/00207219308907191

[13] Abdullah, O.G., Aziz, S.B., Rasheed, M.A. (2017). Effect of silicon powder on the optical characterization of Poly(methyl methacrylate) polymer composites. J. Mater. Sci: Mater. Electron, 28, pp. 4513-4520, 10.1007/s10854-016-6086-9

[14] Rabee, B.H., Al-Kareem, B.A. (2016). Study of Optical Properties of (PMMA-CuO) Nanocomposites. Int. J. Sci. Res., 5, pp. 2319-7064.

[15] Majid, S.S., Faisal, S., Gondal, M.A., Ahad, A., Mustaqeem, M., Khandy, S.A. (2006). Chang-Tang Chang. Structural–Electronic Coupling in BaAl2O4 Drives High-Efficiency Photothermal Water Purification. Langmuir, 42 (9), 6936-6945. https://doi.org/10.1021/acs.langmuir.5c06568

[16] Souri, D., and Shomalian, K.(2009). Band gap determination by absorption spectrum fitting method (ASF) and structural properties of different compositions of (60-x) V_2O_5–$40TeO_2$–xSb_2O_3 glasses. J. Non-Cryst. Solids, 355, pp. 1597-1601, 10.1016/j.jnoncrysol.2009.06.003

[17] Rao, S.L.S., Ramadevudu, G., Shareefuddin, Md., Hameed, A., Chary, M.N, Rao, M.L.(2012). Optical properties of alkaline earth borate glasses. Int. J. Eng. Sci. Technol., 4, pp. 25-35, 10.4314/ijest.v4i4.3

[18] Chopra, N., Mansingh, A., Chadha, G.K.(1990). Electrical, optical and structural properties of amorphous $V_2O_5TeO_2$ blown films. J. Non-Cryst. Solids, 126, pp. 194-201, 10.1016/0022-3093(90)90819-8

[19] Ghobadi, N.(2013). Band gap determination using absorption spectrum fitting procedure Int. Nano Lett., 3, 10.1186/2228-5326-3-2

[20] Rammah, Y.S., El-Sersy, A.R., El-Mesady, I.A., El-Agawany, F.I. (2019). Modifications of Structural, Optical, and Carbonaceous Clusters in Neutron Irradiated $C_{12}H_{18}O_7$ Polymeric Detector. J. Rad. Nucl. Appl., 4, pp. 91-100, 10.18576/jrna/040203

[21] Rabee, B.H., Al-Kareem, B.A.(2016). Study of Optical Properties of (PMMA-CuO) Nanocomposites. Int. J. Sci. Res., 5, pp. 2319-7064

[22] Patel, G., Sureshkumar, M.B., Patel, P.(2011). Effect of TiO_2 on Optical Properties of PMMA: An Optical Characterization. AMR, 383–390, pp. 3249-3256, 10.4028/www.scientific.net/AMR.383-390.3249

[23] Ziman, J.M. (1979). In Principles of the Theory of Solids. Cambridge University Press, Cambridge

THE ROLE OF TOPOLOGICAL THEOREMS IN MODERN MATHEMATICS: MATHEMATICAL SIGNIFICANCE, APPLICATIONS, AND INTERDISCIPLINARY CONNECTIONS*

Güzide Şenel[1]

1 Prof. Dr. Faculty of Science, Department of Mathematics, Amasya University, Amasya, Turkey, g.senel@amasya.edu.tr
ORCID: 0000-0003-4052-2631.
* This work is derived from theses. Thesis Bibliographic Information: This work is derived from theses. Thesis Bibliographic Information: Doctorate Gazıosmanpasa Unıversıty/ Instıtute Of Scıence/Mathematıcs (Dr) Thesis Title: Elastic Metric Spaces (2013) Thesis Supervisor: (Naım Çağman, Serkan Karataş)

1. Introduction

Topology is concerned with the qualitative properties of spaces that remain invariant under continuous transformations. Unlike classical geometry, which focuses on rigid structures and metric properties, topology studies global features such as connectedness, compactness, and continuity.

The modern development of topology can be traced to the work of **Henri Poincaré**, whose seminal paper *Analysis Situs* laid the foundations for algebraic topology by introducing algebraic invariants such as the fundamental group and homology concepts. (2013)

Throughout the twentieth century, topology expanded into several interconnected research areas, including:

- general topology
- algebraic topology
- differential topology
- geometric topology

These fields collectively contribute to the classification and structural understanding of mathematical spaces.

In addition to its theoretical significance, topology has increasingly influenced other scientific disciplines. Topological methods are now widely used in:

- theoretical physics
- data science
- robotics
- network theory
- biological modeling

The objective of this study is to examine the role of fundamental topological theorems within modern mathematical research while highlighting their interdisciplinary impact.

a) Structural Invariants and Classification Problems

A central objective of topology is the identification of properties that remain invariant under continuous deformations. These properties, known as **topological invariants**, play a crucial role in distinguishing and classifying spaces.

Among the most important invariants are:

- Euler characteristic
- homology groups
- cohomology groups
- fundamental groups

The classification theorem for compact surfaces provides a classical example of the power of such invariants. According to this theorem, every compact connected surface is homeomorphic to a sphere with a certain number of handles or cross-caps.

This result represents one of the earliest successful classification results in topology and serves as a prototype for higher-dimensional classification problems.

More generally, classification problems in topology involve determining when two spaces are equivalent under homeomorphisms or homotopy equivalences. These problems have led to the development of powerful algebraic techniques that transform geometric problems into algebraic ones.

b) Fixed Point Theorems and Their Analytical Significance

Fixed point theory occupies a central position in modern topology and nonlinear analysis. Fixed point theorems assert that under certain conditions a continuous mapping from a space to itself must possess a point that remains invariant under the mapping.

One of the most fundamental results in this area is the **Brouwer Fixed Point Theorem**, which states that every continuous mapping from a compact convex subset of Euclidean space into itself has at least one fixed point.

Fixed point theory plays an essential role in the study of nonlinear equations and dynamical systems. In particular, it provides tools for establishing the existence of solutions to differential and integral equations. (routledge.com)

Similarly, the **Banach Fixed Point Theorem**, formulated within metric spaces, provides a constructive approach to proving existence and uniqueness of solutions for various mathematical models.

Modern developments in topological fixed point theory have extended these ideas to multivalued mappings, differential inclusions, and topological vector spaces. (link.springer.com)

Comprehensive treatments of these developments can be found in several monographs that connect fixed point theory with nonlinear functional analysis and topology. (Springer)

c) Homotopy Theory and Algebraic Topology

Homotopy theory represents one of the most powerful frameworks in algebraic topology. The basic idea is to classify spaces according to the continuous deformations of maps between them.

Two continuous functions are said to be homotopic if one can be continuously deformed into the other. This notion leads to the definition of homotopy groups, which capture fundamental topological properties of spaces.

The fundamental group, introduced by Poincaré, provides one of the earliest examples of a homotopy invariant.

Homology theory further extends these ideas by associating algebraic structures—typically groups—with topological spaces. These invariants allow complex geometric objects to be studied using algebraic methods.

One of the most famous problems associated with these concepts is the **Poincaré Conjecture**, which asks whether every closed simply connected three-dimensional manifold is homeomorphic to the three-dimensional sphere.

The conjecture was solved by Grigori Perelman in the early 2000s using Ricci flow techniques developed by Richard Hamilton.

This achievement represents one of the most important breakthroughs in modern geometric topology.

d) Duality Principles in Topology

Duality principles reveal deep symmetries within topological spaces. One of the most fundamental examples is **Poincaré Duality**, which establishes an isomorphism between the homology and cohomology groups of compact orientable manifolds.

Duality theorems provide powerful tools for understanding global geometric structures and have influenced many areas of mathematics, including algebraic geometry and differential geometry.

These principles reveal that local geometric information can often be translated into global topological invariants, providing deeper insights into the structure of manifolds.

2. Applications of Soft Topology in Science and Technology

Although topology is traditionally considered a branch of pure mathematics, many of its ideas have become essential tools in applied sciences.

2.1 Topological Data Analysis

Topological data analysis (TDA) has emerged as a powerful methodology for extracting structural information from complex data sets. Techniques such as persistent homology enable researchers to detect hidden geometric patterns within high-dimensional data.

2.2 Physics and Cosmology

Topology plays a crucial role in modern theoretical physics. In general relativity, spacetime is modeled as a differentiable manifold, allowing topological techniques to be applied to gravitational models.

Topological methods are also central to research in quantum field theory and condensed matter physics.

2.3 Robotics and Motion Planning

In robotics, the configuration space of a mechanical system forms a topological space whose structure determines the feasible motions of the system.

Understanding the topology of configuration spaces is therefore essential for developing collision-free motion planning algorithms.

2.4 Biological and Chemical Systems

Topological methods have also been applied in molecular biology and chemistry. Knot theory has been used to analyze the structure of DNA molecules and the topology of protein folding.

3. Some Topological Theorems in Modern Mathematics

Definition : For given Cartesian coordinate system, the set of points on an n-dimensional unit sphere with radius 1 that are at a distance of 1 from the origin is given.

S^n={$x \in \mathbb{R}^{n+1} : \| x \| = 1$}.

as follows :

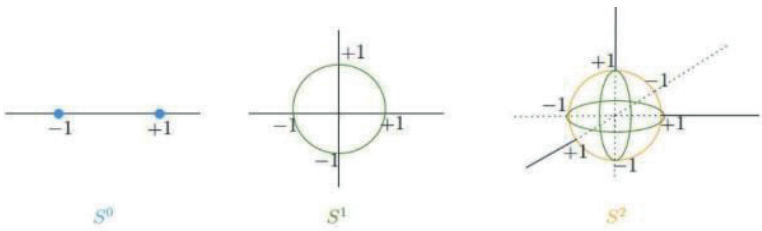

Example: $(\mathbb{R}, U)$The subspace reduced to a set $(S^0, U_{S^0})$from its usual space $S^0$is a disjoint space.

Example: $(\mathbb{R}, \leftarrow D)$The open sets of the subspace reduced $(\mathbb{N}, \tau_{\mathbb{N}})$from the left ray space to the set of natural numbers $\mathbb{N}$ are the closed sets of the topological space.

The vast majority of definitions, theorems, and examples used in this study are cited from source number 21.

Theorem: Let be (X, τ)a topological space and be a subspace $A \subset X$ of (A, τ_A). Then the following expressions hold:

(i) B is a base of the family topologyτ

$$B_A = \{A \cap B : B \in B\}$$

the family $\tau_A$topology.

(ii) A sub-base of the S family topology τ is

$$S_A = \{A \cap S : S \in S\}$$

the family $\tau_A$topology.

(iii) For each $x \in A$ point

$$V_A(x) = \{A \cap V : \in V_{(x)}\}$$

In terms of (A, τ_A)family $x \in A$, it is the family of the neighborhoods in its spatial context.

(iv) For each $x \in A$ point

$$G_A(x) = \{A \cap W : W \in G_{(x)}\}$$

His family It is a basis for the neighborhoods $x \in A$ of a point (A, τ_A)in space.

Proof . (i)$T \in \tau_A$ let it be Let's show T that a set $B_A$can be written as a union of sets belonging to a family of sets.$T \in \tau_A$

$T \in \tau_A \Longrightarrow \exists U \in \tau \ni T = A \cap U$

$\Rightarrow T = A \cap \left(\cup_{(i\in I)} B_i\right)\ldots(U \in \tau \Rightarrow U\tau = \cup_{i\in I} Bi \ni B_i \in B)$

$\Rightarrow T = \cup_{i\in I} (A \cap B_i) \ldots (i \in I, A \cap B_i \in B_A)\ldots(i \in I, A \cap B_i \in B_A)$

In hand It is done .

(ii)$T \in \tau$ Let be a set of finite intersections of sets belonging to the family of sets S_A.T combination aspect that it can be written let's show $T \in \tau$ for

$$T \in \tau_A \Rightarrow \exists U \in \tau \ni T = A \cap U$$

$$\Rightarrow A \cap \left(\cup_{i\in I} \left(\cap_{j=1}^{n} S_{ji}\right)\right)\ldots\left(U \in \tau \Rightarrow U = \left(\cup_{i\in I} \left(\cap_{j=1}^{n} S_{ji}\right)\right) \ni S_i \in B\right)$$

$$\Rightarrow T = \left(\cup_{i\in I} \left(\cap_{j=1}^{n} (A \cap S_{ji})\right)\right)\ldots \qquad (i \in I, A \cap S_{ji} \in B_A)$$

In hand It is done .

(iii) $x \in A$ Let be a set. $A \cap V$ For a point $(A, \tau_A)$of a set $x \in A$ to have a neighborhood in space, it must hold for at least one $U \in \tau_A$open set $x \in U \subset A \cap V$.$V \in V_{(x)}$

$V \in V_{(x)} \Rightarrow \exists U \in \tau \ni x \in U \subset V$

$$\Rightarrow x \in A \cap U \subset A \cap V \ldots(B \subset C \Rightarrow A \cap B \subset A \cap C)$$

$$\Rightarrow A \cap V \in V_{(x)}\ldots(U \in \tau, A \cap U \in \tau_A)$$

In hand It is done .

(iv) $x \in A$ Let the family G_A have a neighborhood basis in the space $x \in A$ of the point such that for (A, τ_A)every $A \cap V$ neighborhood of $x \in W \subset A \cap V$ the point in the space $(A, \tau_A)$of the family $x \in A$ there exists at least one $W \in G_A$.$V \in V_{(x)}$

$$V \in V_{(x)} \implies \exists U \in \tau \ni x \in U \subset V$$

$$\implies \exists W \in G \ni x \in W \subset V \ldots (G \text{ komşuluk tabanı})$$

$$\implies x \in A \cap W \subset A \cap V \ldots (B \subset C \implies A \cap B \subset A \cap C)$$

$$\implies A \cap W \in G_A(x) \ldots \left(A \cap V \in V_{(x)}\right)$$

In hand It is done . (21)

Example: $(\mathbb{Z}, U_z)$ in space One $x \in \mathbb{Z}$ Let's examine the neighborhoods at that point. $(\mathbb{R}, U)$Since for the open set $x \in U \subset U$ from the space, $U = \left[x - \frac{1}{2}, x + \frac{1}{2}\right] \in U$it $U \in V_{(x)}$becomes. $\mathbb{Z}$ If the intersection of the set and is taken,

$$x \in \mathbb{Z} \cap U \subset \mathbb{Z} \cap U$$

And

$$\mathbb{Z} \cap U = \{x\}$$

From what will happen $\{x\} \in V_Z(x)$ in hand We do . One neighborhood every cluster neighborhood because $x \in V$ will be In this way, every $V \subset \mathbb{Z}$ set has a neighborhood.

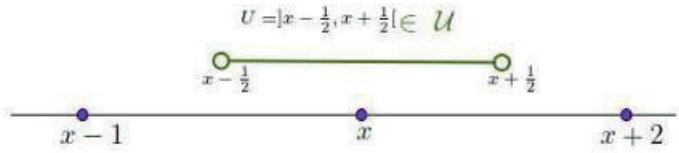

$$\mathbb{Z} \cap U \in V_{(x)} = \{x\} \in V_Z(x)$$

Theorem: Let (X, τ)a topological space $A \subset X$ be given a subspace of a $T \subset A$ given set. For a subspace $(A, \tau_A)$of a given set $(A, \tau_A)$to be a closed set, it is a necessary and sufficient condition $T = A \cap F$ that it has at least one $F \subset X$ closed set.

$$T \subset A, T \in \tau_A^t \iff \exists F \in \tau^t \ni T = A \cap F$$

Proof . Let the set be a closed set in $\Longrightarrow$ T the set $(A,\ \tau_A)$space. From this...

$$T \in \tau_A^t \ \Longrightarrow\ A - T = \tau_A$$

$$\Longrightarrow \exists U \in \tau\ \ni A - T = A \cap U$$

In hand It is done .

$$(X, \tau)$$

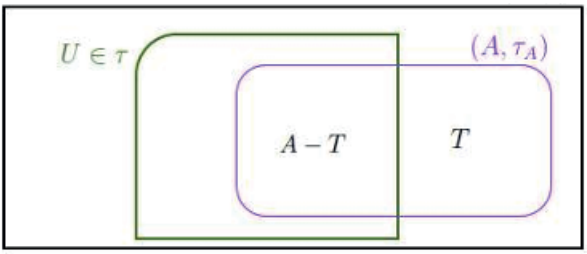

$$T_{\in \tau_A^t} = A \cap (X_{\in \tau^t} - U)$$

T the set $T = A \cap (X - U)$as follows. From this, $U \in \tau$ since T for , $X - U \in \tau^t$the set $(X, \tau)$is obtained as the intersection of $T \in \tau_A^t$a closed set of the set space and set A. As a result $F = X - U$, it becomes.

Let's say $\Longleftarrow F \in \tau^t$it's a closed set $T = A \cap F$. From here:

$$(X, \tau)$$

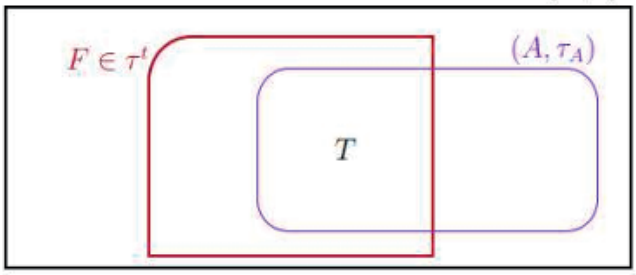

$$A_{\in T_A} - T = A \cap (X_{\in \tau} - F)$$

$F \in \tau^t \Longrightarrow (X - F) \in \tau$

$A - T = A - (A \cap F)$...$(T = A \cap F)$

$$= A \cap (X - F)$$

$$\Longrightarrow A - T \in \tau_A ... (X - F \in \tau_A^t)$$

$$\Longrightarrow T \in \tau_A^t$$

In hand It is done.

Lemma : (X, τ)Given (X, τ)a topological space, $B \subset A \subset X$ the topology reduced from its topology to the set B $(A, \tau_A)$is equal to the topology reduced from its topology to the set B.

every $U \in \tau$ open set such that, **the proof is :**$(A \cap B) \cap U \neq \emptyset$

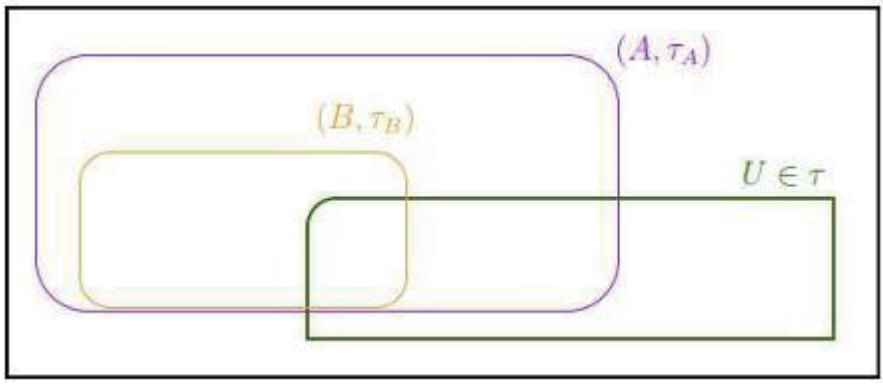

$$(B \cap U_{\in\tau})_{\{\in\tau_B} = \left(B \cap (A \cap U)_{\in\tau_A}\right)_{\{\in(\tau_A)_B}$$

from what it is $\tau_B = (\tau_A)_B$.

Definition: (X, τ)A property (p) in a topological space is called $A \subset X$ **an inherited property if it exists in the space** for every subset of (A, τ_A)that space .

Example: $\left(X, \tau = P(X)\right)$For every disjoint space and $A \subset X$ subset$x \in A$

$$A \cap \{x_{\in\tau}\} = \{x\} \in \tau_A$$

It (A, τ_A) will be a discrete space. Consequently, the property of being a discrete space is an inherited property. (21)

Example: $(\mathbb{R}, U)$in space

$$A1 =]1,2[,\ \ A2 =]1,2],\ \ A3 = [1,2[,\ \ A4 = [1,2]$$

of the sets .

• $1 < x < 2$ for $x \neq 1$ And it exists $x \neq 2$ as it is $d(1,x) = \varepsilon$and $d(x,2) = \delta$will be $\varepsilon, \delta \in \mathbb{R}$.$U = \ \ ]\ x - \frac{\varepsilon}{2}, x + \frac{\delta}{2}[\in U$ for the $U \subset A_1$open set

$A_1^\circ =]1,2\ [$

obtained .

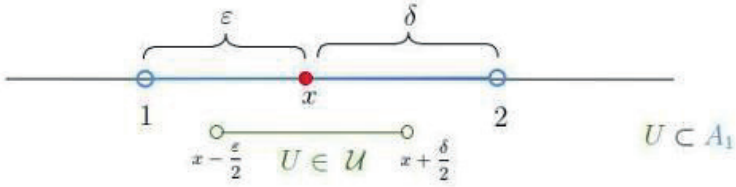

• $1 < x < 2$ for $x \in A_2^\circ$is obtained.$x = 1$ Let's examine $\varepsilon, \delta > 0$ this point .

$U =]x - \varepsilon, , x + \delta[\in U$ Since it is for the $x \notin A_2^\circ$open set $U \not\subseteq A_2$, it is true. As a result

$A_2^\circ =]1,2\ [$

It is obtained.

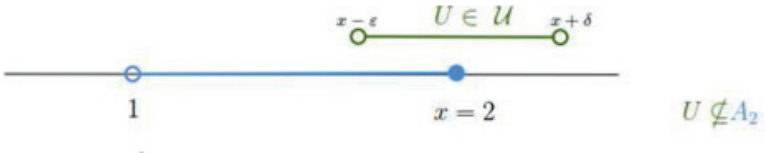

• $1 < x < 2$ for $x \in A_3^\circ$is obtained.$x = 1$ Let's examine this point .$\varepsilon, \delta > 0$ Since for the open set, $U \not\subseteq A_3$it $x \notin A_3^\circ$becomes. As a result$U =]x - \varepsilon, , x + \delta[\in U$

$A_3^\circ =]1,2[$

It is obtained.

• $1 < x < 2$ for $x \in A_4^\circ$It is obtained. Let $x_1 = 1$'s $x_2 = 2$examine the points. $\varepsilon, \delta > 0$ For open sets $U_1 \nsubseteq A_4] \; x_1 - \varepsilon, , x_1 + \delta[\; , \; U_1 =] \; x_1 - \varepsilon, , x_1 + \delta[\in U$ and $U_2 \nsubseteq A_4$since , it becomes. As a result$U_1 =$

$A_4^\circ =]1,2[$

It is obtained.

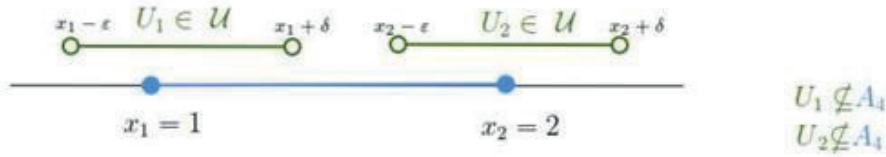

Conclusion: Different sets can have equal interior spaces.

Example: Let's examine the interior points of the set $(\mathbb{R}, U)$A = { 1,2} in space.

Solution:

$x_1 = 1$for $x_2 = 2$the points$\varepsilon, \delta > 0 \quad [\; x_1 - \varepsilon, x_1 + \delta$including $U_1 =]$

$U_2 =] \; x_2 - \varepsilon, x_2 + \delta[\in U$ for open sets $U_1 \not\subset A$and since it $x_1, x_2 \notin A$is. As a result

$$A^\circ = \emptyset$$

It is obtained.

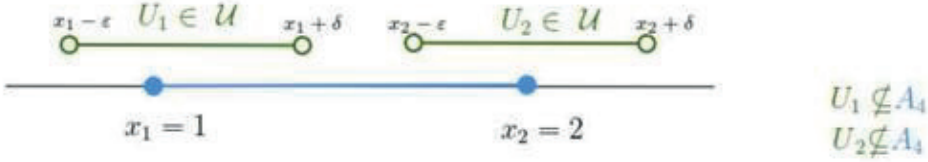

Conclusion: Since $(\mathbb{R}, U)$a finite set A in space is the union of a finite number of odd point sets, $(\mathbb{R}, U)$the set A in space is an empty set.

Example. $(\mathbb{R}, D)$ Let's examine the interior points of the sets $]A_2 = 2,3[, A_3 =]-\infty, 4$ in the space $A_1 = \{0,1\}$.

- $(\mathbb{R}, D)$In the space U=]- ∞ , λ [for an open set U $\nsubseteq A_1$and U $\nsubseteq A_2$since

$$A_1^{\circ} = A_2^{\circ} = \emptyset$$

4. The formal definition of a soft metric space and the difference between a soft metric topology and a fuzzy metric topology

Feature	**Soft Metric Topology**	**Fuzzy Metric Topology**
Foundation	**Soft sets**	**Fuzzy sets**
Uncertainty type	Parameter-based	Degree-based
Distance representation	Parameterized real numbers	Membership values in ([0,1])
Main function	(d_s(x,y,e))	(M(x,y,t))
Interpretation	Multiple criteria distances	Degree of closeness
Structure	Parameter dependence	Gradual truth values
Example meaning	Distance varies by parameter	Closeness varies by degree

Soft metric spaces are useful when:

- parameters are known
- uncertainty comes from multiple criteria.

Fuzzy metric spaces are useful when:

- closeness is inherently vague
- gradation of truth is needed.
- Soft metric topology generalizes metric spaces using parameterized distances.
- Fuzzy metric topology generalizes them using degrees of closeness in [0,1][0,1][0,1].

Both extend classical topology but model **different types of uncertainty**.

Conclusion

Topology has become one of the most influential branches of modern mathematics, providing a framework for studying qualitative properties of geometric and abstract structures. Since the pioneering contributions of Henri Poincaré at the end of the nineteenth century, topology has evolved into several major subfields including general topology, algebraic topology, and differential topology. These areas collectively provide powerful conceptual tools for understanding structural invariants of mathematical spaces.

The present study investigates the theoretical significance of fundamental topological results such as fixed point theorems, classification theorems, duality principles, and developments in homotopy theory. Particular emphasis is placed on their role in the structural analysis of mathematical spaces and their connections with other mathematical disciplines, including analysis, algebra, and differential geometry. Furthermore, the paper discusses the growing importance of topological methods in interdisciplinary contexts such as computer science, robotics, physics, and biological modeling.

The results of this analysis demonstrate that topology functions not only as a central theoretical discipline within pure mathematics but also as a powerful conceptual framework that facilitates the investigation of complex structures across multiple scientific domains.

Topology has become one of the most structurally unifying disciplines in modern mathematics. The study of topological invariants, fixed point

principles, homotopy theory, and duality results has significantly advanced our understanding of mathematical structures.

Beyond its theoretical contributions, topology has also proven to be a powerful interdisciplinary framework with applications in computer science, physics, biology, and engineering.

As modern science increasingly deals with complex and high-dimensional structures, topological methods are expected to play an even greater role in future research.

Keywords

Topology; Algebraic Topology; Fixed Point Theorems; Homotopy Theory; Duality Principles; Mathematical Structures; Interdisciplinary Applications

Funding: This work is supported by the author.
Ethical standard: This article does not contain any studies with human participants or animals performed by the author.

References

1. Poincaré, H. (1895). *Analysis Situs.*
2. Hatcher, A. (2002). *Algebraic Topology.* Cambridge University Press.
3. Munkres, J. (2000). *Topology.* Prentice Hall.
4. Lee, J. (2013). *Introduction to Smooth Manifolds.* Springer.
5. Milnor, J. (1963). *Morse Theory.* Princeton University Press.
6. Bott, R., Tu, L. (1982). *Differential Forms in Algebraic Topology*.
7. Spanier, E. (1966). *Algebraic Topology.*
8. Armstrong, M. (1983). *Basic Topology*.
9. Dugundji, J. (1966). *Topology*.
10. Willard, S. (2004). *General Topology.*
11. Engelking, R. (1989). *General Topology*.
12. May, J. P. (1999). *A Concise Course in Algebraic Topology.*
13. Ghrist, R. (2014). *Elementary Applied Topology.*
14. Brown, R. (2006). *Topology and Groupoids.*
15. Husemoller, D. (1994). *Fibre Bundles.*
16. Bredon, G. (1993). *Topology and Geometry.*
17. Birman, J. (1974). *Braids, Links and Mapping Class Groups.* (Vikipedi)
18. Granas, A., Dugundji, J. (2003). *Fixed Point Theory.* (Springer)
19. Brown, R., Furi, M., Jiang, B. (2005). *Handbook of Topological Fixed Point Theory.* (Springer)
20. Górniewicz, L. (2006). *Topological Fixed Point Theory of Multivalued Mappings.* (Springer)
21. Yılmaz, K., Yılmaz, E.S. (2024). *Step-by-Step Topology: First Step.*
22. Agarwal, R., O'Regan, D. (2022). *Topology and Approximate Fixed Points.* (Springer)
23. Mebarki, K. et al. (2023). *Fixed Point Theorems with Applications.* (Routledge)
24. Perelman, G. (2002). *Ricci Flow and the Poincaré Conjecture*.
25. Edelsbrunner, H., Harer, J. (2010). *Computational Topology.*
26. Carlsson, G. (2009). *Topology and Data.*

Chapter 6

MOLECULAR ELECTRONIC STRUCTURE IN ORGANIC CORROSION INHIBITORS: CHARGE TRANSFER MECHANISMS AND A QUANTUM-CHEMICAL PERSPECTIVE ON ADSORPTION

Yeliz ULAŞ[1]

1 Assoc. Prof. Dr. Yeliz ULAŞ, Bursa Uludag University
Faculty of Arts and Science, Department of Chemistry
ORCID: 0000-0003-2038-1851, yelizulas@uludag.edu.tr

1. Introduction

Metal corrosion is an electrochemical degradation process driven by the thermodynamic tendency of metals to transform into more stable oxide or ionic species. In acidic media, the process typically proceeds through the following half-reactions:

Anodic dissolution

$$M \rightarrow M^{n+} + ne^-$$

Cathodic reaction

$$2H^+ + 2e^- \rightarrow H_2$$

In real systems, these half-reactions occur simultaneously at the metal–electrolyte interface, and the overall kinetics are largely governed by the rate of interfacial charge transfer. Organic inhibitors act by adsorbing onto the metal surface, thereby modulating these charge transfer pathways and reducing the rate of metal dissolution (Chen et al., 2025).

Experimentally, inhibitor performance is evaluated using:

- Weight loss measurements
- Tafel polarization curves
- Electrochemical impedance spectroscopy (EIS)
- Surface characterization techniques

However, these approaches primarily quantify macroscopic outcomes and do not directly reveal the molecular-level mechanism of inhibition.

At the molecular scale, adsorption arises from a combination of interactions:

- Electron donation to the metal surface via the inhibitor HOMO
- Back-donation from the metal to the inhibitor (metal → LUMO interaction)
- Coordinative interactions through heteroatom centers
- π–d orbital overlap
- Dispersion and induced dipole interactions

For this reason, quantum chemical methods provide a rational pre-screening strategy prior to experimental studies, enabling prediction of adsorption tendencies based on electronic structure descriptors (Mohammed et al., 2025).

In this chapter, 2-(naphthalen-1-yl(piperidin-1-yl)methyl)phenol was

selected as a model system, and its adsorption propensity was systematically analyzed through electronic structure parameters(Ulaş, 2020).

This molecule belongs to the alkylaminophenol class, a family of bifunctional compounds combining a phenolic hydroxyl group and an amine functionality within the same molecular framework(Wu et al., 2019). This dual functionality grants these molecules the ability to participate both in proton-transfer processes and in coordinative interactions with metal surfaces. While the phenolic –OH group is electronically conjugated with the aromatic system, the amine moiety provides an electron-rich center. As a result, charge distribution within the molecule is inherently multicentered rather than localized.

The electronic behavior of alkylaminophenols is governed by several key factors:

- Resonance and inductive contributions of the phenolic oxygen
- Electron-donating character of the amine group
- Electronic transmission between aromatic rings via the benzylic carbon
- Intramolecular hydrogen-bonding potential
- Protonation–deprotonation equilibria

The phenolic hydroxyl group can enhance electron density on the aromatic ring via resonance, whereas the amine functionality contributes through inductive and hyperconjugative effects. The interplay of these effects establishes an internal "push–pull" electronic balance. This balance directly influences frontier molecular orbital distribution as well as global reactivity descriptors such as hardness, electronegativity, and electrophilicity (Sehrawat et al., 2024).

In the context of corrosion inhibition, alkylaminophenols are particularly attractive because:

1. They contain dual heteroatom centers (O and N), which can coordinate to metal surfaces.

2. They possess aromatic π-systems, enabling extended surface contact through parallel adsorption.

3. Their electronic structure is tunable; ring substitution can modulate HOMO energy and molecular hardness.

4. They can exhibit significant polarizability, especially in polyaromatic derivatives, enhancing dispersion contributions to adsorption.

Previous studies have reported that aminophenol derivatives exhibit

meaningful inhibition efficiencies on steel and copper surfaces in acidic environments (Balasooriya et al., 2025). Their effectiveness is commonly attributed to coordination through heteroatom centers combined with parallel adsorption of the aromatic framework(Razali et al., 2024).

Another important feature of alkylaminophenols is their ability to transmit electronic effects between two aromatic units through the benzylic carbon bridge. This electronic communication allows substituent-induced changes in electron density to propagate throughout the molecular framework. Consequently, adsorption behavior cannot be reduced to a single functional group; rather, the entire electronic architecture must be considered.

Furthermore, the nature of the amine ring (e.g., piperidine, pyrrolidine, morpholine) influences both steric volume and electron-donating capacity. Bulky secondary amines may act not only as coordination centers but also as structural elements that determine molecular orientation on the surface. This can influence whether adsorption occurs in a planar or tilted configuration.

Taken together, alkylaminophenols offer a threefold advantage as corrosion inhibitors:

- Electron-donating heteroatom centers
- Extended π-contact surface
- Electronically tunable molecular scaffold

These structural characteristics render this class of compounds particularly suitable for quantum-chemical pre-screening studies. The selected derivative, 2-(naphthalen-1-yl(piperidin-1-yl)methyl)phenol, represents a structurally informative example due to its combined phenolic and amine functionalities and its extended naphthalene π-system, making it an appropriate model for evaluating adsorption potential within the alkylaminophenol framework.

2. Conceptual Repositioning of the Model Molecule

Over the past two decades, density functional theory (DFT)-based analyses of corrosion inhibitors have increased significantly (Mamand et al., 2024). Most studies have focused on a common set of quantum-chemical descriptors, including:

- E_{HOMO}
- E_{LUMO}
- Energy gap (ΔE)
- Global hardness (η) and softness (σ)
- Electronegativity (χ)

- Electrophilicity index (ω)
- Dipole moment
- Polarizability

Numerous reports have attempted to establish correlations between these parameters and experimentally determined inhibition efficiencies (Ebenso et al., 2021).

However, a recurring limitation in the literature is the reduction of inhibition performance to a single descriptor—most commonly a high EHOMO value—without considering the multidimensional nature of adsorption (Ouakki et al., 2022). Such simplification is conceptually insufficient. Adsorption is not governed by one parameter but emerges from the interplay of orbital localization, charge density distribution, molecular polarizability, and dispersion contributions.

The alkylaminophenol derivative examined in the present study has previously been analyzed in a spectroscopic context (Ulaş, 2020). Yet, when the same molecule is evaluated within a surface chemistry framework, the central questions change fundamentally:

- Where is the electron density predominantly localized?
- Which heteroatom center is more prone to coordinative interaction with the metal surface?
- Does the molecular polarizability permit surface-induced reorientation?
- Is the π-system structurally and electronically suitable for parallel adsorption?

These questions reposition the molecule within a different conceptual framework. Rather than treating quantum descriptors as isolated numerical values, they must be reinterpreted collectively in relation to surface interaction mechanisms. In this sense, electronic structure parameters are not endpoints, but mechanistic indicators that require contextual analysis within the adsorption process.

3.Geometri Optimizasyonu ve Fonksiyonel Seçimi

Frontier molecular orbital (FMO) theory proposes that chemical reactivity is primarily governed by the highest occupied molecular orbital (HOMO) and the lowest unoccupied molecular orbital (LUMO). In the context of surface chemistry and corrosion inhibition, these orbitals serve as key indicators defining both the direction and character of metal–molecule interactions. The HOMO quantitatively reflects the electron-donating capacity of the inhibitor, whereas the LUMO represents its electron-accepting potential.

At metal surfaces, partially filled or vacant d-orbitals interact with the frontier orbitals of organic molecules. The energetic alignment and spatial overlap between these orbitals constitute one of the principal determinants of adsorption strength (Sujatha & Lavanya, 2023). When the HOMO energy is favorably aligned with the metal surface orbitals, electron donation becomes energetically accessible, enhancing the likelihood of coordinative bonding. Conversely, the LUMO energy level and distribution influence the possibility of metal-to-molecule back-donation, a process that may contribute to adsorption complex stabilization.

Importantly, FMO analysis extends beyond simple orbital energy comparison. Spatial localization, nodal structure, phase characteristics, and heteroatom contributions must also be considered. In heteroatom-containing aromatic systems, the manner in which the HOMO is distributed between the π-framework and donor centers determines the relative contributions of coordinative bonding versus parallel π-interaction with the surface. Therefore, frontier orbital analysis represents a fundamental theoretical tool for predicting the interaction sites and mechanisms through which inhibitor molecules engage metal surfaces (Boussalah et al., 2012).

HOMO Analysis

The calculated HOMO energy (–7.8195 eV) quantitatively reflects the molecule's electron-donating tendency. Examination of the HOMO distribution reveals pronounced delocalization across the aromatic π-system, with significant contribution localized around the phenolic oxygen.

This distribution suggests two mechanistic implications:

1. The extended π-system may facilitate parallel surface alignment, providing a broad contact area that strengthens dispersion and π–metal interactions.

2. The electron density concentrated on the phenolic oxygen indicates that this site serves as a plausible donor center for coordinative interaction.

In contrast, the piperidine nitrogen exhibits comparatively limited HOMO contribution. This observation implies that, rather than acting as the dominant orbital donor, the amine center may contribute more substantially to the overall electrostatic environment and structural orientation of the molecule at the interface.

LUMO Analysis

The LUMO energy (+0.1240 eV) reflects the molecule's electron-accepting potential. Although corrosion inhibition is often interpreted primarily in terms of electron donation from the inhibitor to the metal surface, metal-to-molecule back-donation cannot be excluded. In particular, interactions

between transition-metal d-orbitals and aromatic π^* orbitals may enable bidirectional charge transfer, enhancing adsorption stability.

Accordingly, both the energy level and spatial distribution of the LUMO are relevant—not only for reactivity assessment but also for understanding the thermodynamic stabilization of the adsorption comp

HOMO–LUMO Energy Gap (ΔE)

The HOMO–LUMO energy gap (ΔE = 7.9435 eV) serves as an indicator of relative chemical hardness. A relatively large ΔE value suggests electronic stability and comparatively low intrinsic polarizability. However, ΔE alone cannot determine inhibition performance. It must be evaluated alongside charge distribution, polarizability, and global reactivity descriptors to obtain mechanistic insight.

Global reactivity descriptors provide a quantitative description of a molecule's charge-transfer tendency and electronic deformation capacity.

The ionization potential (I) corresponds to the energy required to remove an electron and is inversely related to electron-donating ability; systems with lower I values can donate electrons more readily. The electron affinity (A) reflects the ability to accept an electron and is particularly relevant for assessing possible back-donation from the metal surface.

Chemical hardness (η) represents resistance to electronic deformation under external perturbation. High η values correspond to rigid, less polarizable systems, whereas low η values indicate greater electronic flexibility. Softness (σ), defined as the reciprocal of hardness, reflects the capacity for electron density redistribution upon interaction with a surface.

Electronegativity (χ) provides an averaged measure of electron-attracting tendency and is useful for predicting the direction of charge equilibration at the metal–molecule interface. The electrophilicity index (ω) represents the overall capacity of a system to accept electronic charge and becomes particularly relevant in adsorption processes involving bidirectional charge transfer.

When evaluated collectively, these descriptors allow differentiation between a purely donor-type inhibitor and a dynamically adaptive system capable of mutual charge exchange. In corrosion inhibition, excessively high hardness (η) may indicate weak surface interaction, whereas excessively low hardness may correspond to uncontrolled reactivity. Therefore, a balanced η–σ profile, accompanied by moderate χ and reasonable ω values, can be interpreted as indicative of an electronic structure conducive to stable yet reversible adsorption behavior at the metal interface.

Table 1. *Quantum-Chemical Electronic Descriptors of the Model Alkylaminophenol*

WB97XD	E_{HOMO}	E_{LUMO}	?E	?	?	?	?
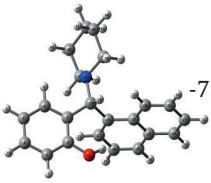	-7.8195	0.1240	7.9435	3.9718	1.9859	3.8478	1.8638

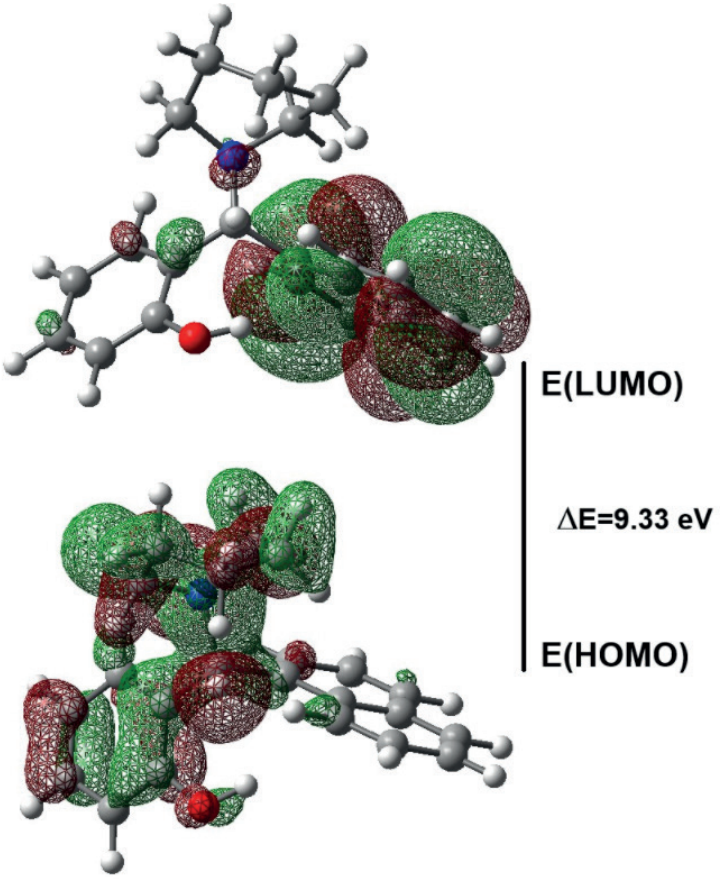

Figure 1. *HOMO and LUMO orbital distributions (ωB97XD/6-311++G(d,p)).*

5. Molecular Electrostatic Potential (MEP) Analysis

Molecular electrostatic potential (MEP) surfaces provide a spatial visualization of charge distribution, allowing identification of electrostatically

reactive regions within a molecule. In the context of metal–molecule interactions, MEP maps are particularly valuable because they distinguish electron-rich (nucleophilic) regions from electron-deficient (electrophilic) ones. This approach complements frontier orbital analysis: while orbital energies describe charge-transfer propensity, MEP distributions indicate the spatial initiation sites of electrostatic interaction (Ferkous et al., 2025).

For the investigated molecule, the most negative electrostatic potential is localized around the phenolic oxygen atom. This finding indicates a high electron density at this site, identifying it as a primary candidate for interaction with electrophilic centers on the metal surface. The lone pairs of the phenolic oxygen are especially well-suited for coordinative interaction with partially vacant d-orbitals of transition metals.

In addition to this localized negative region, a moderately negative potential is distributed across the aromatic π-system. This delocalized character demonstrates that electron density is not confined to a single atom but extends over a broader electronic surface. Such delocalization suggests that adsorption may not be restricted to point coordination but could occur via a parallel, surface-contact configuration. The extended and planar structure of the naphthalene ring is particularly relevant in this regard, as it can maximize contact area with the surface and enhance dispersion and π–metal interactions.

Regions of positive electrostatic potential are observed near protonatable centers and hydrogen atoms. Although these sites are not primary coordination points, they may contribute to electrostatic stabilization and influence molecular orientation at the interface by interacting with the surface charge distribution.

The dipole moment reflects the overall asymmetry of charge distribution and the molecule's response to an interfacial electric field. A significant dipole moment may enable reorientation of the molecule along the electric field present at the metal–electrolyte interface, indicating that adsorption involves not only chemical bonding but also electrostatic contributions.

Total polarizability describes the ability of the electron cloud to deform under an external electric field or in the presence of a metal surface. Molecules with higher polarizability can gain additional stabilization through induced dipole–induced dipole interactions. In systems containing extended π-frameworks, such as polyaromatic structures, facile deformation of the electron cloud enhances dispersion contributions and may strengthen adsorption energy.

Partial negative charges localized on heteroatoms—particularly oxygen and nitrogen—indicate potential binding regions for local coordinative

interaction. Meanwhile, the delocalized charge distribution across the aromatic framework suggests the possibility of multicentered surface contact. This holistic distribution underscores that adsorption cannot be reduced to a single donor–acceptor interaction; rather, electrostatic, orbital, and dispersion effects collectively govern interfacial behavior.

When interpreted alongside frontier orbital results, MEP analysis provides a spatially resolved prediction of adsorption sites, preferred orientations, and interaction modes. Thus, rational inhibitor design must consider not only energetic descriptors but also the spatial organization of charge distribution.

In Figure 3, the MEP surface is mapped over the range -4.205×10^{-2} to $+4.205 \times 10^{-2}$ a.u. The most intense negative potential (red regions) is clearly localized around the phenolic oxygen, confirming its role as the strongest nucleophilic center. Moderate negative potential (yellow–green regions) distributed over the naphthalene ring highlights the delocalized character of the π-system and supports the feasibility of parallel π-interaction with the metal surface. More positive regions elsewhere in the molecule may contribute to electrostatic balance and facilitate appropriate adsorption orientation.

Taken together, the MEP distribution indicates that the molecule possesses an electronic architecture capable of interacting with the metal surface through both localized coordinative bonding via the phenolic oxygen and multicentered contact mediated by its extended π-surface.

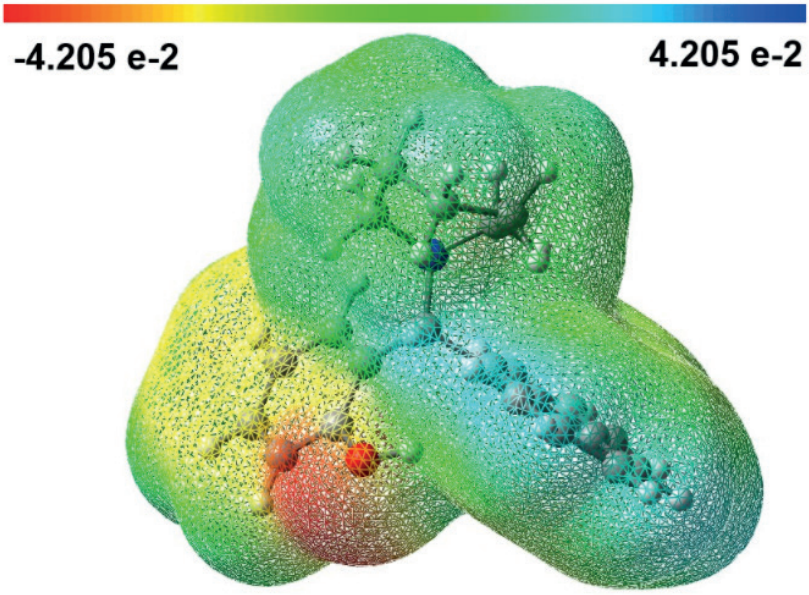

Figure 3. *Molecular electrostatic potential (MEP) surface (ωB97XD/6-311++G(d,p)).*

5. Molecular Interpretation of Adsorption Tendency

Metal surface adsorption is a complex phenomenon that cannot be explained by a single interaction type; rather, it arises from the combined contribution of multiple electronic and physical effects. For the investigated molecule, the potential interaction mechanisms may be summarized as follows:

- Electron donation to the metal surface via the HOMO
- Coordinative interaction through heteroatom centers
- Parallel surface alignment enabled by the extended π-system
- Dispersion and induced dipole contributions

The concentration of HOMO density over the phenolic oxygen and aromatic framework suggests that initial surface contact may occur through both a localized donor center and the π-surface. In particular, the phenolic oxygen possesses the capacity to interact coordinatively with partially vacant metal d-orbitals. Such localized donor–metal interactions may play a decisive role during the initial stage of adsorption.

In addition, the planar and extended structure of the naphthalene ring allows for maximized surface contact in a parallel adsorption configuration. This geometry enhances not only orbital overlap but also dispersion and π–metal interactions. In transition-metal systems, molecules possessing extended π-clouds have been reported to achieve enhanced stabilization when adsorbed in parallel orientations.

Although dispersion interactions are often considered weak individually, their cumulative contribution in extended aromatic systems is non-negligible. The use of the dispersion-corrected ωB97XD functional in this study enables a more realistic description of such weak yet pervasive interactions. Consequently, not only covalent-like coordinative bonding but also physical stabilization contributions between surface and molecule are indirectly accounted for.

The moderate hardness and appreciable softness values indicate an electronic profile capable of controlled charge exchange with the surface. Excessively rigid (high-η) systems may interact weakly, whereas overly soft systems may display uncontrolled reactivity. The present structure appears positioned between these extremes, theoretically supporting stable yet reversible adsorption behavior.

MEP analysis reinforces the likelihood of coordinative bonding via the phenolic oxygen, while the delocalized charge distribution across the aromatic system suggests multicentered surface contact. Together, these observations support a hybrid adsorption mechanism in which localized coordination and parallel π-interaction act cooperatively rather than independently.

Overall, the analysis of this model molecule demonstrates that inhibition cannot be reduced to a single electronic parameter. HOMO energy, LUMO level, hardness–softness balance, electrostatic potential distribution, dipole moment, and polarizability collectively define a multidimensional electronic architecture governing adsorption tendency. This perspective emphasizes that rational inhibitor selection should rely on holistic electronic profiling rather than a simplistic "high HOMO" criterion.

7. Relating Molecular Tendencies to Adsorption Isotherms

Experimentally, metal surface adsorption is commonly analyzed using Langmuir and Temkin isotherm models. These models describe the relationship between surface coverage (θ) and inhibitor concentration (C), providing insight into whether adsorption proceeds as a monolayer process or involves lateral interactions between adsorbed species.

The Langmuir model represents the ideal case of a homogeneous surface with negligible interactions among adsorbed molecules. In this framework, the adsorption equilibrium constant (K_ads) quantitatively reflects the binding tendency of the inhibitor to the surface.

The Temkin model, in contrast, assumes that adsorption energy varies with surface coverage and accounts for lateral interactions between adsorbed molecules. This approach may be more realistic for systems containing large π-frameworks and high polarizability.

In the absence of experimental θ–C data, isotherm parameters were not directly calculated in this study. Nevertheless, DFT-derived molecular descriptors provide theoretical insight into probable adsorption behavior.

The investigated 2-(naphthalen-1-yl(piperidin-1-yl)methyl)phenol molecule:

· Possesses an extended naphthalene π-system conducive to parallel surface alignment,

· Can exhibit coordinative interaction via both the piperidine nitrogen and phenolic oxygen,

· Displays delocalized electronic structure suggestive of enhanced polarizability.

These features are compatible with ordered monolayer formation and thus consistent with Langmuir-type adsorption tendencies. However, the π–π interaction potential of the naphthalene ring and possible electrostatic contributions may also promote lateral interactions between adsorbed species, providing a basis for Temkin-type behavior.

Thus, although DFT descriptors do not directly yield adsorption constants,

they establish a molecular-level framework for interpreting experimentally derived isotherm parameters (Farag & Toghan, 2025).

8. Generalizability of the Methodological Approach

The systematic framework applied in this chapter consists of the following steps:

1. Geometry optimization and confirmation of a true minimum
2. Frontier molecular orbital (FMO) analysis
3. Evaluation of global reactivity descriptors
4. MEP and atomic charge distribution analysis
5. Dipole moment and polarizability assessment
6. Integrated mechanistic interpretation of multiple descriptors

The principal advantage of this approach lies in its multidimensional nature. It avoids reliance on a single electronic indicator and instead evaluates the electronic architecture comprehensively. Geometry optimization ensures a realistic conformational model; FMO analysis clarifies charge-transfer direction; global descriptors quantify electronic flexibility; MEP maps visualize spatial interaction sites; and dipole moment and polarizability analyses assess interfacial adaptability.

This framework is not limited to alkylaminophenols. It is directly applicable to amines, phenols, Schiff bases, heterocyclic compounds, polyaromatic systems, and multi-heteroatom inhibitor candidates. In substituted aromatic series, electronic transmission and charge delocalization effects can be systematically compared using this methodology. Consequently, large molecular libraries may be theoretically screened prior to experimental investigation, allowing early elimination of low-performance candidates.

By shifting inhibitor design from intuitive selection toward electronically informed decision-making, this approach provides a rational pre-screening platform.

9. Conclusion

In this chapter, an alkylaminophenol derivative was systematically evaluated from a corrosion inhibition perspective using a dispersion-corrected DFT approach. Frontier orbital distributions, global reactivity descriptors, electrostatic potential maps, and polarizability analyses were interpreted collectively to establish a comprehensive electronic profile of adsorption tendency.

The findings indicate that the molecule:

· Is capable of coordinative interaction through heteroatom centers,

· Possesses an extended π-system favoring parallel surface alignment and increased contact area,

· Exhibits a moderately soft electronic character suitable for balanced charge transfer,

· Requires consideration of dispersion contributions, particularly due to its aromatic framework.

This study does not directly calculate adsorption energies or inhibition efficiencies; rather, it provides a molecular-level electronic interpretation of adsorption propensity. It demonstrates that quantum chemical methods can function as rational pre-screening tools, potentially reducing experimental trial-and-error processes.

Quantitative determination of adsorption energies and binding geometries would require explicit metal–molecule complex calculations or periodic slab models. Nevertheless, the framework presented here offers a robust theoretical basis for evaluating electronic suitability before proceeding to advanced surface modeling.

Ultimately, successful inhibitor design depends not solely on experimental measurements but on accurate interpretation of molecular electronic architecture. Multidimensional quantum-chemical analysis remains one of the most powerful tools for understanding and predicting surface interactions.

References:

Balasooriya, H., Li, C., & Wang, F. (2025). Understanding Steel Corrosion: Surface Chemistry and Defects Explored Through DFT Modelling—A Review. *Processes*, *13*(7), 1–38. https://doi.org/10.3390/pr13071971

Boussalah, N., Ghalem, S., Kadiri, S. El, Hammouti, B., & Touzani, R. (2012). Theoretical study of the corrosion inhibition of some bipyrazolic derivatives: A conceptual DFT investigation. *Research on Chemical Intermediates*, *38*(8), 2009–2023. https://doi.org/10.1007/s11164-012-0522-0

Chen, D., Zhou, W., Ji, Y., & Dong, C. (2025). Applications of density functional theory to corrosion and corrosion prevention of metals: A review. *Materials Genome Engineering Advances*, *3*(1). https://doi.org/10.1002/mgea.83

Ebenso, E. E., Verma, C., Olasunkanmi, L. O., Akpan, E. D., Verma, D. K., Lgaz, H., Guo, L., Kaya, S., & Quraishi, M. A. (2021). Molecular modelling of compounds used for corrosion inhibition studies: a review. *Physical Chemistry Chemical Physics*, *23*(36), 19987–20027. https://doi.org/10.1039/d1cp00244a

Farag, A. A., & Toghan, A. (2025). Unravelling the adsorption and anti-corrosion potency of newly synthesized thiazole Schiff bases on C-steel in 1 M HCl: Computational and experimental implementations. *Results in Engineering*, *25*(December 2024). https://doi.org/10.1016/j.rineng.2025.104504

Ferkous, H., Guezane-Lakoud, S., Sedik, A., Boublia, A., Delimi, A., Kahlouche, A., Boulechfar, C., Dilgin, Y., Halim, K. S. A., Albrahim, M., & Benguerba, Y. (2025). Tailored α-hydroxyphosphonate derivatives: Green synthesis, spectroscopic characterization, DFT analysis, and high-efficiency corrosion protection for copper in acidic media. *Sustainable Materials and Technologies*, *43*(December 2024). https://doi.org/10.1016/j.susmat.2025.e01282

Mamand, D. M., Anwer, T. M. K., & Qadr, H. M. (2024). Corrosion inhibition performance of organic compounds and theoretical calculations based on density functional theory (DFT). *Corrosion Reviews*, *42*(1), 1–15. https://doi.org/10.1515/corrrev-2022-0112

Mohammed, W. A., Rashid, K. H., AL-Azawi, K. F., Khadom, A. A., Kadhum, A. A. H., & Al-Amiery, A. A. (2025). A Review On Corrosion Inhibition Performance of Chalcones: A Multi-Technique Study Using Weight Loss, EIS, Polarization, and Quantum Chemical Calculations. *Moroccan Journal of Chemistry*, *13*(3), 1138–1167. https://doi.org/10.48317/IMIST.PRSM/morjchem-v13i3.57205

Ouakki, M., Galai, M., & Cherkaoui, M. (2022). Imidazole derivatives as efficient and potential class of corrosion inhibitors for metals and alloys in aqueous electrolytes: A review. *Journal of Molecular Liquids*, *345*. https://doi.org/10.1016/j.molliq.2021.117815

Razali, N. Z. K., Wan Hassan, W. N. S., Sheikh Mohd Ghazali, S. A. I., Mohd Shotor, S. N., & Dzulkifli, N. N. (2024). DFT, Fukui indices, and molecular dynamic simulation studies on corrosion inhibition characteristics: a review. *Chemical*

Papers, *78*(2), 715–731. https://doi.org/10.1007/s11696-023-03148-w

Sehrawat, R., Vashishth, P., Bairagi, H., Shukla, S. K., Kumar, H., Ji, G., & Mangla, B. (2024). Coordination bonding and corrosion inhibition characteristics of chalcone compounds for metals: An inclusive review based on experimental as well as theoretical perspectives. *Coordination Chemistry Reviews*, *514*. https://doi.org/10.1016/j.ccr.2024.215820

Sujatha, H. S., & Lavanya, M. (2023). An insight to HOMO LUMO aspects in corrosion applications. *Canadian Metallurgical Quarterly*, *62*(4), 761–772. https://doi.org/10.1080/00084433.2022.2140398

Ulaş, Y. (2020). Experimental and Theoretical Studies of 2-(naphthalen-1-yl (piperidin-1-yl) methyl)phenol Compound. In *Yeliz Ulaş J.Chem.Soc.Pak* (Vol. 42, Issue 06).

Wu, P., Givskov, M., & Nielsen, T. E. (2019). Reactivity and Synthetic Applications of Multicomponent Petasis Reactions [Review-article]. *Chemical Reviews*, *119*(20), 11245–11290. https://doi.org/10.1021/acs.chemrev.9b00214

Chapter 7

BEYOND CONVENTIONAL ANTIOXIDANTS: NEW MOLECULAR APPROACHES IN NEURODEGENERATIVE DISORDERS

Hüsna SEKBAN[1]

Elif Naz GÜRSOY[2]

Kubra SENER[3]

Şule COŞKUN CEVHER[4]

1 Gazi University, Faculty of Science, Department of Biology, Ankara, Türkiye, ORCID: 0009-0008-8175-9575.
2 Res.Asst. Elif Naz GÜRSOY, Gazi University, Faculty of Science, Department of Biology, Ankara, Türkiye, ORCID: 0000-0003-4946-1185.
3 Res. Asst. Kubra SENER, Gazi University, Faculty of Science, Department of Biology, Ankara, Türkiye, ORCID: 0000-0002-8759-9444.
4 Prof. Dr. Şule Coşkun Cevher, Gazi University, Faculty of Science, Department of Biology, Ankara, Türkiye, ORCID: 0000-0001-6204-2845.

1. Introduction

Neurodegenerative diseases represent a broad spectrum of disorders characterized by the progressive loss of neuronal structure and function. This group includes Alzheimer's Disease (AD), Parkinson's Disease (PD), Huntington's Disease (HD), Amyotrophic Lateral Sclerosis (ALS), Multiple Sclerosis (MS), and ischemic stroke. These disorders cause substantial deterioration in cognitive, motor, and sensory functions and irreversibly impair activities of daily living and overall quality of life (Wilson et al., 2023). With population aging, the global burden of neurodegenerative diseases continues to increase. Nevertheless, there is still no definitive therapy capable of completely halting disease progression. Current pharmacological approaches largely provide palliative care and symptomatic relief, which underscores the need for more effective strategies with disease-modifying potential (Lamptey et al., 2022). An important biological basis for this unmet need is the multifactorial nature of neurodegeneration. In particular, mitochondrial dysfunction and oxidative stress constitute central mechanisms that drive disease progression. These processes impair cellular metabolism and shift redox balance toward excessive reactive oxygen species (ROS) generation (Lin & Beal, 2006). When endogenous antioxidant defenses fail to neutralize ROS, lipid peroxidation and protein oxidation occur, ultimately leading to neuronal injury and cell death (Ayala, Muñoz, & Argüelles, 2014). The brain is especially vulnerable to oxidative damage due to its high oxygen demand and limited regenerative capacity (Cobley, Fiorello, & Bailey, 2018). Therefore, interventions targeting oxidative mechanisms are considered key components of future neuroprotective strategies.

This pathophysiological background explains why currently available medications remain insufficient in neurodegenerative disorders. In Alzheimer's disease, donepezil, and in Parkinson's disease, levodopa-based therapies alleviate clinical symptoms, yet they do not interfere with the underlying molecular cascade (Yiannopoulou & Papageorgiou, 2013). Consequently, disease progression continues in most patients despite treatment. Similarly, many antioxidants that demonstrate promising results in experimental models fail to show comparable efficacy in human studies. The major reasons for this failure include inadequate penetration across the Blood-Brain Barrier (BBB), low bioavailability, and rapid metabolic degradation (Tönnies & Trushina, 2017). These limitations have reinforced the need for novel molecular strategies that extend beyond existing approaches. Therefore, recent research has increasingly focused on molecules with higher lipophilicity, prolonged half-life, and the ability to modulate multiple signaling pathways rather than on conventional radical scavenger (Weinreb, Amit, Bar-Am, & Youdim, 2016).

Within this emerging perspective, interest has grown toward naturally derived yet relatively underexplored compounds. Citrus polymethoxyflavones

such as nobiletin and tangeretin (Braidy et al., 2017), marine-derived carotenoids (Gammone, Riccioni, & D'Orazio, 2015), as well as fisetin (Khan, Syed, Ahmad, & Mukhtar, 2013), deferiprone (Dusek, Schneider, & Aaseth, 2016), and ergothioneine (Cheah & Halliwell, 2012) have gained attention as promising candidates. These molecules exhibit more favorable pharmacokinetic characteristics and may cross the BBB more efficiently than classical antioxidants. Moreover, they function not only as free radical scavengers but also as regulators of cellular defense networks. In particular, they can activate endogenous protective systems, especially the nuclear factor erythroid 2-related factor 2 (Nrf2) signaling pathway, and exert modulatory effects on mitochondrial and inflammatory mechanisms.

In this section, the selected antioxidants are presented as emerging candidates for neuroprotection. Their mechanisms of action, bioavailability characteristics, and safety considerations are discussed in relation to different stages of disease.

2. Neurodegenerative Diseases and Oxidative Stress

Oxidative stress is widely recognized as a common hallmark of neurodegenerative pathologies, despite the multifactorial nature of their etiology and progression. The brain accounts for only about two percent of total body weight, yet it is responsible for nearly twenty percent of overall oxygen consumption (Cobley et al., 2018). This high metabolic demand makes the generation of ROS within the mitochondrial electron transport chain inevitable. Under physiological conditions, ROS are effectively controlled by endogenous antioxidant systems. However, during aging and pathological processes, ROS production increases and, once cellular defense capacity is exceeded, redox homeostasis becomes disrupted (Lin & Beal, 2006).

The heightened vulnerability of the brain to oxidative stress largely results from the abundance of polyunsaturated fatty acids in neuronal membranes. These lipids constitute primary targets for ROS attack and initiate cascading lipid peroxidation reactions. Lipid peroxidation can impair membrane fluidity and selective permeability. It may also lead to the loss of membrane potential and disruption of intracellular calcium homeostasis. These alterations render neurons prone to excitotoxicity (Ayala et al., 2014).

In addition, the accumulation of misfolded proteins observed in disorders such as Alzheimer's and Parkinson's disease progressively aggravates mitochondrial dysfunction. As damaged neurons become unable to maintain efficient energy production, cellular stress responses intensify and ROS generation further increases (Lin & Beal, 2006). Age-related accumulation of redox-active metals, including iron and copper, can also exacerbate this process. These metals catalyze the formation of highly toxic hydroxyl radicals through the Fenton reaction. The resulting radicals induce irreversible damage

to DNA, proteins, and lipids, potentially triggering apoptosis and other programmed cell death pathways (Urrutia, Mena, & Núñez, 2014). Therefore, oxidative stress is considered not merely a consequence of neurodegeneration but a major pathological driver that accelerates disease progression.

This framework supports therapeutic approaches that modulate redox balance, preserve mitochondrial function, and strengthen endogenous antioxidant defenses.

3. Potential Therapeutic Agents

The limited efficacy of current pharmacological approaches in halting the progression of neurodegenerative diseases has directed attention toward next-generation therapeutic molecules. Conventional antioxidants generally show restricted clinical benefit because they do not adequately target the intracellular compartments where major pathological damage occurs. Most classical agents exhibit hydrophilic properties and therefore display poor penetration across the BBB (Forman & Zhang, 2021). In addition, they often fail to reach mitochondria, which represent a central hub of oxidative injury (Jiang et al., 2020).

Within this framework, several specialized bioactive compounds have emerged as promising candidates. Owing to their high lipophilicity, these agents are able to cross the BBB more efficiently and modulate intracellular signaling pathways beyond simple ROS scavenging (Braidy et al., 2017). Some of these molecules also support mitochondrial function and may even promote mitochondrial biogenesis. The following section focuses on polymethoxylated flavones, marine-derived carotenoids, senolytic agents, and mitochondria-targeted protectors, which possess considerable therapeutic potential but have not yet achieved full clinical translation.

3.1. Polymethoxylated Flavones

Polymethoxylated flavones (PMFs), isolated from citrus (*Citrus sp.*) peels, possess multiple methoxyl groups that structurally distinguish them from classical flavonoids (Li et al., 2009). This unique hydrophobic architecture grants Nobiletin and Tangeretin high intrinsic lipophilicity, enabling them to traverse the BBB efficiently via passive diffusion (Braidy et al., 2017).

Nobiletin

Nobiletin ($C_{21}H_{22}O_8$), acts as a direct ligand for the retinoic acid receptor-related orphan receptors (RORα/γ) nuclear receptors, which serve as the master regulators of the circadian clock, thereby activating the *Bmal1* gene. This molecular mechanism holds significant potential for restoring the sleep-wake cycle disturbances frequently observed in patients with neurodegenerative disorders (He et al., 2016). Furthermore, the resynchronization of the circadian

rhythm enhances glymphatic system activity, which accelerates the clearance of amyloid-beta plaques, a hallmark of AD pathology (Lee et al., 2020).

Beyond its chronobiological effects, Nobiletin provides neuroprotection by modulating intracellular secondary messengers, specifically cyclic adenosine monophosphate (cAMP) levels. The initial step in this signaling cascade involves the inhibition of phosphodiesterase (PDE) enzymes, which leads to an elevation in intracellular cAMP concentrations. This surge initiates the activation of the Protein Kinase A (PKA) cascade (Onozuka et al., 2008). Upon activation, PKA phosphorylates the transcription factor cAMP response element-binding protein (CREB) at the Serine-133 residue, facilitating its translocation into the nucleus (Matsuzaki et al., 2006). The binding of phosphorylated CREB to specific DNA promoter regions upregulates the expression of brain-derived neurotrophic factor (BDNF). This enhancement in BDNF levels plays a pivotal role in maintaining synaptic plasticity and preserving long-term memory functions (Nakajima, Ohizumi, & Yamada, 2014).

Tangeretin

Tangeretin ($C_{20}H_{20}O_7$), preserves the integrity of dopaminergic neurons within the *substantia nigra* in PD models, thereby sustaining tyrosine hydroxylase activity. Consequently, it prevents the decline in motor coordination and locomotor function (Datla, Christidou, Widmer, Rooprai, & Dexter, 2001).

However, the greatest obstacle encountered in the clinical phase trials of these molecules is the potential for drug-drug interactions. Based on the study by Gao et al., while it is known that Nobiletin and Tangeretin suppress hepatic cytochrome P450 enzymes, particularly CYP3A4, whether this situation increases the toxicity of existing treatments in the elderly population using multiple drugs has not been sufficiently elucidated in the literature (Gao, Gao, Zeng, Li, & Liu, 2018). In the same study, although the binding affinity of Nobiletin to ROR receptors has been demonstrated, whether this activation increases the expression of the *Trem2* receptor responsible for phagocytosis in microglial cells directly or by regulating the circadian rhythm has not been thoroughly investigated at the molecular level.

3.2.2. Marine-Derived Carotenoids

Xanthophyll group carotenoids obtained from the marine ecosystem display superior properties in protecting neuronal membrane stability thanks to their unique molecular structures (Galasso et al., 2018).

Fucoxanthin

In contrast to the Astaxanthin molecule, about which more is known, Fucoxanthin ($C_{42}H_{58}O_6$), which is a molecule showing similar properties

obtained from brown algae, is less studied but holds promise especially in neuroinflammation processes. Due to the allenic bonds and unique carbonyl groups in its structure providing an amphiphilic character to the molecule, in complete contrast to other apolar carotenoids known to settle only parallel to the hydrophobic part of the membrane, it can bind vertically or at an angle to the double layer of the neuronal cell membrane as well. This is beneficial in optimizing membrane fluidity and selective permeability (Mikami & Hosokawa, 2013; L. Zhang et al., 2017).

Fucoxanthin modulates the nuclear factor kappa B (NF-κB) pathway in microglial cells by protecting the stability of the IκB-α protein. Under normal conditions, the p65 and p60 subunits of NF-κB remain in an inactive state bound to the IκB-α inhibitor protein. However, when stimulated by various inducers that cause the emergence of oxidative stress or neurodegenerative diseases, the IκB kinase complex is activated, leading to the initiation of IκB-α phosphorylation and subsequently causing the progression of intracellular damage (Mattson & Camandola, 2001). In studies conducted by Zhang et al., it has been revealed that Fucoxanthin suppresses this phosphorylation step and prevents the degradation of IκB-α. Thus, the translocation of the p65 subunit into the nucleus is blocked. As a result, the gene expression of pro-inflammatory cytokines TNF-α and IL-6 is suppressed (Figure 1.). In this way, the potential for reduced motor neuron loss has emerged not only in AD and PD but also in ALS models (Alghazwi, Smid, Musgrave, & Zhang, 2019; Zeng et al., 2018).

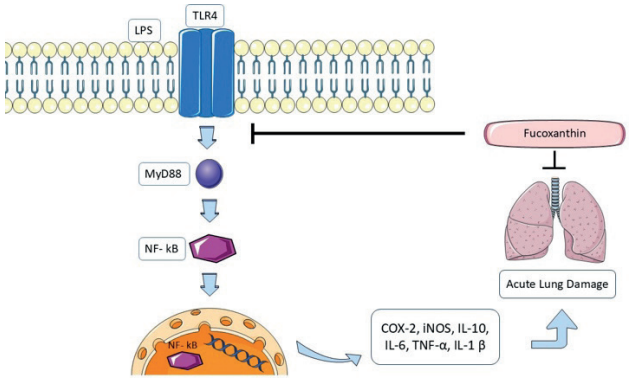

Figure 1. *Fucoxanthin prevents the nuclear entry of NF-κB, leading to the downregulation of pro-inflammatory cytokine production (Li X, 2020)***.** *Adapted from Servier Medical Art (https://smart.servier.com), licensed under CC BY 4.0 (https://creativecommons.org/licenses/by/4.0/).*

The most prominent gap in the current literature is related to the metabolic stability of Fucoxanthin in the body. It has not been clarified from a pharmacokinetic perspective whether the active form reaching the brain

tissue of this compound, which is rapidly metabolized and converted into the Fucoxantinol molecule as soon as it enters the human body, is the parent molecule or one of the intermediate metabolites, and how this conversion changes the therapeutic efficacy (Kim & Pangestuti, 2011). Especially, investigations on the interactions of Fucoxantinol with P-glycoprotein (P-gp/ABCB1) efflux pumps, which are located on the outer surfaces of BBB endothelial cells and significantly limit the entry of drugs into the brain, are quite limited (Méresse, Fodil, Fleury, & Chénais, 2020; Peng, Yuan, Wu, & Wang, 2011).

In addition to this, it is seen that a very large portion of the studies conducted to bring the neuroprotective effects of this molecule to light remain limited to AD models (Alghazwi et al., 2019). In contrast, data regarding the molecular activities of other neurodegenerative diseases characterized by protein degradation or accumulation are limited. Especially, the molecular mechanisms regarding how Fucoxanthin modulates autophagy on the alpha-synuclein accumulation involved in PD pathophysiology or the degeneration of motor neurons in ALS disease have not yet been clarified (Mohibbullah et al., 2022). On the other hand, studies on how chronically applied Fucoxanthin affects the membrane integrity of neuronal cells in the long term have been found lacking (Méresse et al., 2020; Sun et al., 2023).

3.2.3. Senolytic, Autophagic, and Anti-Inflammatory Flavonoids

In neurodegenerative disease conditions, the clearance of aged cells accumulated in the body and especially in brain tissue is critical for preventing the accumulation of inflammation.

Fisetin

Senolytic agents such as Fisetin ($C_{15}H_{10}O_6$) stand out for researchers in this regard. This molecule, found most abundantly in strawberries in nature, selectively inhibits the PI3K/AKT/mTOR pathway. Suppression of the mTORC1 complex drives these cells toward apoptosis by preventing the expression of anti-apoptotic Bcl-2 family proteins that enable aged cells to survive. In this way, while the accumulation of damaged glial cells is prevented, the protection of healthy neurons and the maintenance of their functions are supported (Maher, 2019, 2020). Additionally, it has been shown that this molecule prevents the cleavage of p35, a cyclin-dependent kinase 5 (Cdk5) activator, into the toxic p25 form in AD models. It has been reported that a regularly applied Fisetin diet protects synaptic functions and prevents cognitive decline by suppressing neuroinflammation, even if it does not disrupt the integrity of amyloid plaques accumulated in the brain (Currais et al., 2014).

Apigenin

Apigenin ($C_{15}H_{10}O_5$), is a flavone found abundantly in parsley and celery, and is an antioxidant that stands out with its property of promoting new neuron formation by crossing the BBB. At the molecular level, it initiates the phosphorylation of CREB by activating the PI3K/Akt and ERK1/2 signaling cascades (Taupin, 2009). Phosphorylated CREB translocating into the nucleus increases the expression of BDNF and the TrkB receptor, which are of critical importance for the growth and maintenance of viability of neurons. This mechanism has been directly associated with synaptic transmission and long-term memory, especially in AD models (Zhao et al., 2013). It has been stated that the Apigenin and Scutellarein flavonoids in this group are especially effective in preventing reperfusion injury after ischemic stroke and in protecting the myelin sheath on cells in MS models (Wang et al., 2016).

Scutellarein

Scutellarein ($C_{15}H_{10}O_6$), which is the active metabolite of Scutellarin obtained from the *Scutellaria baicalensis* plant, is especially critical in ischemic neurodegeneration processes. The NF-κB pathway activated during ischemia increases the expression of the Matrix Metalloproteinase-9 (MMP-9) enzyme that breaks down the BBB. Scutellarein stops MMP-9 production before it starts by blocking the translocation of the p65 subunit of NF-κB to the nucleus (Y. Zhang et al., 2022). Additionally, by preventing the degradation of tight junction proteins such as occludin and claudin, which are the building blocks of the BBB, and even by promoting their production, it prevents the infiltration of neurotoxic substances into the brain tissue (Zhong, Luo, Deng, & Zhao, 2019).

However, one of the main deficiencies in the transition of studies conducted with these molecules to clinical application is that dosage protocols have not been determined. Especially since the effects of continuous use of agents with senolytic effects such as Fisetin on healthy tissues are unknown, critical indicators such as the appropriate dose and frequency of intake to be applied in humans have not yet been standardized (Currais et al., 2014). In addition to this, despite the therapeutic potential of Scutellarein, its high hydrophobic property and rapid metabolism limit its clinical use (Salehi et al., 2019). Although studies conducted to overcome this obstacle are quite limited in the literature, Chen et al. have obtained remarkable results with the Self-Micro-Emulsifying Drug Delivery System (SMEDDS) they developed. This nano-carrier system has increased the oral bioavailability of Scutellarein by 4.6 times compared to its pure form, being an important step in the development of the pharmacological activities of the molecule and possessing the quality of being a pioneer for new studies (Sha, Wu, Chen, & Fang, 2012).

Trehalose

Trehalose ($C_{12}H_{22}O_{11}$) is a naturally occurring disaccharide that can induce autophagy through an alternative mechanism that is independent of the mechanistic target of rapamycin (mTOR) pathway, which commonly regulates canonical autophagy (Sarkar, Davies, Huang, Tunnacliffe, & Rubinsztein, 2007). In this context, trehalose promotes the nuclear translocation of transcription factor EB (TFEB) and forkhead box O1 (FoxO1), thereby enhancing the transcriptional program required for autophagic flux.

Mechanistically, trehalose stimulates a transient Ca^{2+} release at the lysosomal membrane and activates calcineurin, a calcium dependent phosphatase. Activated calcineurin dephosphorylates TFEB and FoxO1, which facilitates their translocation from the cytoplasm into the nucleus. In models of Alzheimer's disease and Huntington's disease, nuclear FoxO1 has been shown to bind promoter regions of autophagy related genes, including LC3 and Bnip3, and to promote their transcription (Rusmini et al., 2019). This signaling axis supports lysosomal biogenesis and facilitates the clearance of intracellular toxic protein aggregates through macroautophagy. Trehalose has also been described as a chemical chaperone that can stabilize protein structure under stress conditions (Crowe, 2007).

Despite these promising mechanisms, the doses required for trehalose to exert meaningful central effects in humans are expected to be high due to limitations in BBB penetration. High dose oral administration may lead to intestinal degradation by trehalase and can cause significant gastrointestinal adverse effects (Emanuele, 2014). Moreover, studies addressing synthetic analogs or trehalase resistant delivery systems that could improve trehalose bioavailability while reducing side effects remain limited (Rusmini et al., 2019; Yap et al., 2023).

3.2.4 Endogenous Defense Supporting Agents

Sulforaphane

Sulforaphane ($C_6H_{11}NOS_2$) is an isothiocyanate derivative isolated from broccoli sprouts and is considered one of the strongest natural inducers of the Keap1-Nrf2-ARE pathway, which provides cellular adaptation against oxidative stress (Dinkova-Kostova, Fahey, Kostov, & Kensler, 2017). Under physiological conditions, the transcription factor Nrf2 is retained in the cytoplasm by the Keap1 protein and is targeted for ubiquitination through the Cul3-based E3 ligase complex. Sulforaphane interacts with the reactive carbon atom in its structure and targets specific cysteine residues of Keap1, particularly Cys151, Cys273, and Cys288, forming covalent bonds (Baird & Yamamoto, 2020). This interaction alters the conformation and regulatory function of Keap1 and leads to the release of Nrf2.

Following its release, Nrf2 translocates to the nucleus and forms a heterodimer with small Maf proteins (sMaf). The complex binds to antioxidant response element (ARE) promoter regions on DNA and initiates transcriptional activation. This activation markedly increases the expression of several cytoprotective genes, including heme oxygenase-1 (HO-1), NAD(P)H quinone dehydrogenase 1 (NQO1), and glutamate-cysteine ligase (GCL), which is the rate-limiting enzyme of glutathione synthesis (Figure 2.) (Bellezza, Giambanco, Minelli, & Donato, 2018).

In addition to its antioxidant actions, sulforaphane modulates neuroinflammatory pathways. It suppresses microglial activation by inhibiting the nuclear translocation of the p65 subunit of NF-κB, a central regulator of inflammatory signaling, through direct cysteine modification (Subedi, Lee, Yumnam, Ji, & Kim, 2019). Through these combined mechanisms, sulforaphane contributes to cellular protection against oxidative stress and supports the efficient resolution of inflammation (Tarozzi et al., 2013).

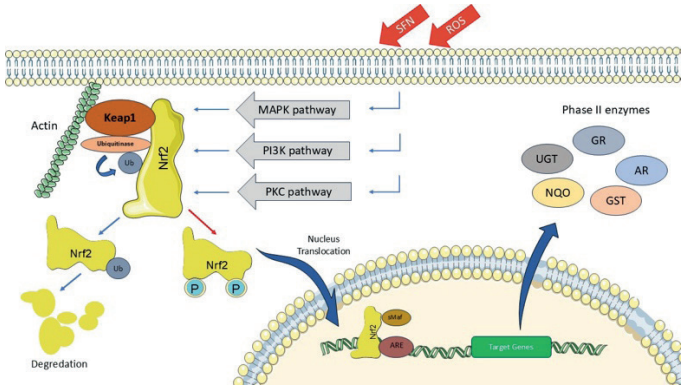

Figure 2. *Sulforaphane alleviates Keap1 inhibition, leading to the activation of the Nrf2-driven antioxidant response (Yin, Wang, Qing, Lin, & Wu, 2016). Adapted from Servier Medical Art (https://smart.servier.com), licensed under CC BY 4.0 (https://creativecommons.org/licenses/by/4.0/).*

Although Sulforaphane is known as an antioxidant with high popularity among research topics, it has not made much progress in the clinical phase. The main reasons for this are that the boundary between the beneficial dose and the toxic dose is quite narrow and that the sensitivity of the molecule to changing conditions such as heat and pH is difficult to optimize (Vanduchova, Anzenbacher, & Anzenbacherova, 2019). It exists in the plants where it is found in the form of glucoraphanin, its inactive precursor, and is dependent on the myrosinase enzyme for activation. Since the human genome does not encode this enzyme, activation is completely dependent on the diversity of the gut microbiota. This causes differences of up to 40% between individuals in benefiting from the antioxidant (Fahey et al., 2015). Finally, Sulforaphane is

known to exhibit a U-shaped effect. While it is cytoprotective at physiological doses (1-5 μM) under normal conditions, it has been shown in in vitro studies that it can trigger apoptosis by disrupting the mitochondrial membrane potential at supraphysiological doses (>20 μM). However, the determination of a safe therapeutic dose for the human brain has not yet been standardized (Santín-Márquez, Alarcón-Aguilar, López-Diazguerrero, Chondrogianni, & Königsberg, 2019).

Withaferin A and Withanolide A

Ashwagandha (*Withania somnifera*), one of the fundamental components of Indian medicine, supports the restoration of impaired protein structures and synaptic transmission functions in the pathophysiology of neurodegeneration thanks to the Withaferin A and Withanolide A compounds it contains. Withaferin A ($C_{28}H_{38}O_6$), activates the Ubiquitin-Proteasome System (UPS) and the Autophagy-Lysosome pathway responsible for the degradation of misfolded and accumulated proteins. It accelerates the autophagy process via the p62/SQSTM1 protein and physically limits protein aggregation by increasing the expression of HSP70 and HSP90 proteins (Sehgal et al., 2012).

Withanolide A ($C_{28}H_{38}O_6$), on the other hand, ensures the re-establishment of damaged neuronal networks by promoting axon and dendrite growth. This effect occurs through the increase in the expression of the post-synaptic density protein PSD-95 and the growth cone marker Growth Associated Protein 43 (GAP-43) (Kuboyama, Tohda, & Komatsu, 2014). Additionally, it opens post-synaptic Cl^- channels by mimicking GABA release from pre-synaptic terminals. This provides hyperpolarization properties to the cell, ensuring the protection of neurons from damage, especially in externally influenced stress conditions such as anxiety (Dar, Hamid, & Ahmad, 2015). In HD models, it has been reported to reduce the aggregation of the mutant huntingtin protein (Kuboyama et al., 2014).

However, the greatest obstacle to this molecule passing through clinical processes and becoming a sustainable drug is the difficulties experienced in the standardization of herbal extracts. Depending on the geographical origin, harvest time, and the polarity values of the extraction solvent used for the *Withania somnifera* samples, the active properties of the bioactive components in the product show significant variations. This incompatibility and imbalance in the extracts used in commercial preparations and experimental studies prevent the determination of a reliable dose and weaken the reproducibility of study results (Mirjalili, Moyano, Bonfill, Cusido, & Palazón, 2009).

3.2.5. Mitochondrial Protectors and Mitochondrial Biogenesis

Among the primary causes of the emergence of neurodegenerative diseases, not only oxidative stress but also mitochondrial dysfunction and the

pathological accumulation of metal ions, primarily iron, play a central role. Molecules that show mitochondrial function-protecting activity aim to protect the energy metabolism of neurons with specialized transport systems and chelation mechanisms, unlike standard radical scavengers (Urrutia et al., 2014).

Ergothioneine

Ergothioneine ($C_9H_{15}N_3O_2S$), is a natural metabolite found in some plants and animals, especially mushrooms. Although it cannot be synthesized by the body, it crosses the BBB through a specific protein transporter called OCTN1 and is taken into neurons and subsequently into the mitochondria. This selective permeability mechanism and its long half-life of approximately 30 days make Ergothioneine a unique protector in preventing mitochondrial DNA damage (Cheah & Halliwell, 2012).

Regarding Ergothioneine, whether the low blood levels observed in neurodegenerative patients are a cause or a consequence of the disease has not yet been fully elucidated (Cheah & Halliwell, 2012).

Deferiprone

It is aimed to stop iron accumulation, which is another critical dimension of neuronal damage, and the resulting ferroptosis with Deferiprone ($C_7H_9NO_2$), a synthetic iron chelator. Free iron, which increases in the brain tissue of patients with AD and PD, triggers ROS formation. Deferiprone, thanks to its low molecular weight structure that can cross the BBB, breaks this destructive cycle by binding excess iron and prevents ferroptosis (Devos et al., 2014).

Even though the neuroprotective efficacy of Deferiprone has been proven, the fact that it carries serious side effect risks such as the loss of immune cells in long-term use keeps its study at uninformed doses under risk. In the literature, synergistic study models where Deferiprone is combined with natural antioxidants to reduce its high impact are lacking (Tricta et al., 2016).

Alpha-Tocopherol Quinone

Similarly, Alpha-Tocopherol Quinone (ATQ) ($C_{26}H_{44}O_3$), which is an advanced metabolite of vitamin E, shows structural similarity to Coenzyme Q10 (Ubiquinone), a mitochondrial electron carrier. In diseases where mitochondrial Complex I (NADH dehydrogenase) dysfunction is observed, such as Leber's Hereditary Optic Neuropathy (LHON) and PD, ATQ ensures the continuity of energy production by leading the repair of disruptions in the electron transport chain (Shrader et al., 2011). This mechanism prevents electrons from escaping the chain and combining with oxygen to form superoxide radicals at the source. That is, instead of scavenging ROS after they are formed, ATQ follows a strategy that prevents ROS formation (Enns et al., 2012; Oyewole & Birch-Machin, 2015).

Unlike classic vitamin E, ATQ physically prevents the conversion of misfolded peptides into toxic fibrils by directly interacting with amyloid-beta plaques, which are at the center of AD pathology, and degrades already formed fibrils. This anti-amyloidogenic effect stops ROS production and apoptosis linked to caspase-3 activation by reducing the cytotoxic pressure on the mitochondria (Yang et al., 2010).

Although ATQ is an endogenous advanced product, its concentration changes in brain tissue during neurodegenerative processes and its potential as a biomarker have not been sufficiently characterized. A more critical molecular gap is related to the chemical reactivity of ATQ. It is known that quinone-structured compounds form covalent bonds by entering into Michael addition reactions with thiol (-SH) groups on proteins (Bolton & Dunlap, 2017). Whether this alkylating property of ATQ affects only the targeted mitochondrial complexes in long-term use or leads to unwanted toxicity at off-target sites by blocking the active sites of other critical enzymes is a safety question that has not yet been elucidated in the literature (Bolton, Trush, Penning, Dryhurst, & Monks, 2000; Kumagai, Shinkai, Miura, & Cho, 2012).

Pyrroloquinoline quinone

Pyrroloquinoline quinone (PQQ) ($C_{14}H_6N_2O_8$) serves as a water-soluble vitamin, cofactor, antioxidant, and anti-inflammatory agent. While most known antioxidants protect existing mitochondria, PQQ is one of the rare agents that trigger mitochondrial biogenesis as a redox cofactor (Rucker, Chowanadisai, & Nakano, 2009).

It initiates its effect by activating the CREB and NAD^+-dependent deacetylase SIRT1 pathway. Activated SIRT1 activates the transcriptional co-activator Peroxisome proliferator-activated receptor-gamma coactivator 1-alpha (PGC-1α), which forms the basis of mitochondrial biogenesis, by deacetylating it (Chowanadisai et al., 2010). Nuclear activation of PGC-1α initiates mitochondrial DNA replication and Mitochondrial Transcription Factor A (TFAM) expression by stimulating NRF-1 and NRF-2 transcription factors. Thus, by increasing the number of mitochondria in neurons, it aims to restore the metabolic capacity lost along with neurodegeneration (Figure 3.) (Hwang & Willoughby, 2018).

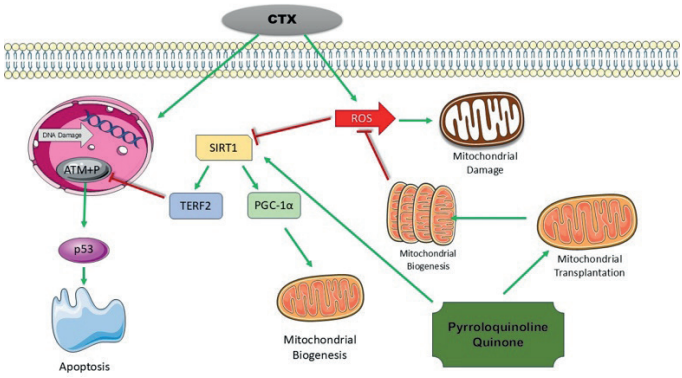

Figure 3. *PQQ triggers mitochondrial biogenesis by upregulating PGC-1α expression through intracellular signaling pathways (Liu et al., 2024). Adapted from Servier Medical Art (https://smart.servier.com), licensed under CC BY 4.0 (https://creativecommons.org/licenses/by/4.0/).*

The greatest obstacle in the clinical application of PQQ is the limited safe dose range and toxicological risks. Studies conducted in animal models have shown that high-dose PQQ administration can lead to acute renal tubular necrosis by interacting with organic anion transporters in the renal tubules (Liang, Zhang, Wang, Song, & Jia, 2015; Watanabe, Hobara, Ohsawa, Higashi, & Tsuji, 1989). Furthermore, at high concentrations, PQQ can lose its antioxidant property and trigger ROS production by assuming a pro-oxidant character, contrary to its normal effect (Misra, Rajpurohit, & Khairnar, 2012). The fact that the safe dose range in humans and the effects it shows while crossing the BBB have not been clarified limits the systemic use of PQQ (Q. Zhang, Shen, Ding, Shen, & Ding, 2011).

4. CONCLUSION

Neurodegenerative diseases arise from intersecting pathological mechanisms, most notably oxidative injury, impaired proteostasis, and mitochondrial dysfunction (Jurcau, 2021). Because these processes reinforce one another, sustained neuroprotection is unlikely to be achieved through single-target approaches. This perspective motivates therapeutic strategies that modulate multiple pathways while also meeting translational requirements such as brain accessibility and tolerability (Cavalli et al., 2008; Cheong et al., 2022).

To provide a concise comparison of the compounds discussed in this chapter, Table 4.1 summarizes their primary targets, dominant effects and key translational limitations.

Table 4.1. *Key mechanisms and translational limitations of selected agents*

Molecule Name	Primary Targets	Dominant and Unique Efficacy	Factors Limiting Use	References
Nobiletin	RORα/γ, Bmal1 Gene	Increasing glymphatic clearance by regulating the biological clock.	Risk of drug interaction as a result of CYP450 suppression.	(Gao et al., 2018; He et al., 2016; Lee et al., 2020)
Tangeretin	*Substantia Nigra*, CYP3A4	Preserves tyrosine hydroxylase activity and maintains motor coordination in PD models.	Potential toxicity in polypharmacy via CYP3A4 inhibition.	(Datla et al., 2001; Gao et al., 2018)
Fucoxanthin	NF-κB, Cell Membrane	Protecting the structure by settling vertically into the cell membrane and suppressing neuroinflammation.	Uncertainty of entry into the brain due to rapid metabolism and P-gp pumps.	(Alghazwi et al., 2019; Kim & Pangestuti, 2011; Mattson & Camandola, 2001; Zeng et al., 2018)
Fisetin	mTOR, Cdk5/p35	Selectively clearing aged cells.	Lack of safe dosage and frequency of use protocols in humans.	(Currais et al., 2014; Maher, 2020)
Apigenin	PI3K/Akt, ERK1/2, BDNF/TrkB	Promotes neurogenesis and synaptic plasticity by activating the CREB pathway, crosses the BBB efficiently.	High concentrations may interfere with GABAergic signaling	(Taupin, 2009; Wang et al., 2016; Zhao et al., 2013)
Scutellarein	MMP-9, Tight Junction Proteins	Protecting the barrier by stopping the enzymes that break down the BBB.	Very low oral bioavailability due to high hydrophobic structure.	(Salehi et al., 2019; Wang et al., 2016; Y. Zhang et al., 2022)
Trehalose	Calcineurin, TFEB, Lysosome	Initiating the removal of wastes and chemical chaperoning without stopping cell growth.	Rapid degradation by the Trehalase enzyme in the intestine and GI side effects.	(Crowe, 2007; Emanuele, 2014; Sarkar et al., 2007)

Sulforaphane	Keap1-Nrf2-ARE Pathway	Stimulating antioxidant defense enzymes most strongly at the genetic level.	Activation being dependent on gut microbiota and narrow therapeutic range.	(Bellezza et al., 2018; Dinkova-Kostova et al., 2017; Santín-Márquez et al., 2019; Subedi et al., 2019; Vanduchova et al., 2019)
Ashwagandha (Withaferin A, Withanolide A)	UPS, HSP70/90, GAP-43	Repairing broken neuronal networks by promoting axon and dendrite growth.	Standardization problem of herbal extracts.	(Dar et al., 2015; Kuboyama et al., 2014; Mirjalili et al., 2009; Sehgal et al., 2012)
Ergothioneine	OCTN1 Transporter, Mitochondria	Protecting mitochondrial DNA by remaining undeclared in the body for approximately 30 days.	Unclear causal relationship between disease pathology and blood levels.	(Cheah & Halliwell, 2012)
Deferiprone	Labile Iron Pool	Preventing cell membrane dysfunction by binding excess iron.	Risk of immune cell loss in long-term use.	(Devos et al., 2014; Tricta et al., 2016)
Alpha-Tocopherol Quinone (ATQ)	Mitochondrial Complex I	Preventing ROS formation at the source instead of scavenging them.	Risk of creating off-target toxicity by binding to proteins (Michael addition).	(Bolton et al., 2000; Enns et al., 2012; Kumagai et al., 2012; Oyewole & Birch-Machin, 2015; Shrader et al., 2011)
Pyrroloquinoline Quinone (PQQ)	SIRT1, PGC-1α	Triggering mitochondrial biogenesis.	Risk of kidney toxicity and showing pro-oxidant effect at high doses.	(Chowanadisai et al., 2010; Hwang & Willoughby, 2018; Liang et al., 2015; Misra et al., 2012; Rucker et al., 2009)

Across the reviewed candidates, three recurring constraints shape clinical translation. These include limited blood–brain barrier penetration, insufficient systemic exposure due to poor bioavailability or rapid metabolism, and dose-

limiting safety concerns such as drug–drug interactions or pro-oxidant shifts at higher exposure. Addressing these barriers will likely require optimized formulations and rational combination strategies that jointly support redox balance, mitochondrial resilience, and protein homeostasis.

5. FUTURE PERSPECTIVES

Future progress in neuroprotective therapy will depend on integrating molecular pharmacology with advanced delivery technologies. For many candidates discussed in this chapter, the main limitation is not mechanistic plausibility but insufficient brain exposure due to suboptimal pharmacokinetics. Accordingly, blood–brain barrier–oriented nano-carrier platforms, enzyme-resistant derivatives, and rational prodrug strategies are expected to play a decisive role. These approaches may enable effective concentrations to be achieved in vulnerable neuronal compartments while reducing systemic adverse effects.

A second priority involves improving precision in patient selection and therapeutic monitoring. Inter-individual variability in metabolism, microbiota composition, and comedication profiles can substantially influence both activation and safety, particularly for agents such as sulforaphane and polymethoxylated flavones. Biomarkers reflecting Nrf2 pathway engagement, autophagic flux, mitochondrial function, and glymphatic activity may support stratification and response tracking. In parallel, combination regimens that integrate complementary mechanisms may offer a more coherent strategy than single-compound interventions for multifactorial neurodegenerative pathology.

From a translational perspective, preclinical development must be aligned with clinical feasibility. Early-phase studies should prioritize dose optimization, long-term safety profiling, and systematic evaluation of interaction risks, especially in elderly populations exposed to polypharmacy. Collaboration between neuroscientists, formulation scientists, and clinicians will be essential to bridge mechanistic insights and practical implementation. With these advances, next-generation antioxidants and related bioactive molecules may gradually become components of mechanism-based neuroprotective strategies.

REFERENCES

Alghazwi, M., Smid, S., Musgrave, I., & Zhang, W. (2019). In vitro studies of the neuroprotective activities of astaxanthin and fucoxanthin against amyloid beta (Aβ1-42) toxicity and aggregation. *Neurochemistry International, 124*, 215-224.

Ayala, A., Muñoz, M. F., & Argüelles, S. (2014). Lipid peroxidation: production, metabolism, and signaling mechanisms of malondialdehyde and 4-hydroxy-2-nonenal. *Oxid Med Cell Longev, 2014*, 360438.

Baird, L., & Yamamoto, M. (2020). The Molecular Mechanisms Regulating the KEAP1-NRF2 Pathway. *Mol Cell Biol, 40*(13).

Bellezza, I., Giambanco, I., Minelli, A., & Donato, R. (2018). Nrf2-Keap1 signaling in oxidative and reductive stress. *Biochimica et Biophysica Acta (BBA) - Molecular Cell Research, 1865*(5), 721-733.

Bolton, J. L., & Dunlap, T. (2017). Formation and Biological Targets of Quinones: Cytotoxic versus Cytoprotective Effects. *Chem Res Toxicol, 30*(1), 13-37.

Bolton, J. L., Trush, M. A., Penning, T. M., Dryhurst, G., & Monks, T. J. (2000). Role of quinones in toxicology. *Chem Res Toxicol, 13*(3), 135-160.

Braidy, N., Behzad, S., Habtemariam, S., Ahmed, T., Daglia, M., Nabavi, S. M., . . . Nabavi, S. F. (2017). Neuroprotective Effects of Citrus Fruit-Derived Flavonoids, Nobiletin and Tangeretin in Alzheimer's and Parkinson's Disease. *CNS Neurol Disord Drug Targets, 16*(4), 387-397.

Cavalli, A., Bolognesi, M. L., Minarini, A., Rosini, M., Tumiatti, V., Recanatini, M., & Melchiorre, C. (2008). Multi-target-directed ligands to combat neurodegenerative diseases. *J Med Chem, 51*(3), 347-372.

Cheah, I. K., & Halliwell, B. (2012). Ergothioneine; antioxidant potential, physiological function and role in disease. *Biochim Biophys Acta, 1822*(5), 784-793.

Cheong, S. L., Tiew, J. K., Fong, Y. H., Leong, H. W., Chan, Y. M., Chan, Z. L., & Kong, E. W. J. (2022). Current Pharmacotherapy and Multi-Target Approaches for Alzheimer's Disease. *Pharmaceuticals (Basel), 15*(12).

Chowanadisai, W., Bauerly, K. A., Tchaparian, E., Wong, A., Cortopassi, G. A., & Rucker, R. B. (2010). Pyrroloquinoline quinone stimulates mitochondrial biogenesis through cAMP response element-binding protein phosphorylation and increased PGC-1alpha expression. *J Biol Chem, 285*(1), 142-152.

Cobley, J. N., Fiorello, M. L., & Bailey, D. M. (2018). 13 reasons why the brain is susceptible to oxidative stress. *Redox Biol, 15*, 490-503.

Crowe, J. (2007). Trehalose as a "chemical chaperone": Fact and fantasy. *Advances in experimental medicine and biology, 594*, 143-158.

Currais, A., Prior, M., Dargusch, R., Armando, A., Ehren, J., Schubert, D., . . . Maher, P. (2014). Modulation of p25 and inflammatory pathways by fisetin maintains cognitive function in Alzheimer's disease transgenic mice. *Aging Cell, 13*(2),

379-390.

Dar, N. J., Hamid, A., & Ahmad, M. (2015). Pharmacologic overview of Withania somnifera, the Indian Ginseng. *Cell Mol Life Sci, 72*(23), 4445-4460.

Datla, K. P., Christidou, M., Widmer, W. W., Rooprai, H. K., & Dexter, D. T. (2001). Tissue distribution and neuroprotective effects of citrus flavonoid tangeretin in a rat model of Parkinson's disease. *NeuroReport, 12*(17), 3871-3875.

Devos, D., Moreau, C., Devedjian, J. C., Kluza, J., Petrault, M., Laloux, C., . . . Bordet, R. (2014). Targeting chelatable iron as a therapeutic modality in Parkinson's disease. *Antioxid Redox Signal, 21*(2), 195-210.

Dinkova-Kostova, A. T., Fahey, J. W., Kostov, R. V., & Kensler, T. W. (2017). KEAP1 and Done? Targeting the NRF2 Pathway with Sulforaphane. *Trends Food Sci Technol, 69*(Pt B), 257-269.

Dusek, P., Schneider, S. A., & Aaseth, J. (2016). Iron chelation in the treatment of neurodegenerative diseases. *J Trace Elem Med Biol, 38*, 81-92.

Emanuele, E. (2014). Can Trehalose Prevent Neurodegeneration? Insights from Experimental Studies. *Current drug targets, 15*.

Enns, G. M., Kinsman, S. L., Perlman, S. L., Spicer, K. M., Abdenur, J. E., Cohen, B. H., . . . Miller, G. (2012). Initial experience in the treatment of inherited mitochondrial disease with EPI-743. *Mol Genet Metab, 105*(1), 91-102.

Fahey, J. W., Holtzclaw, W. D., Wehage, S. L., Wade, K. L., Stephenson, K. K., & Talalay, P. (2015). Sulforaphane Bioavailability from Glucoraphanin-Rich Broccoli: Control by Active Endogenous Myrosinase. *PLoS One, 10*(11), e0140963.

Forman, H. J., & Zhang, H. (2021). Targeting oxidative stress in disease: promise and limitations of antioxidant therapy. *Nat Rev Drug Discov, 20*(9), 689-709.

Galasso, C., Orefice, I., Pellone, P., Cirino, P., Miele, R., Ianora, A., . . . Sansone, C. (2018). On the Neuroprotective Role of Astaxanthin: New Perspectives? *Mar Drugs, 16*(8).

Gammone, M. A., Riccioni, G., & D'Orazio, N. (2015). Marine Carotenoids against Oxidative Stress: Effects on Human Health. *Mar Drugs, 13*(10), 6226-6246.

Gao, Z., Gao, W., Zeng, S.-L., Li, P., & Liu, E. H. (2018). Chemical structures, bioactivities and molecular mechanisms of citrus polymethoxyflavones. *Journal of Functional Foods, 40*, 498-509.

He, B., Nohara, K., Park, N., Park, Y. S., Guillory, B., Zhao, Z., . . . Chen, Z. (2016). The Small Molecule Nobiletin Targets the Molecular Oscillator to Enhance Circadian Rhythms and Protect against Metabolic Syndrome. *Cell Metab, 23*(4), 610-621.

Hwang, P., & Willoughby, D. S. (2018). Mechanisms Behind Pyrroloquinoline Quinone Supplementation on Skeletal Muscle Mitochondrial Biogenesis: Possible Synergistic Effects with Exercise. *J Am Coll Nutr, 37*(8), 738-748.

Jiang, Q., Yin, J., Chen, J., Ma, X., Wu, M., Liu, G., . . . Yin, Y. (2020). Mitochond-

ria-Targeted Antioxidants: A Step towards Disease Treatment. *Oxid Med Cell Longev, 2020*, 8837893.

Jurcau, A. (2021). Insights into the Pathogenesis of Neurodegenerative Diseases: Focus on Mitochondrial Dysfunction and Oxidative Stress. *Int J Mol Sci, 22*(21).

Khan, N., Syed, D. N., Ahmad, N., & Mukhtar, H. (2013). Fisetin: a dietary antioxidant for health promotion. *Antioxid Redox Signal, 19*(2), 151-162.

Kim, S. K., & Pangestuti, R. (2011). Biological activities and potential health benefits of fucoxanthin derived from marine brown algae. *Adv Food Nutr Res, 64*, 111-128.

Kuboyama, T., Tohda, C., & Komatsu, K. (2014). Effects of Ashwagandha (roots of Withania somnifera) on neurodegenerative diseases. *Biological and Pharmaceutical Bulletin, 37*(6), 892-897.

Kumagai, Y., Shinkai, Y., Miura, T., & Cho, A. K. (2012). The chemical biology of naphthoquinones and its environmental implications. *Annual review of pharmacology and toxicology, 52*(1), 221-247.

Lamptey, R. N. L., Chaulagain, B., Trivedi, R., Gothwal, A., Layek, B., & Singh, J. (2022). A Review of the Common Neurodegenerative Disorders: Current Therapeutic Approaches and the Potential Role of Nanotherapeutics. *Int J Mol Sci, 23*(3).

Lee, J., Kim, D. E., Griffin, P., Sheehan, P. W., Kim, D. H., Musiek, E. S., & Yoon, S. Y. (2020). Inhibition of REV-ERBs stimulates microglial amyloid-beta clearance and reduces amyloid plaque deposition in the 5XFAD mouse model of Alzheimer's disease. *Aging Cell, 19*(2), e13078.

Li, S., Pan, M.-H., Lo, C.-Y., Tan, D., Wang, Y., Shahidi, F., & Ho, C.-T. (2009). Chemistry and health effects of polymethoxyflavones and hydroxylated polymethoxyflavones. *Journal of Functional Foods, 1*(1), 2-12.

Li X, H. R., Liu K, Liu M, Luo H, Huang L, Luo L. (2020). Fucoxanthin attenuates LPS-induced acute lung injury via inhibition of the TLR4/MyD88 signaling axis. *Aging (Albany NY). 13*.

Liang, C., Zhang, X., Wang, W., Song, Y., & Jia, X. (2015). A subchronic oral toxicity study on pyrroloquinoline quinone (PQQ) disodium salt in rats. *Food Chem Toxicol, 75*, 146-150.

Lin, M. T., & Beal, M. F. (2006). Mitochondrial dysfunction and oxidative stress in neurodegenerative diseases. *Nature, 443*(7113), 787-795.

Liu, S., Wang, Y., Yang, H., Tan, J., Zhang, J., & Zi, D. (2024). Pyrroloquinoline quinone promotes human mesenchymal stem cell-derived mitochondria to improve premature ovarian insufficiency in mice through the SIRT1/ATM/p53 pathway. *Stem Cell Research & Therapy, 15*.

Maher, P. (2019). The potential of flavonoids for the treatment of neurodegenerative diseases. *International Journal of Molecular Sciences, 20*(12), 3056.

Maher, P. (2020). Preventing and Treating Neurological Disorders with the Flavonol Fisetin. *Brain Plasticity, 6*(2), 155-166.

Matsuzaki, K., Yamakuni, T., Hashimoto, M., Haque, A. M., Shido, O., Mimaki, Y., . . . Ohizumi, Y. (2006). Nobiletin restoring beta-amyloid-impaired CREB phosphorylation rescues memory deterioration in Alzheimer's disease model rats. *Neurosci Lett, 400*(3), 230-234.

Mattson, M. P., & Camandola, S. (2001). NF-kappaB in neuronal plasticity and neurodegenerative disorders. *J Clin Invest, 107*(3), 247-254.

Méresse, S., Fodil, M., Fleury, F., & Chénais, B. (2020). Fucoxanthin, a Marine-Derived Carotenoid from Brown Seaweeds and Microalgae: A Promising Bioactive Compound for Cancer Therapy. *International Journal of Molecular Sciences, 21*(23), 9273.

Mikami, K., & Hosokawa, M. (2013). Biosynthetic pathway and health benefits of fucoxanthin, an algae-specific xanthophyll in brown seaweeds. *Int J Mol Sci, 14*(7), 13763-13781.

Mirjalili, M. H., Moyano, E., Bonfill, M., Cusido, R. M., & Palazón, J. (2009). Steroidal lactones from Withania somnifera, an ancient plant for novel medicine. *Molecules, 14*(7), 2373-2393.

Misra, H. S., Rajpurohit, Y. S., & Khairnar, N. P. (2012). Pyrroloquinoline-quinone and its versatile roles in biological processes. *J Biosci, 37*(2), 313-325.

Mohibbullah, M., Haque, M. N., Sohag, A. A. M., Hossain, M. T., Zahan, M. S., Uddin, M. J., . . . Choi, J.-S. (2022). A Systematic Review on Marine Algae-Derived Fucoxanthin: An Update of Pharmacological Insights. *Marine Drugs, 20*(5), 279.

Nakajima, A., Ohizumi, Y., & Yamada, K. (2014). Anti-dementia Activity of Nobiletin, a Citrus Flavonoid: A Review of Animal Studies. *Clin Psychopharmacol Neurosci, 12*(2), 75-82.

Onozuka, H., Nakajima, A., Matsuzaki, K., Shin, R.-W., Ogino, K., Saigusa, D., . . . Mimaki, Y. (2008). Nobiletin, a citrus flavonoid, improves memory impairment and Aβ pathology in a transgenic mouse model of Alzheimer's disease. *The Journal of pharmacology and experimental therapeutics, 326*(3), 739-744.

Oyewole, A. O., & Birch-Machin, M. A. (2015). Mitochondria-targeted antioxidants. *Faseb j, 29*(12), 4766-4771.

Peng, J., Yuan, J. P., Wu, C. F., & Wang, J. H. (2011). Fucoxanthin, a marine carotenoid present in brown seaweeds and diatoms: metabolism and bioactivities relevant to human health. *Mar Drugs, 9*(10), 1806-1828.

Rucker, R., Chowanadisai, W., & Nakano, M. (2009). Potential physiological importance of pyrroloquinoline quinone. *Altern Med Rev, 14*(3), 268-277.

Rusmini, P., Cortese, K., Crippa, V., Cristofani, R., Cicardi, M. E., Ferrari, V., . . . Poletti, A. (2019). Trehalose induces autophagy via lysosomal-mediated TFEB activation in models of motoneuron degeneration. *Autophagy, 15*(4), 631-651.

Salehi, B., Venditti, A., Sharifi-Rad, M., Kręgiel, D., Sharifi-Rad, J., Durazzo, A., . . . Novellino, E. (2019). The therapeutic potential of apigenin. *International Journal of Molecular Sciences, 20*(6), 1305.

Santín-Márquez, R., Alarcón-Aguilar, A., López-Diazguerrero, N. E., Chondrogianni, N., & Königsberg, M. (2019). Sulforaphane - role in aging and neurodegeneration. *Geroscience, 41*(5), 655-670.

Sarkar, S., Davies, J. E., Huang, Z., Tunnacliffe, A., & Rubinsztein, D. C. (2007). Trehalose, a novel mTOR-independent autophagy enhancer, accelerates the clearance of mutant huntingtin and alpha-synuclein. *J Biol Chem, 282*(8), 5641-5652.

Sehgal, N., Gupta, A., Valli, R. K., Joshi, S. D., Mills, J. T., Hamel, E., . . . Ravindranath, V. (2012). Withania somnifera reverses Alzheimer's disease pathology by enhancing low-density lipoprotein receptor-related protein in liver. *Proc Natl Acad Sci U S A, 109*(9), 3510-3515.

Sha, X., Wu, J., Chen, Y., & Fang, X. (2012). Self-microemulsifying drug-delivery system for improved oral bioavailability of probucol: preparation and evaluation. *Int J Nanomedicine, 7*, 705-712.

Shrader, W. D., Amagata, A., Barnes, A., Enns, G. M., Hinman, A., Jankowski, O., . . . Mollard, P. (2011). α-Tocotrienol quinone modulates oxidative stress response and the biochemistry of aging. *Bioorganic & medicinal chemistry letters, 21*(12), 3693-3698.

Subedi, L., Lee, J. H., Yumnam, S., Ji, E., & Kim, S. Y. (2019). Anti-Inflammatory Effect of Sulforaphane on LPS-Activated Microglia Potentially through JNK/AP-1/NF-κB Inhibition and Nrf2/HO-1 Activation. *Cells, 8*(2).

Sun, H., Yang, S., Zhao, W., Kong, Q., Zhu, C., Fu, X., . . . He, Y. (2023). Fucoxanthin from marine microalgae: A promising bioactive compound for industrial production and food application. *Crit Rev Food Sci Nutr, 63*(26), 7996-8012.

Tarozzi, A., Angeloni, C., Malaguti, M., Morroni, F., Hrelia, S., & Hrelia, P. (2013). Sulforaphane as a potential protective phytochemical against neurodegenerative diseases. *Oxid Med Cell Longev, 2013*, 415078.

Taupin, P. (2009). Apigenin and related compounds stimulate adult neurogenesis. Mars, Inc., the Salk Institute for Biological Studies: WO2008147483. *Expert Opin Ther Pat, 19*(4), 523-527.

Tönnies, E., & Trushina, E. (2017). Oxidative Stress, Synaptic Dysfunction, and Alzheimer's Disease. *J Alzheimers Dis, 57*(4), 1105-1121.

Tricta, F., Uetrecht, J., Galanello, R., Connelly, J., Rozova, A., Spino, M., & Palmblad, J. (2016). Deferiprone-induced agranulocytosis: 20 years of clinical observations. *Am J Hematol, 91*(10), 1026-1031.

Urrutia, P. J., Mena, N. P., & Núñez, M. T. (2014). The interplay between iron accumulation, mitochondrial dysfunction, and inflammation during the execution step of neurodegenerative disorders. *Front Pharmacol, 5*, 38.

Vanduchova, A., Anzenbacher, P., & Anzenbacherova, E. (2019). Isothiocyanate from Broccoli, Sulforaphane, and Its Properties. *J Med Food, 22*(2), 121-126.

Wang, Z., Yu, J., Wu, J., Qi, F., Wang, H., Wang, Z., & Xu, Z. (2016). Scutellarin protects cardiomyocyte ischemia–reperfusion injury by reducing apoptosis and oxida-

tive stress. *Life Sciences, 157*, 200-207.

Watanabe, A., Hobara, N., Ohsawa, T., Higashi, T., & Tsuji, T. (1989). Nephrotoxicity of pyrroloquinoline quinone in rats. *Hiroshima J Med Sci, 38*(1), 49-51.

Weinreb, O., Amit, T., Bar-Am, O., & Youdim, M. B. (2016). Neuroprotective effects of multifaceted hybrid agents targeting MAO, cholinesterase, iron and β-amyloid in ageing and Alzheimer's disease. *Br J Pharmacol, 173*(13), 2080-2094.

Wilson, D. M., 3rd, Cookson, M. R., Van Den Bosch, L., Zetterberg, H., Holtzman, D. M., & Dewachter, I. (2023). Hallmarks of neurodegenerative diseases. *Cell, 186*(4), 693-714.

Yang, S. G., Wang, W. Y., Ling, T. J., Feng, Y., Du, X. T., Zhang, X., . . . Liu, R. T. (2010). α-Tocopherol quinone inhibits β-amyloid aggregation and cytotoxicity, disaggregates preformed fibrils and decreases the production of reactive oxygen species, NO and inflammatory cytokines. *Neurochem Int, 57*(8), 914-922.

Yap, K. H., Azmin, S., Makpol, S., Damanhuri, H. A., Mustapha, M., Hamzah, J. C., & Ibrahim, N. M. (2023). Profiling neuroprotective potential of trehalose in animal models of neurodegenerative diseases: a systematic review. *Neural Regeneration Research, 18*(6), 1179-1185.

Yiannopoulou, K. G., & Papageorgiou, S. G. (2013). Current and future treatments for Alzheimer's disease. *Ther Adv Neurol Disord, 6*(1), 19-33.

Yin, T.-F., Wang, M., Qing, Y., Lin, Y.-M., & Wu, D. (2016). Research progress on chemopreventive effects of phytochemicals on colorectal cancer and their mechanisms. *World Journal of Gastroenterology, 22*, 7058.

Zeng, J., Zhang, Y., Ruan, J., Yang, Z., Wang, C., Hong, Z., & Zuo, Z. (2018). Protective effects of fucoxanthin and fucoxanthinol against tributyltin-induced oxidative stress in HepG2 cells. *Environmental Science and Pollution Research, 25*(6), 5582-5589.

Zhang, L., Wang, H., Fan, Y., Gao, Y., Li, X., Hu, Z., . . . Wang, X. (2017). Fucoxanthin provides neuroprotection in models of traumatic brain injury via the Nrf2-ARE and Nrf2-autophagy pathways. *Scientific Reports, 7*(1), 46763.

Zhang, Q., Shen, M., Ding, M., Shen, D., & Ding, F. (2011). The neuroprotective action of pyrroloquinoline quinone against glutamate-induced apoptosis in hippocampal neurons is mediated through the activation of PI3K/Akt pathway. *Toxicology and Applied Pharmacology, 252*(1), 62-72.

Zhang, Y., Zhang, Z., Wang, J., Zhang, X., Zhao, J., Bai, N., . . . Huo, Q. (2022). Scutellarin alleviates cerebral ischemia/reperfusion by suppressing oxidative stress and inflammatory responses via MAPK/NF-κB pathways in rats. *Environ Toxicol, 37*(12), 2889-2896.

Zhao, L., Wang, J.-L., Liu, R., Li, X.-X., Li, J.-F., & Zhang, L. (2013). Neuroprotective, anti-amyloidogenic and neurotrophic effects of apigenin in an Alzheimer's disease mouse model. *Molecules, 18*(8), 9949-9965.

Zhong, X., Luo, C., Deng, M., & Zhao, M. (2019). Scutellarin-treated exosomes incre-

ase claudin 5, occludin and ZO1 expression in rat brain microvascular endothelial cells. *Exp Ther Med, 18*(1), 33-40.